NAD metabolism modulates mitochondrial function and inflammation and prevents progression of diabetic kidney disease

Komuraiah Myakala[1], Xiaoxin X Wang[1], Bryce A. Jones[2], Matthew D Hirschey[3], Xiaoping Yang[4], Avi Z Rosenberg[4], Brandon Ginley[5], Pinaki Sarder[5], Leonid Brodsky[6], Yura Jang[7], Chan Hyun Na[7], Yue Qi[8], Xu Zhang[8], Udayan Guha[8], Pierce Lewien[9], Ci Wu[11], Shivani Bansal[11], Junfeng Ma[11], Amrita Cheema[11], Julia Panov[6,10], and Moshe Levi[1]

[1]Department of Biochemistry and Molecular & Cellular Biology, Georgetown University, Washington, DC; [2]Department of Pharmacology and Physiology, Georgetown University, Washington, DC; [3]Departments of Medicine, Division of Endocrinology, Metabolism, and Nutrition, and Pharmacology and Cancer Biology, Duke University, Durham, North Carolina; [4]Department of Pathology, Johns Hopkins University, Baltimore, Maryland; [5]Departments of Pathology and Anatomical Sciences, SUNY at Buffalo, Buffalo, New York; [6]Tauber Bioinformatics Research Center, University of Haifa, Mount Carmel, Haifa, 31905, Israel; [7]Department of Neurology, Institute for Cell Engineering, Johns Hopkins University, Baltimore, MD; [8]Thoracic and GI Malignancies Branch, National Cancer Institute, National Institutes of Health, Bethesda, MD 20814; [9]Department of Medicine, University of Colorado School of Medicine, Aurora, Colorado 80045; [10]Sagol Department of Neurobiology, University of Haifa, Mount Carmel, Haifa, 31905, Israel; [11] Department of Oncology, Lombardi Comprehensive Cancer Center, Georgetown University, Washington DC

Running Head: NAD metabolism and diabetic kidney disease

Correspondence: Moshe Levi, MD. Georgetown University, Department of Biochemistry and Molecular & Cellular Biology, 3900 Reservoir Road, Basic Science 353, Washington, DC 20007. Email: Moshe.Levi@georgetown.edu

ABSTRACT

Background: Diabetes mellitus is the leading cause of cardiovascular and renal disease in the United States. In spite of all of the beneficial interventions implemented in patients with diabetes, there remains a need for additional therapeutic targets in diabetic kidney disease (DKD). Mitochondrial dysfunction and inflammation are increasingly recognized as important causes of the development and progression of DKD. However, the molecular connection between mitochondrial function, inflammation, and fibrosis remains to be elucidated.

Methods: In the present studies we tested the hypothesis that enhancing NAD metabolism could increase mitochondrial sirtuin 3 (SIRT3) activity, improve mitochondrial function, decrease mitochondrial DNA damage, and prevent inflammation and progression of DKD.

Results: We found that treatment of db-db mice with type 2 diabetes with nicotinamide riboside (NR) prevented albuminuria, increased urinary KIM1 excretion, and several parameters of DKD. These effects were associated with increased SIRT3 activity, improved mitochondrial function, and decreased inflammation at least in part via inhibiting the activation of the cyclic GMP-AMP synthase-stimulator of interferon genes (cGAS-STING) signaling pathway.

Conclusions: NR supplementation boosted the NAD metabolism to modulate mitochondrial function and inflammation and prevent progression of diabetic kidney disease.

INTRODUCTION

Diabetes mellitus is the leading cause of cardiovascular and renal disease in the United States [1-5]. Data from the National Diabetes Statistics Report in 2020 estimated that more than 34 million Americans, or 10.5% of the population, had diabetes (https://www.cdc.gov/diabetes/pdfs/data/statistics/national-diabetes-statistics-report.pdf). As many as one in four Americans are expected to become diabetic by the year 2050 [4, 6].

The beneficial interventions implemented in patients with diabetes, including tight glucose control, stringent BP control, angiotensin-converting enzyme inhibition (ACEI), angiotensin II receptor blockade (ARB), mineralocorticoid receptor antagonism, sodium glucose cotransport-2 (SGLT2) inhibition and GLP-1 receptor agonism [7-12], indicate additional new therapeutic targets in DKD, which can further understanding of the mechanisms that cause progression and/or prevention of DKD.

Inflammation and mitochondrial dysfunction are increasingly recognized as important causes of renal diseases [13-18] . Kidney is the organ with the second highest oxygen consumption in our body; it is distinctly sensitive to mitochondrial dysfunction, which promotes kidney injury and inflammation [19, 20]. On the other hand, innate immunity-mediated inflammation is closely associated with mitochondria damage. In LPS-induced acute kidney injury model, activation of innate immune response via stimulator of interferon genes (STING) was associated with decreased mitochondrial complex I

activity. Other factors involved in the mitochondrial homeostasis were also found to be decreased in LPS kidneys, such as NAD+ level, and expression of PGC-1a, ERRα and Sirt3 (**Supplementary Figure S1**). The molecular connection between inflammation and mitochondrial metabolism remains to be elucidated.

By contrasting the bulk RNAseq data and the total proteomics data between non-diabetic db/m and diabetic db/db mouse kidneys, we have found that mitochondria and immunity pathways are disrupted in diabetic kidneys. Analysis of transcriptome data revealed that 'mitochondria' and 'immunity' gene ontology (GO) terms were enriched by genes differentially expressed in db/db kidneys compared with db/m mouse kidneys (**Supplementary Figure S2 A-B, Supplementary Table S1**). Similarly, enrichment analysis of differentially expressed proteins in db/db kidneys vs. db/m kidneys also showed GO terms related to mitochondrial function and to immunity (**Supplementary Figure S2 D-E, Supplementary Table S2**). A more detailed examination of the dysregulated genes in db/db kidneys revealed that many of these genes known to localize to mitochondria (**Supplementary Table S3**, based on the MitoCarta3 database) specifically function in fatty acid oxidation (FAO) (**Supplementary Figure S2C**). Our proteomics data analyses also showed that proteins involved in FAO were downregulated in db/db kidneys (**Supplementary Figure S2F**). The downregulation of their expression suggests that defects in FAO in db/db kidneys may contribute to the mitochondrial dysfunction [21, 22]. Of special interest is SIRT3 protein which we found to be downregulated in db/db mice kidneys (**Supplementary Figure S3**). SIRT3 is known to play a major role in regulating the activity of acyl-CoA dehydrogenases in FAO [23], of

which Acadm gene coding for MCAD protein and Acad9 gene were found to be downregulated in our transcriptome data from db/db kidneys (**Supplementary Figure S2C**). We therefore hypothesized that increasing SIRT3 activity could restore the expression of critical FAO genes and that SIRT3 represents a potential therapeutic target.

SIRT3 is an NAD+-dependent deacetylase whose activity depends on the cellular levels of NAD+. Due to the higher Km value for NAD+, SIRT3 activity is more sensitive to the fluctuation of NAD+ availability than other mitochondrial sirtuins [24-26]. Supplementation with NAD+ precursor, nicotinamide riboside (NR) can efficiently enhance NAD+ biosynthesis [27-29].

In the present studies, we administered NR to db/db mice, a model of type 2 diabetes, to evaluate its effects in diabetic nephropathy. We found that long-term NR treatment improved DKD in the db/db mice via restoring the mitochondrial function and preventing the renal inflammation, at least in part by inhibiting the activation of the cyclic GMP-AMP synthase-stimulator of interferon genes (cGAS-STING) signaling pathway.

RESULTS

NR treatment improved the diabetic kidney disease

In this study, we treated the db/db mice with type 2 diabetes with NR for 20 weeks (**Figure 1A**). NR treatment did not change the body weight, kidney weight, or blood glucose, but the serum cholesterol and triglyceride levels were decreased in NR treated db/db mice (**Table 1**). We found that NR treated db/db mice had a significant decrease in albuminuria (**Figure 1B**) and the urinary kidney injury marker Kim1 excretion (**Figure 1C**), indicating NR's effects in improving both podocyte and tubular injury in diabetic kidney disease.

NR treatment improved mesangial expansion in db/db mice based on PAS staining (**Figure 1D**). Immunofluorescence microscopy showed increased extracellular matrix protein (collagen IV and fibronectin) deposition in the glomeruli of db/db kidneys indicating the presence of glomerulosclerosis, which was improved with the NR treatment (**Figure 1E-F, Supplementary Figure S4**). TGFβ, PAI-1 and CTGF, profibrotic growth factors, and αSMA, marker of fibrosis, were increased in db/db kidneys. Treatment with NR decreased mRNA abundance of TGFβ, PAI-1 and αSMA, but not CTGF (**Figure 1G**).

We determined potential podocyte loss with the podocyte nuclear marker p57. The immunohistochemistry of p57 showed the decreased numbers of podocytes in db/db kidneys which was prevented by the NR treatment (**Figure 1H**).

NR treatment improved renal oxidative stress

We found that urinary TBARS level, kidney NADPH oxidase 4 (NOX4) mRNA and kidney 4-hydroxynonenal (4-HNE) protein levels, markers of lipid peroxidation, were increased in diabetic db/db mice. NR treatment decreased urinary TBARS level, kidney NOX4 mRNA and 4-HNE protein level in db/db mice (**Figures 2A-C**). By lipidomics we found that lactosylceramide was also increased in the db/db kidneys and decreased with the NR treatment (**Figure 2D**). Lactosylceramide is known to activate NADPH oxidase to generate oxidative stress [30].

NR treatment increased NAD+ level and increased SIRT3 expression and activity

To assess the effects of NR treatment in the kidneys, we measured NAD+ levels in db/m and db/db kidneys. Although there was no change in baseline NAD+ levels between db/m and db/db kidneys, NR significantly increased NAD+ levels in both db/m and db/db kidneys (**Figure 3A**). With metabolomics we further noticed that there was also increased methylated NAD+ metabolite (1-methylnicotinamide) in NR treated kidneys (**Figure 3A**).

There were increases in acetylated lysine level of whole kidney lysate **(Figure 3B)** and mitochondrial kidney proteins **(Figure 3C)** in db/db mice, an indication of decreased deacetylase activity. Treatment with NR restored acetylated lysine proteins to levels seen in db/m mice, suggesting the improved deacetylase activity in the mitochondria. SIRT3 is the main mitochondrial deacetylase and is involved in regulating mitochondria functions including FAO. To explore whether SIRT3 was involved in the NR effect, we

examined the SIRT3 expression and activity. SIRT3 protein abundance (**Figure 3D**) and activity (**Figure 3E**) were reduced in the diabetic kidney. NR treatment increased SIRT3 protein abundance **(Figure 3D)** and SIRT3 activity **(Figure 3E)**. In human diabetic kidneys, SIRT3 expression (**Figure 3F**, **Supplementary Table S5**) was also decreased. Another NAD+-dependent deacetylase Sirt1 expression did not change in human diabetic kidneys when compared with the non-diabetic controls (**Figure 3G, Supplementary Table S5**).

To further determine a role for SIRT3 in regulating acetylated lysine protein in the kidney, we studied SIRT3 knockout mice [31, 32]. In the kidneys of SIRT3 knockout mice, we found that total protein acetylation level was increased, as well as the acetylation for SOD2 and IDH2 (**Figure 3H)**, two proteins previously found as SIRT3 targets [33, 34]. In diabetic kidneys, acetylated SOD2 and IDH2 protein levels are increased, and NR treatment decreased acetylated SOD2 and IDH2 protein levels (**Figure 3I and 3J**). Acetylation on K68 and K122 of SOD2 has been reported to regulate SOD2 activity [34]. We further performed acetylomics and found that acetylation on K68 instead of K122 of SOD2 was increased in db/db kidneys.

NR treatment enhanced mitochondrial biogenesis in diabetic kidneys

NR treatment increased the mitochondrial DNA/nuclear DNA ratio in db-db diabetic kidneys, indicative of increased mitochondrial biogenesis (**Figure 4A**). NR treatment also increased PGC1α mRNA and protein abundance (**Figure 4B**). PGC1α is a master mitochondrial biogenesis regulator [35]. As expected, the direct targets of PGC1α, *Nrf1*

and the mitochondrial transcription factor *Tfam1,* expression were increased in the diabetic kidney following the NR treatment (**Figure 4C**).

The increased mitochondrial biogenesis was accompanied by increased expression of genes related to the mitochondrial ETC complexes, including complex I subunit *Ndufa4*, complex III subunit *Uqcrc2* and complex IV subunit *Cox6a2* (**Figure 4D**). Complex I activity was decreased in the diabetic kidneys and treatment with NR increased Complex I activity. NR treatment also increased Complex IV activity (**Figure 4E**).

In addition, enzymes that mediate mitochondrial fatty acid β-oxidation, including *Cpt1a* mRNA, *Lcad* mRNA, and *Mcad* mRNA and MCAD protein, were upregulated by the NR treatment in db/db kidneys (**Figure 4F**), suggesting that NR treatment promotes mitochondrial fatty acid β-oxidation. Consistent with these effects, we found that the NR treatment prevented triglyceride accumulation in the kidney (**Supplementary Figure S5**).

NR treatment decreased inflammation in diabetic kidneys

We found significant increases in the expression of MCP-1, TNFα, IL-6, TIMP1 and CD68 mRNA in diabetic kidneys. Toll-like receptor 2 (TLR2), a marker of innate immune pathway triggered by damage-associated molecular patterns, was also increased in db/db kidneys. NR treatment successfully prevented their increases (**Figure 5A**). The staining of CD45 and CD68, markers of leukocytes and macrophages, respectively, showed immune cells infiltration in the glomeruli of db/db kidney, which was prevented in the NR treated group (**Figure 5B and 5C**).

NR treatment decreased cGAS-STING activation in diabetic kidneys

To explore how NR treatment can exert anti-inflammatory effects, we analyzed the RNAseq and whole proteomics data and found that NR treatment downregulates many of the inflammatory genes and proteins upregulated in db/db kidneys (**Figure 6 A-E, Supplementary Tables S6-7 and Figure S6**). Interestingly, the expression of IFITM genes [36] which belong to interferon stimulated genes (ISG) was upregulated in db/db kidneys and was ameliorated by NR treatment (**Figure 6E**). In a non-virus infected environment, ISG induction can be triggered by activated nucleic acid sensors, such as cyclic GMP-AMP synthase (cGAS) and stimulator of interferon genes (STING), which respond to the leaking nuclear or mitochondrial DNA [37-39]. We have found that there was increased mtDNA damage in the db/db kidneys and NR treatment protected the kidney from mtDNA damage (**Figure 6F**). mtDNA damage will trigger the leaking of mtDNA into cytosol, activating the nucleic acid sensors such as cGAS and STING. In the diabetic kidneys, we found marked increases in the cGAS mRNA, STING mRNA and STING protein levels. cGAS and STING levels were significantly decreased by treatment with NR (**Figure 6G**). Activation of STING will turn on the downstream effectors TBK1 and IRF3 by promoting their phosphorylation. We found that STING was activated in db/db kidneys as determined by increases in phosphorylation of its downstream proteins TBK1 **(Figure 6H)** and IRF3 **(Figure 6I)**. NR treatment significantly reduced STING activation (**Figure 6H-I**). We further examined the downstream response and we found that both Stat3 **(Figure 6J)** and NFκB **(Figure 6K)**

were activated in db/db kidneys. Their activation as determined by their active forms phospho-Stat3 and phospho-p65 were reduced by NR treatment.

To further determine STING activation in the kidneys, we performed the immunostaining of STING on kidney tissues. In human diabetic kidneys, STING expression is also increased compared with the controls. Control human kidney biopsies showed endothelial staining of STING in glomeruli, peritubular capillaries and larger vessels with sparse staining of interstitial inflammatory cells. In diabetic renal parenchyma, an expanded pattern of STING staining is observed. There is increased endovascular STING staining in glomeruli correlating with segments with prominent endothelium and endocapillary inflammatory cells including lymphocytes and monocyte/macrophages. Prominent parietal epithelial cells showed increased STING expression. By far, the most prominent compartment with STING expression are the interstitial inflammatory cells. Also noted is enhanced staining in two tubular elements: atrophic tubule and distal nephron (**Figure 6L**). In diabetic mouse kidneys, the increased STING signal was mostly found in inflammatory cells within glomeruli (**Figure 6M**).

STING inhibition decreased inflammation in diabetic kidneys

To determine the role of the increased STING activity *per se* in mediating the inflammation in the diabetic kidney we treated db/m and db/db mice with the STING inhibitor C176 [40-42] **(Figure 7A)**. Treatment of db/db mice with C176 prevented the increases in IRF3 and phospho-IRF3 **(Figure 7B)**. C176 also prevented the increases in the inflammatory markers phospho-STAT3 protein and IL-1β mRNA levels **(Figure 7C)**.

To determine a direct role for STING, independent of the potential off-target effects of C176, we performed studies with the STING KO mice **(Figure 7D)**. In these studies, wild type and STING KO mice were made diabetic with the administration of streptozotocin (STZ). In the STZ mice there was a significant increase in STING protein level, which was prevented in the STING KO mice made diabetic with STZ **(Figure 7E)**. STZ induced increases in urinary albumin and urinary KIM-1 which were significantly attenuated in STING KO mice **(Figure 7F)**. In the STZ mice there was increased protein abundance of phospho-Stat3 which was also significantly decreased in STING KO mice **(Figure 7G)**.

DISCUSSION

Mitochondrial dysfunction and inflammation have been proposed to play an important role in the progression of diabetic kidney disease [13, 15, 16, 19]. It is not known whether these two processes are linked with each other. We have found that treating diabetic mice with nicotinamide riboside (NR), an NAD+ precursor, improves several parameters of mitochondrial dysfunction including restoration of mitochondrial fatty acid β-oxidation. This may be mediated by increasing the mitochondrial sirtuin 3 activity. The increase in sirtuin 3 activity was associated with decreasing the acetylation of proteins important for mitochondrial function including SOD2 and IDH2. The increase in the mitochondrial antioxidant SOD2 is reflected by the ability of NR to decrease renal oxidative stress. NR treatment also induced an increase in mitochondrial DNA/nuclear DNA ratio, indicative of an increase in mitochondrial biogenesis, as well as increases in Tfam, Nrf1, and PGC-1α, complex I and complex IV activities, and enzymes that mediate mitochondrial fatty acid β-oxidation. Other NAD+ precursors have also been reported beneficial renal effects [29, 43]. However, in this report, we further connected the NAD+ effects in diabetic kidney disease model to its direct target SIRT3 by showing the increase in SIRT3 deacetylase activity and the decrease of acetylation level in the mitochondrial targets of SIRT3. SIRT3 relies on the availability of NAD+ level to improve the mitochondrial functions including FAO [44-46]. Restoring FAO is a critical step to reverse the kidney injury. Recently, increasing the FAO enzyme Cpt1a in renal tubules was shown to protect against kidney fibrosis [47].

How these mitochondrial functional changes relate to regulation of inflammation is not known, however in diabetes there is evidence for increased mitochondrial DNA damage which is prevented by NR treatment. The increase in mitochondrial DNA damage may be mediated by increased oxidative stress and also by decreases in Tfam and Nrf1 [48]. The increase in mitochondrial DNA damage on the other hand can result in activation of cGAS-STING and STING signaling, which are major mediators of inflammation via inducing the NFκB and STAT3 regulated inflammatory pathways. In addition, we have found significant increases of the interferon-induced transmembrane proteins 1,2, and 3 [36]. Treatment with NR prevents the decreases in Tfam and Nrf1, the increase in mitochondrial damage, and the increases in the interferon-induced transmembrane proteins 1,2, and 3, NFκB and STAT3.

STING expression is also increased in the kidneys of human subjects with diabetes. STING staining of control kidney biopsies show endothelial staining in glomeruli, peritubular capillaries and larger vessels with sparse staining of interstitial inflammatory cells. In diabetic renal parenchyma, an expanded pattern of staining is observed. There is increased endovascular staining in glomeruli correlating with segments with prominent endothelium and endocapillary inflammatory cells including lymphocytes and monocyte/macrophages. Prominent parietal epithelial cells show increased expression. By far, the most prominent compartment with STING expression are interstitial inflammatory cells. Also noted is enhanced staining in two tubular elements: atrophic tubule and distal nephron.

A role for increased STING expression and activity per se in mediating inflammation is demonstrated in studies where we inhibited STING with a well-established inhibitor C-176 and also in STING knockout mice made diabetic with streptozotocin. In both studies we found that STING inhibition prevents inflammation. In addition, and importantly we determined that STING inhibition prevents diabetic kidney injury as demonstrated by preventing increases in urine albumin and urine KIM1 excretion. Although STING has been previously reported in other kidney injury models [40, 42, 49], this is the first time that the localization of STING activation in the kidney has been examined. In contrast to the data from the cultured cells, the proximal tubules did not seem to be a major site for STING activation in diabetic kidneys. The infiltrated immune cells express most of the STING found in the kidney. This raises the question of how the mitochondrial DNA damage in the tubules relates to STING activation in the immune cells, which warrants further investigation.

METHODS

Animal studies

All mouse experiments were conducted according with the Guide for Care and Use of Laboratory Animals, National Institute of Health, Bethesda, MD and were approved by Institutional Animal Care and Use Committee of Georgetown University, Washington, D.C.

10-week-old male db/m (non-diabetic controls) (catalog # 00662) and db/db (diabetic) (catalog # 00642) mice were obtained from Jackson Laboratories (Bar Harbor, ME). The mice were housed in animal care facility with 12/12-hour light-dark cycle and fed for 20 weeks on regular chow diet (TD 190694, Envigo, Madison, WI) or chow diet supplemented with 500 mg/kg body weight nicotinamide riboside (NR) (ChromaDex, Irvine, CA) (TD 190695, Envigo, Madison, WI). One week prior to the end of the study, the mice were placed in metabolic cages for a 24-hour urine collection. At the end of the study, heparinized plasma and kidneys were harvested for further processing.

To determine the role of SIRT3, whole body SIRT3 knockout mice on C57BL/6 background were obtained from Matthew Hirschey (Duke University) [32] to compare their kidneys with the age, gender matched wild-type control kidneys.

To determine the role of STING inhibition in the diabetic kidneys, 20-week-old male db/m and db/db mice were treated with C-176 [41] (Focus Biomolecules, Plymouth Meeting, PA) at 1.2mg/kg body weight dose with daily i.p. injection for 4 weeks.

To further determine the role of STING in the diabetic kidneys, 12-week-old male wild type and whole-body STING knockout mice on C57BL/6J background (JAX catalog #025805) were treated with streptozotocin at 50mg/kg body weight as 5-day daily consecutive i.p. injection to induce diabetes. These mice were sacrificed after 12 weeks on diabetes.

Blood and urine biochemical analysis

Blood glucose levels were assessed with a glucometer (Elite XL, Bayer, Tarrytown, NY). Blood urea nitrogen (BUN) was measured with colorimetric QuantiChrom assay kit (Bioassay systems, Hayward, CA). Total cholesterol and triglycerides levels in plasma were determined with calorimetric assay kit provided by Pointe Scientific (Canton, MI, USA). Urine assays followed the instructions from the kits listed in **Supplementary Table S4.**

NAD^+ measurement

20 mg of kidney tissue was homogenized in extraction buffer provided by the kit (E2ND-100, Bioassay systems) and NAD^+ was determined immediately according to manufacturer's protocol.

Immunoblotting

Total protein was quantified using the BCA protein assay kit (Thermo Scientific, Rockford, IL). Western blotting was done as previously described [50]. Antibody information can be found in **Supplementary Table S4.**

Quantitative Real-Time PCR

Total RNA from kidneys were isolated according to manufacturer's protocol with Qiagen RNeasy mini kit (Qiagen, Gaithersburg, MD) and cDNA was made using reverse transcript reagents from Thermo Scientific (Catalog # 4374967). qRT–PCR was performed using Quant Studio Real-Time PCR machine (Thermo Fisher Scientific). Expression levels of target genes were normalized to 18S level. Primer sequences are listed in **Supplementary Table S4.**

Mitochondrial enzymatic complex activity assay and sirtuin 3 activity assay

Mitochondrial fraction was isolated according to previously described protocol [50]. Isolated mitochondria were assayed for the complex I (Catalog # ab109729), complex IV (Catalog # ab109911) and sirtuin 3 activity (Catalog # ab156067) with the kits purchased from Abcam, Boston, MA.

Analysis of mitochondrial DNA damage

Total DNA from kidney tissue was isolated using Genomic Tip (Qiagen, Valencia, CA), and its concentration was measured by PicoGreen dye (Invitrogen, Carlsbad, CA). 15 ng DNA was used to amplify a long 10kb mitochondria DNA target followed by real-

time PCR based quantification to determine mitochondria DNA lesions, as previously described [51].

Immunohistochemical (IHC) and PAS staining

Immunohistochemical staining was performed on formalin fixed and paraffin embedded 5 µm kidney sections. Following deparaffinization and rehydration, the slides were subjected to heat mediated antigen retrieval in citrate buffer pH 6 and blocked with 3% BSA. The sections were probed with Sirt1 (Abcam catalogue # ab110304), Sirt3 (Sigma catalogue # S4072) or STING (Cell Signaling, catalogue # 13647S) antibody and incubated in room temperature for 1.5 hours. Mouse/Rabbit PolyDetector reagent (Bio SB, Catalog No. BSB 0269) or UnoVue HRP secondary antibody detection reagent (Diagnostic BioSystems, Pleasanton, CA) was applied followed by DAB chromogen. The Periodic Acid-Schiff (PAS) staining was performed with a PAS stain kit (Thermo Scientific, Catalog No. 87007). Imaging was done with Nanozoomer (Hamamatsu Photonics, Japan) and Motic Digital Slide Scanner (Richmond, BC, Canada).

Quantification of Morphology

Glomeruli were extracted from images of PAS staining and the PAS components of each glomerulus were segmented as described before [52]. To quantify mesangial expansion, the ratio of PAS positive pixels to detected glomerular pixels was used.

Immunofluorescence microscopy

The kidney tissue was snap frozen by embedding in to optimum cutting temperature (OCT) medium (Thermo Scientific, CA). The tissues were sectioned at 5-µm in thickness and transferred over the superfrost slides. Immunofluorescence staining performed as descried previously [50, 53]. Antibody information can be found in **Supplementary Table S4.**

Bulk RNA-seq

One microgram of total RNA samples was sent to Novogene (Sacramento, CA) for mRNA sequencing. RNA-seq fastQ files were filtered and trimmed from adaptors using Trimmomatic algorithm [54]. The reads were aligned to *Mus musculus* genome assembly and annotation file GRCM38:mm10 using STAR algorithm [55]. Gene expression was estimated in FPKM counts using RSEM algorithm [56]. Differential expression was quantified with DeSeq2 algorithm [57]. Absolute fold change of 1.5 and Bonferroni adjusted p-value of less than 0.05 was considered as significant change. All bioinformatics analysis was performed on T-BioInfo Platform (http://tauber-data2.haifa.ac.il:3000/). DAVID Bioinformatics [58, 59] and PANTHER Classification System (http://PANTHERdb.org/) were used to classify the differentially expressed genes into functional groups. To identify proteins that are localized to mitochondria, we used a curated database of mitochondrial localized proteins – MitoCarta3 database [60].

Proteomic analysis

Frozen mouse kidney samples were lysed in 8 M urea and 50 mM triethylammonium bicarbonate (TEAB). Proteins were then reduced and alkylated followed by digestion with

LysC (Fujifilm Wako Pure Chemical, Osaka, Japan) in the ratio of 1:100 (enzyme-to-protein, w/w) at 37°C for 3 hours. Subsequently, the proteins were further digested with trypsin (Promega, Fitchburg, WI) in the ratio of 1:50 (enzyme-to-protein, w/w) at 37°C overnight after diluting the urea concentration from 8 M to 2 M. Proteins were then acidified, desalted, and lyophilized sequentially. The dried peptides were labeled with 16-plex TMT reagents (Thermo Scientific). The labeled peptides was fractionated using basic pH RPLC for total proteome analysis as described previously [61]. The LC-MS/MS was analyzed on an Orbitrap Fusion Lumos Tribrid Mass Spectrometer coupled with an Ultimate3000 RSLCnano nano-flow liquid chromatography system (Thermo Scientific). The resulting spectra were analyzed by Proteome Discoverer (version 2.4.1.15 software package, Thermo Scientific) following standard procedures. Downstream analysis was performed with Perseus [62] using log2 normalized intensities of protein abundance. Absolute fold change of 1.5 and Bonferroni adjusted p-value of less than 0.05 was considered as significant change.

Acetylomics analysis

Proteins in tissue lysates were reduced and alkylated followed by digestion with sequencing-grade Lys-C/trypsin (Promega) by incubation at 37°C overnight. The resulting peptides were eluted and dried down with a SpeedVac (Fisher Scientific). Acetyl-lysine (AcK) peptides were then enriched by using sequential enrichment with AcK Affinity Beads (Cytoskeleton, Denver, CO and ImmuneChem, British Columbia, Canada) and analyzed with a nanoAcquity UPLC system (Waters) coupled with Orbitrap Fusion Lumos Mass Spectrometer (Thermo Fisher). The resulting spectra were analyzed by using

SpectronautTM v14 (Biognosys, Switzerland) in directDIA mode with the mouse database downloaded from UniProt.

Metabolomics: This method is developed to quantitate endogenous molecules using QTRAP® 5500 LC-MS/MS System (Sciex, Framingham, MA). For the purpose, kidney samples were pulverized in liquid nitrogen and dissolved in 150 µl of extraction buffer (methanol/water 50/50) containing 200 ng/mL of debrisoquine (DBQ) as internal standard for positive mode and 200 ng/mL of 4-nitrobenzoic acid as internal standard for negative mode. The samples were vortexed for 30 seconds and homogenized for 1-2 min on ice and incubated on ice for 20 min followed by addition of 150 µl of acetonitrile and incubation at -20 ℃ for 20 min. Samples were centrifuged at 13,000 rpm for 20 min at 4 ℃. The supernatant was transferred to MS vial for LC-MS analysis.

Lipidomics: This method is designed to measure 21 classes of lipid molecules which includes diacylglycerols (DAG), cholesterol esters (CE), sphingomyelins (SM), phosphatidylcholine (PC), triacylglycerols (TAG), free fatty acids (FFA), ceramides (CE), dihydroceramides (DCER), hexosylceramide (HCER), lactosylceramide (LCER), phosphatidylethanolamine (PE), lysophosphtatidylchloine (LPC), lysophosphatidylethnolamine (LPE), phosphatidic acid (PA), lysophosphatidic acid (LPA), phosphatidylinositol (PI), lysophosphotidylinositol (LPI), phosphatidylglycerol (PG), acylcarnitines and phosphatidylserine (PS) using QTRAP® 5500 LC-MS/MS System (Sciex). For the purpose, kidney samples were pulverized in liquid nitrogen and dissolved in 300 µL of extraction buffer (IPA) containing internal standard for lipid classes. The samples were vortexed for 30 seconds and homogenized for 1-2 min on ice and incubated

on ice for 20 min followed by incubation at -20 ℃ for 20 min. Samples were centrifuged at 13,000 rpm for 20 min at 4 ℃. The supernatant was transferred to MS vial for LC-MS analysis.

Statistical Analysis

All the resulted data sets were calculated and presented as mean ± SEM. One-way ANOVA fallowed by Student-Newman-Keuls post hoc analysis were used to analyze the variance among multiple groups and between two groups. The statistically significant differences were designated as a *P* values of <0.05. GraphPad prism 8.1.2 software package was used for statistical analysis (www.graphpad.com).

Data and Resource Availability

All reagents and data from this article are available from the corresponding author upon request.

Acknowledgements

Funding. This study was funded by NIH R01 Grants DK116567 (ML), DK127830 (ML), F30 Fellowship DK129003 (BAJ), AHA Postdoctoral Fellowship 19POST34381041 (KM), and National Center for Advancing Translational Sciences of NIH under Award Number TL1TR001431 (BAJ). We also thank Chromadex (Los Angeles, CA) for supplying us NR.

Duality of Interest. No potential conflicts of interest relevant to this article were reported.

Author Contributions. ML and XXW conceived and designed research; KM, XXW performed most experiments; BAJ, MDH, XY, AZR, BG and PS performed the histology work; LB, YJ, CHN, YQ, XZ, UG, PL, CW, JM, AC, and JP conducted the –omics work and analysis. KM and XXW analyzed data and interpreted results of experiments; KM, XXW and JP prepared figures; XXW, KM, JP and ML wrote the manuscript with input from all the co-authors; ML is the guarantor of this work and, as such, had full access to all the data in the study and takes responsibility for the integrity of the data and the accuracy of the data analysis.

Table 1. Metabolic data for db-m and db-db mice.

	DB/M	DB/M + NR	DB/DB	DB/DB + NR
Body weight (g)	30.8±2.28	31.7±1.67	33.8±2.7	27.8±2.39
Food intake (mouse/day)	3.1±0.06	3.03±0.06	5.4±2.60[a]	5.2±0.21
Kidney weight (g)	0.29±0.02	0.24±0.02	0.31±0.02	0.26±0.02
Kidney weight/body weight ratio (%)	0.90±0.11	0.77±0.1	0.98±0.11	0.94±0.1
glucose (mg/dL)	145.8±11	156.8±7.78	783.3±29[a]	787.2±3.83
Plasma TG (mg/dL)	55.6±15.2	46.9±8.7	137.1±15.2[a]	72.0±64.9[b]
Plasma TC (mg/dL)	86.5±2.3	84.2±9.6	121±34.4[c]	89.2±31.7[d]

Data are means ± SE (N=6 mice in each group): [a] $p < 0.0001$ vs. DB/M, [b] $p < 0.001$ vs. DB/M, [c] $p < 0.05$ vs. DB/M, [d] $p < 0.05$ vs. DB/DB.

Figure Legends

Figure 1. Effect of nicotinamide riboside (NR) treatment on diabetes induced podocyte and tubular dysfunction. A) Experimental scheme for the study with NR treatment. B) Urinary albumin and C) KIM1 normalized to creatinine ratio was measured in 24-hour urine. Albumin and KIM1 excretion were significantly increased in db/db compared to non-diabetic db/m mice. Dietary supplementation with NR significantly reduced the urinary excretion of albumin and KIM1. D) PAS stained images indicating, increased PAS positive area with mesangial matrix expansion, glomeruli size and pathological changes were suppressed upon NR treatment in db/db mice with unchanged glomerular size. E) & F) Immunofluorescence images indicating the collagen IV and fibronectin fluorescence signals were increased in db/db kidney and reduced significantly in NR treated mice. G) TGFβ, PAI1, CTGF and αSMA mRNA levels were higher in the db/db kidneys. TGFβ, PAI1, and αSMA mRNA levels were significantly decreased upon NR treatment. H) Immunochemistry images of podocyte positive marker p57 is markedly reduced in kidney of db/db mice and depletion was prevented upon NR treatment. p57 positive areas were quantified per each glomerulus of kidney section. n=6-8 per group, values presented as mean ± SEM with variance is calculated using one-way ANOVA.

Figure 2: Effect of NR treatment on markers related to oxidative stress in diabetic mice. A) Urinary thiobarbituric acid reactive substances (TBARS), B) NADPH oxidase 4 (NOX4) mRNA levels were significantly higher in db/db mice and NR treatment prevented increases in TBARS and NOX4 mRNA. C) Western blot analysis showing 4-hydroxynonenal (4-HNE) protein expression levels were upregulated and abrogated

upon NR treatment in kidney of db/db mice. D) Metabolomics revealed the regulation of lactosylceramides. n=6 per group for A-C) and n=3 per group for D), values presented as mean ± SEM with variance is calculated using one-way ANOVA.

Figure 3: Effect of NR treatment on NAD^+ levels, SIRT3 expression and activity in the kidney as well as expression of total acetylated proteins in the kidney of SIRT3 KO mice. A) NAD^+ levels were measured in kidney and comparable in both db/m and db/db mice. 1-methyl-nicotinamide was measured with metabolomics. NR treatment increased NAD^+ level and 1-methyl-nicotinamide level in both groups. B) & C) Acetylated-lysine protein expression levels in total kidney lysates and mitochondrial fractions were increased in db/db mice and NR supplementation decreased its abundance. D) SIRT3 protein abundance in whole tissue lysate and E) SIRT3 enzyme activity in mitochondrial fraction were reduced significantly in db/db kidney and reduction was prevented upon NR treatment. In human diabetic kidneys F) Immunohistochemical (IHC) staining showing the SIRT3 protein abundance is significantly lower compared to non-diabetic human kidneys G) Histology quantification of nuclear Sirt1 expression levels were unchanged between non-diabetic and diabetic human kidneys. Western blot analysis of kidney mitochondrial lysates showing increased H) protein expression levels of total acetylated lysine and acetylated superoxide dismutase 2 (SOD2) and isocitrate dehydrogenase (NADP+) 2 (IDH2) in kidney of SIRT3 KO mice. In total kidney lysates, the abundance of I) acetylated SOD2 and J) acetylated IDH2 were increased in db/db mice and prevented in mice treated with NR. n=6 per group, values presented as mean ± SEM with variance is calculated using one-way ANOVA

Figure 4: Effect of NR treatment on mitochondria in the kidney of diabetic db/db mice. A) mitochondrial DNA/nuclear DNA ratio was unchanged in db/db mice and NR supplementation increased the ratio of mito DNA. B) mRNA and protein expression levels of PGC1a a master regulator of mitochondrial biogenesis was increased with NR treatment in db/db mice though there is comparable differences between db/m and db/db mice. C) mRNA levels of *Nrf2* and *Tfam* were decreased in db/db mice and prevented the decreasing upon NR treatment. D) Complex 1 and III subunits *Ndufa4* and *Uqcrc2* mRNA levels were reduced significantly in db/db kidney and reduction was inhibited with NR treatment. Complex IV subunit *Cox6a2* mRNA levels were increased in both db/m and db/db kidney with NR supplementation. E) Complex 1 enzyme activity was markedly decreased in db/db mice and reversed in response to NR treatment. In addition, complex IV activity also increased by NR treatment in db/db mice. F) The fatty acid β-oxidation enzymes *Cpt1a*, *Lcad* mRNA and *Mcad* mRNA and protein levels were increased with NR administration in db/db mice. n=5-6 per group, values presented as mean ± SEM with variance is calculated using one-way ANOVA.

Figure 5: Effect of NR treatment on inflammation in the kidney of db/db mice. A) The inflammatory cytokine markers MCP-1, TNFα, IL-6, TIMP1 and CD68 transcript levels were significantly higher in db/db mice. Also TLR2 an innate immune response marker increased in db/db mice. NR treatment successfully prevented their increases. Immunofluorescence microscopic images B) CD45 stained in green, phalloidin as red and C) CD68 stained in green showing the infiltration of immune cells in the glomeruli of

db/db kidney which was prevented in the NR treated db/db mice. n=5-6 per group, values presented as mean ± SEM with variance is calculated using one-way ANOVA.

Figure 6: NR treatment inhibit the cGAS-STING activation in the kidney of db/db mice. A & B) Transcriptome and C & D) proteomics analysis of kidney indicating the upregulation of pathways related to immunity in the kidney of db/db mice compared to db/m controls. E) Transcriptomic analysis found IFITM genes which belong to interferon stimulated genes (ISG) was upregulated in db/db kidneys and inhibited by NR treatment. F) Mitochondrial DNA (mtDNA) damage markedly increased in db/db mice and damage was prevented by NR. G) cGAS mRNA and Sting mRNA and proteins levels were increased in db/db mice and NR treatment decreased their levels. Downstream of cGAS-Sting singling proteins, active form of H) phosphorylated TBK1, I) phosphorylated IRF3, J) phosphorylated Stat3, K) phosphorylated p65 protein abundance were increased in db/db mice and normalized upon NR treatment, although total p65 levels were unchanged. Immunohistochemistry indicating L) Sting protein expression was increased in the kidney of humans with diabetes. M) Similar to humans, Sting expression levels were increased in glomeruli and interstitial kidney of db/db mice and reduced with NR treatment. The western blot images were quantified and normalized to the total protein or phosphorylated active form divided inactive total protein as loading control. n=5-6 per group, values presented as mean ± SEM with variance is calculated using one-way ANOVA.

Figure 7: Effects of STING inhibitor C176 or STING knockout (KO) on the inflammatory response and kidney function in db/db and streptozotocin (STZ) induced diabetic mice. A) Experimental scheme for the study with C176 treatment. B) total and phosphorylated IRF3 protein levels were decreased significantly in db/db mice treated with C176. C) phosphorylated Stat3 protein levels were higher in db/db mice and C176 treatment decreased their levels. IL1-β mRNA levels increased in kidney and decreased with C176 treatment in db/db compared to control db/m mice. D) Experimental scheme for the study with STING KO mice. E) Sting protein levels were significantly increased in wild type (WT) mice with STZ induced diabetes and markedly decreased in Sting KO mice made diabetic with STZ. F) Urinary albumin/creatinine and urinary KIM1/creatinine ratio were increased significantly in wild type mice with STZ-induced diabetes and they were markedly reduced in the Sting KO mice made diabetic with STZ. G) Phosphorylation of stat3 protein levels were higher in kidney of WT mice with STZ-induced diabetes and normalized in STZ induced diabetic Sting KO mice. n=4-6 per group, values presented as mean ± SEM with variance is calculated using one-way ANOVA.

REFERENCES

1. Sedor, JR, Freedman, BI: Biologic Underpinnings of Type 1 Diabetic Kidney Disease. *J Am Soc Nephrol*, 30**:** 1782-1783, 2019.
2. Thomas, MC, Cooper, ME, Zimmet, P: Changing epidemiology of type 2 diabetes mellitus and associated chronic kidney disease. *Nat Rev Nephrol*, 12**:** 73-81, 2016.
3. Breyer, MD, Coffman, TM, Flessner, MF, Fried, LF, Harris, RC, Ketchum, CJ, Kretzler, M, Nelson, RG, Sedor, JR, Susztak, K, Kidney Research National, D: Diabetic nephropathy: a national dialogue. *Clin J Am Soc Nephrol*, 8**:** 1603-1605, 2013.
4. Boyle, JP, Thompson, TJ, Gregg, EW, Barker, LE, Williamson, DF: Projection of the year 2050 burden of diabetes in the US adult population: dynamic modeling of incidence, mortality, and prediabetes prevalence. *Popul Health Metr*, 8**:** 29, 2010.
5. Reidy, K, Kang, HM, Hostetter, T, Susztak, K: Molecular mechanisms of diabetic kidney disease. *J Clin Invest*, 124**:** 2333-2340, 2014.
6. Gregg, EW, Li, Y, Wang, J, Burrows, NR, Ali, MK, Rolka, D, Williams, DE, Geiss, L: Changes in diabetes-related complications in the United States, 1990-2010. *N Engl J Med*, 370**:** 1514-1523, 2014.
7. Barrera-Chimal, J, Jaisser, F: Pathophysiologic mechanisms in diabetic kidney disease: A focus on current and future therapeutic targets. *Diabetes Obes Metab*, 22 Suppl 1**:** 16-31, 2020.
8. Matthews, DR, Paldanius, PM, Proot, P, Chiang, Y, Stumvoll, M, Del Prato, S, group, Vs: Glycaemic durability of an early combination therapy with vildagliptin and metformin versus sequential metformin monotherapy in newly diagnosed type 2 diabetes (VERIFY): a 5-year, multicentre, randomised, double-blind trial. *Lancet*, 394**:** 1519-1529, 2019.
9. Davies, MJ, D'Alessio, DA, Fradkin, J, Kernan, WN, Mathieu, C, Mingrone, G, Rossing, P, Tsapas, A, Wexler, DJ, Buse, JB: Management of Hyperglycemia in Type 2 Diabetes, 2018. A Consensus Report by the American Diabetes Association (ADA) and the European Association for the Study of Diabetes (EASD). *Diabetes Care*, 41**:** 2669-2701, 2018.
10. Alicic, RZ, Rooney, MT, Tuttle, KR: Diabetic Kidney Disease: Challenges, Progress, and Possibilities. *Clin J Am Soc Nephrol*, 12**:** 2032-2045, 2017.
11. Perkovic, V, Jardine, MJ, Neal, B, Bompoint, S, Heerspink, HJL, Charytan, DM, Edwards, R, Agarwal, R, Bakris, G, Bull, S, Cannon, CP, Capuano, G, Chu, PL, de Zeeuw, D, Greene, T, Levin, A, Pollock, C, Wheeler, DC, Yavin, Y, Zhang, H, Zinman, B, Meininger, G, Brenner, BM, Mahaffey, KW, Investigators, CT: Canagliflozin and Renal Outcomes in Type 2 Diabetes and Nephropathy. *N Engl J Med*, 380**:** 2295-2306, 2019.
12. Michos, ED, Tuttle, KR: GLP-1 Receptor Agonists in Diabetic Kidney Disease. *Clin J Am Soc Nephrol*, 2021.
13. Mise, K, Galvan, DL, Danesh, FR: Shaping Up Mitochondria in Diabetic Nephropathy. *Kidney360*, 1**:** 982-992, 2020.
14. Ducasa, GM, Mitrofanova, A, Fornoni, A: Crosstalk Between Lipids and Mitochondria in Diabetic Kidney Disease. *Curr Diab Rep*, 19**:** 144, 2019.
15. Forbes, JM, Thorburn, DR: Mitochondrial dysfunction in diabetic kidney disease. *Nat Rev Nephrol*, 14**:** 291-312, 2018.
16. Sharma, K, Karl, B, Mathew, AV, Gangoiti, JA, Wassel, CL, Saito, R, Pu, M, Sharma, S, You, YH, Wang, L, Diamond-Stanic, M, Lindenmeyer, MT, Forsblom, C, Wu, W, Ix,

JH, Ideker, T, Kopp, JB, Nigam, SK, Cohen, CD, Groop, PH, Barshop, BA, Natarajan, L, Nyhan, WL, Naviaux, RK: Metabolomics reveals signature of mitochondrial dysfunction in diabetic kidney disease. *J Am Soc Nephrol,* 24**:** 1901-1912, 2013.

17. Winiarska, A, Knysak, M, Nabrdalik, K, Gumprecht, J, Stompor, T: Inflammation and Oxidative Stress in Diabetic Kidney Disease: The Targets for SGLT2 Inhibitors and GLP-1 Receptor Agonists. *Int J Mol Sci,* 22, 2021.
18. Andrade-Oliveira, V, Foresto-Neto, O, Watanabe, IKM, Zatz, R, Camara, NOS: Inflammation in Renal Diseases: New and Old Players. *Front Pharmacol,* 10**:** 1192, 2019.
19. Tang, SCW, Yiu, WH: Innate immunity in diabetic kidney disease. *Nat Rev Nephrol,* 16**:** 206-222, 2020.
20. Perez-Morales, RE, Del Pino, MD, Valdivielso, JM, Ortiz, A, Mora-Fernandez, C, Navarro-Gonzalez, JF: Inflammation in Diabetic Kidney Disease. *Nephron,* 143**:** 12-16, 2019.
21. Reidy, KJ, Ross, MJ: Re-energizing the kidney: targeting fatty acid metabolism protects against kidney fibrosis. *Kidney Int,* 2021.
22. Mori, Y, Ajay, AK, Chang, JH, Mou, S, Zhao, H, Kishi, S, Li, J, Brooks, CR, Xiao, S, Woo, HM, Sabbisetti, VS, Palmer, SC, Galichon, P, Li, L, Henderson, JM, Kuchroo, VK, Hawkins, J, Ichimura, T, Bonventre, JV: KIM-1 mediates fatty acid uptake by renal tubular cells to promote progressive diabetic kidney disease. *Cell Metab,* 33**:** 1042-1061 e1047, 2021.
23. Li, M, Li, CM, Ye, ZC, Huang, J, Li, Y, Lai, W, Peng, H, Lou, TQ: Sirt3 modulates fatty acid oxidation and attenuates cisplatin-induced AKI in mice. *J Cell Mol Med,* 24**:** 5109-5121, 2020.
24. Ralto, KM, Rhee, EP, Parikh, SM: NAD(+) homeostasis in renal health and disease. *Nat Rev Nephrol,* 16**:** 99-111, 2020.
25. Morigi, M, Perico, L, Benigni, A: Sirtuins in Renal Health and Disease. *J Am Soc Nephrol,* 29**:** 1799-1809, 2018.
26. Katsyuba, E, Romani, M, Hofer, D, Auwerx, J: NAD(+) homeostasis in health and disease. *Nat Metab,* 2**:** 9-31, 2020.
27. Katsyuba, E, Mottis, A, Zietak, M, De Franco, F, van der Velpen, V, Gariani, K, Ryu, D, Cialabrini, L, Matilainen, O, Liscio, P, Giacche, N, Stokar-Regenscheit, N, Legouis, D, de Seigneux, S, Ivanisevic, J, Raffaelli, N, Schoonjans, K, Pellicciari, R, Auwerx, J: De novo NAD(+) synthesis enhances mitochondrial function and improves health. *Nature,* 563**:** 354-359, 2018.
28. Rajman, L, Chwalek, K, Sinclair, DA: Therapeutic Potential of NAD-Boosting Molecules: The In Vivo Evidence. *Cell Metab,* 27**:** 529-547, 2018.
29. Tran, MT, Zsengeller, ZK, Berg, AH, Khankin, EV, Bhasin, MK, Kim, W, Clish, CB, Stillman, IE, Karumanchi, SA, Rhee, EP, Parikh, SM: PGC1alpha drives NAD biosynthesis linking oxidative metabolism to renal protection. *Nature,* 531**:** 528-532, 2016.
30. Chatterjee, S, Balram, A, Li, W: Convergence: Lactosylceramide-Centric Signaling Pathways Induce Inflammation, Oxidative Stress, and Other Phenotypic Outcomes. *Int J Mol Sci,* 22, 2021.
31. Shimazu, T, Hirschey, MD, Hua, L, Dittenhafer-Reed, KE, Schwer, B, Lombard, DB, Li, Y, Bunkenborg, J, Alt, FW, Denu, JM, Jacobson, MP, Verdin, E: SIRT3 deacetylates

mitochondrial 3-hydroxy-3-methylglutaryl CoA synthase 2 and regulates ketone body production. *Cell Metab*, 12**:** 654-661, 2010.

32. Hirschey, MD, Shimazu, T, Goetzman, E, Jing, E, Schwer, B, Lombard, DB, Grueter, CA, Harris, C, Biddinger, S, Ilkayeva, OR, Stevens, RD, Li, Y, Saha, AK, Ruderman, NB, Bain, JR, Newgard, CB, Farese, RV, Jr., Alt, FW, Kahn, CR, Verdin, E: SIRT3 regulates mitochondrial fatty-acid oxidation by reversible enzyme deacetylation. *Nature,* 464**:** 121-125, 2010.
33. Someya, S, Yu, W, Hallows, WC, Xu, J, Vann, JM, Leeuwenburgh, C, Tanokura, M, Denu, JM, Prolla, TA: Sirt3 mediates reduction of oxidative damage and prevention of age-related hearing loss under caloric restriction. *Cell*, 143**:** 802-812, 2010.
34. Tao, R, Vassilopoulos, A, Parisiadou, L, Yan, Y, Gius, D: Regulation of MnSOD enzymatic activity by Sirt3 connects the mitochondrial acetylome signaling networks to aging and carcinogenesis. *Antioxid Redox Signal*, 20**:** 1646-1654, 2014.
35. Fernandez-Marcos, PJ, Auwerx, J: Regulation of PGC-1alpha, a nodal regulator of mitochondrial biogenesis. *Am J Clin Nutr*, 93**:** 884S-890, 2011.
36. Schneider, WM, Chevillotte, MD, Rice, CM: Interferon-stimulated genes: a complex web of host defenses. *Annu Rev Immunol*, 32**:** 513-545, 2014.
37. Decout, A, Katz, JD, Venkatraman, S, Ablasser, A: The cGAS-STING pathway as a therapeutic target in inflammatory diseases. *Nat Rev Immunol*, 2021.
38. Ablasser, A, Hur, S: Regulation of cGAS- and RLR-mediated immunity to nucleic acids. *Nat Immunol*, 21**:** 17-29, 2020.
39. Ablasser, A, Chen, ZJ: cGAS in action: Expanding roles in immunity and inflammation. *Science*, 363, 2019.
40. Chung, KW, Dhillon, P, Huang, S, Sheng, X, Shrestha, R, Qiu, C, Kaufman, BA, Park, J, Pei, L, Baur, J, Palmer, M, Susztak, K: Mitochondrial Damage and Activation of the STING Pathway Lead to Renal Inflammation and Fibrosis. *Cell Metab*, 30**:** 784-799 e785, 2019.
41. Haag, SM, Gulen, MF, Reymond, L, Gibelin, A, Abrami, L, Decout, A, Heymann, M, van der Goot, FG, Turcatti, G, Behrendt, R, Ablasser, A: Targeting STING with covalent small-molecule inhibitors. *Nature*, 559**:** 269-273, 2018.
42. Maekawa, H, Inoue, T, Ouchi, H, Jao, TM, Inoue, R, Nishi, H, Fujii, R, Ishidate, F, Tanaka, T, Tanaka, Y, Hirokawa, N, Nangaku, M, Inagi, R: Mitochondrial Damage Causes Inflammation via cGAS-STING Signaling in Acute Kidney Injury. *Cell Rep*, 29**:** 1261-1273 e1266, 2019.
43. Yasuda, I, Hasegawa, K, Sakamaki, Y, Muraoka, H, Kawaguchi, T, Kusahana, E, Ono, T, Kanda, T, Tokuyama, H, Wakino, S, Itoh, H: Pre-emptive Short-term Nicotinamide Mononucleotide Treatment in a Mouse Model of Diabetic Nephropathy. *J Am Soc Nephrol*, 32**:** 1355-1370, 2021.
44. Srivastava, SP, Li, J, Takagaki, Y, Kitada, M, Goodwin, JE, Kanasaki, K, Koya, D: Endothelial SIRT3 regulates myofibroblast metabolic shifts in diabetic kidneys. *iScience*, 24**:** 102390, 2021.
45. Srivastava, SP, Li, J, Kitada, M, Fujita, H, Yamada, Y, Goodwin, JE, Kanasaki, K, Koya, D: SIRT3 deficiency leads to induction of abnormal glycolysis in diabetic kidney with fibrosis. *Cell Death Dis*, 9**:** 997, 2018.

46. Morigi, M, Perico, L, Rota, C, Longaretti, L, Conti, S, Rottoli, D, Novelli, R, Remuzzi, G, Benigni, A: Sirtuin 3-dependent mitochondrial dynamic improvements protect against acute kidney injury. *J Clin Invest,* 125**:** 715-726, 2015.
47. Miguel, V, Tituana, J, Herrero, JI, Herrero, L, Serra, D, Cuevas, P, Barbas, C, Puyol, DR, Marquez-Exposito, L, Ruiz-Ortega, M, Castillo, C, Sheng, X, Susztak, K, Ruiz-Canela, M, Salas-Salvado, J, Gonzalez, MAM, Ortega, S, Ramos, R, Lamas, S: Renal tubule Cpt1a overexpression protects from kidney fibrosis by restoring mitochondrial homeostasis. *J Clin Invest,* 131, 2021.
48. Xu, W, Boyd, RM, Tree, MO, Samkari, F, Zhao, L: Mitochondrial transcription factor A promotes DNA strand cleavage at abasic sites. *Proc Natl Acad Sci U S A,* 116**:** 17792-17799, 2019.
49. Wu, J, Raman, A, Coffey, NJ, Sheng, X, Wahba, J, Seasock, MJ, Ma, Z, Beckerman, P, Laczko, D, Palmer, MB, Kopp, JB, Kuo, JJ, Pullen, SS, Boustany-Kari, CM, Linkermann, A, Susztak, K: The key role of NLRP3 and STING in APOL1-associated podocytopathy. *J Clin Invest,* 131, 2021.
50. Myakala, K, Jones, BA, Wang, XX, Levi, M: Sacubitril/valsartan treatment has differential effects in modulating diabetic kidney disease in db/db mice and KKAy mice compared with valsartan treatment. *Am J Physiol Renal Physiol,* 320**:** F1133-F1151, 2021.
51. Furda, A, Santos, JH, Meyer, JN, Van Houten, B: Quantitative PCR-based measurement of nuclear and mitochondrial DNA damage and repair in mammalian cells. *Methods Mol Biol,* 1105**:** 419-437, 2014.
52. Ginley, B, Lutnick, B, Jen, KY, Fogo, AB, Jain, S, Rosenberg, A, Walavalkar, V, Wilding, G, Tomaszewski, JE, Yacoub, R, Rossi, GM, Sarder, P: Computational Segmentation and Classification of Diabetic Glomerulosclerosis. *J Am Soc Nephrol,* 30**:** 1953-1967, 2019.
53. Wang, XX, Jiang, T, Shen, Y, Adorini, L, Pruzanski, M, Gonzalez, FJ, Scherzer, P, Lewis, L, Miyazaki-Anzai, S, Levi, M: The farnesoid X receptor modulates renal lipid metabolism and diet-induced renal inflammation, fibrosis, and proteinuria. *Am J Physiol Renal Physiol,* 297**:** F1587-1596, 2009.
54. Bolger, AM, Lohse, M, Usadel, B: Trimmomatic: a flexible trimmer for Illumina sequence data. *Bioinformatics,* 30**:** 2114-2120, 2014.
55. Dobin, A, Davis, CA, Schlesinger, F, Drenkow, J, Zaleski, C, Jha, S, Batut, P, Chaisson, M, Gingeras, TR: STAR: ultrafast universal RNA-seq aligner. *Bioinformatics,* 29**:** 15-21, 2013.
56. Li, B, Dewey, CN: RSEM: accurate transcript quantification from RNA-Seq data with or without a reference genome. *BMC Bioinformatics,* 12**:** 323, 2011.
57. Love, MI, Huber, W, Anders, S: Moderated estimation of fold change and dispersion for RNA-seq data with DESeq2. *Genome Biol,* 15**:** 550, 2014.
58. Huang da, W, Sherman, BT, Lempicki, RA: Systematic and integrative analysis of large gene lists using DAVID bioinformatics resources. *Nat Protoc,* 4**:** 44-57, 2009.
59. Huang, DW, Sherman, BT, Tan, Q, Collins, JR, Alvord, WG, Roayaei, J, Stephens, R, Baseler, MW, Lane, HC, Lempicki, RA: The DAVID Gene Functional Classification Tool: a novel biological module-centric algorithm to functionally analyze large gene lists. *Genome Biol,* 8**:** R183, 2007.
60. Rath, S, Sharma, R, Gupta, R, Ast, T, Chan, C, Durham, TJ, Goodman, RP, Grabarek, Z, Haas, ME, Hung, WHW, Joshi, PR, Jourdain, AA, Kim, SH, Kotrys, AV, Lam, SS, McCoy, JG, Meisel, JD, Miranda, M, Panda, A, Patgiri, A, Rogers, R, Sadre, S, Shah, H,

Skinner, OS, To, TL, Walker, MA, Wang, H, Ward, PS, Wengrod, J, Yuan, CC, Calvo, SE, Mootha, VK: MitoCarta3.0: an updated mitochondrial proteome now with sub-organelle localization and pathway annotations. *Nucleic Acids Res,* 49**:** D1541-D1547, 2021.

61. Tahir, R, Renuse, S, Udainiya, S, Madugundu, AK, Cutler, JA, Nirujogi, RS, Na, CH, Xu, Y, Wu, X, Pandey, A: Mutation-Specific and Common Phosphotyrosine Signatures of KRAS G12D and G13D Alleles. *J Proteome Res,* 20**:** 670-683, 2021.
62. Tyanova, S, Cox, J: Perseus: A Bioinformatics Platform for Integrative Analysis of Proteomics Data in Cancer Research. *Methods Mol Biol,* 1711**:** 133-148, 2018.

Figure 1

A

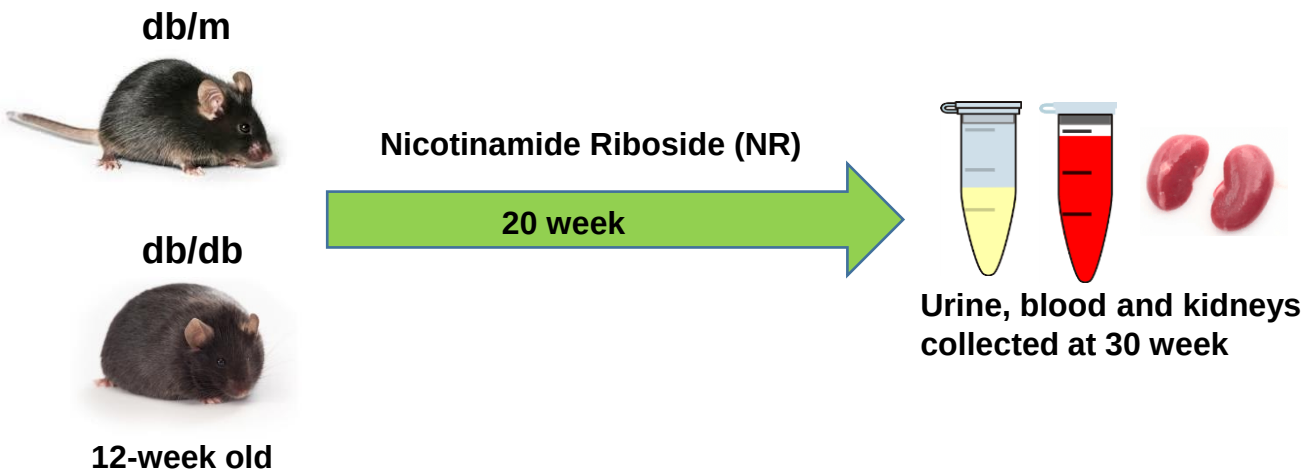

Figure 1

B

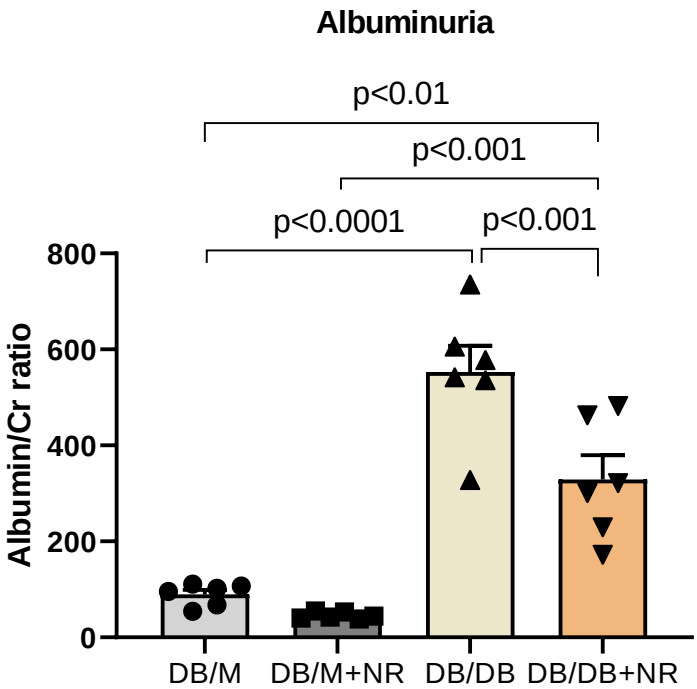

C

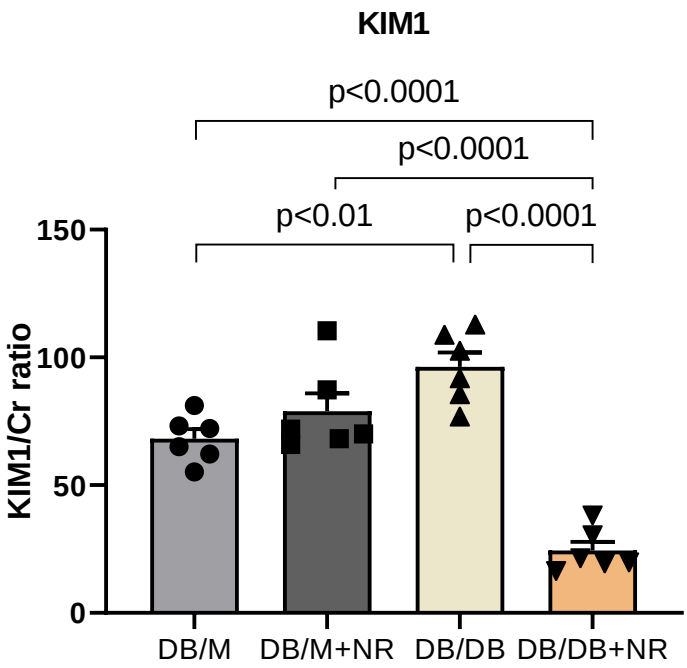

Figure 1

D

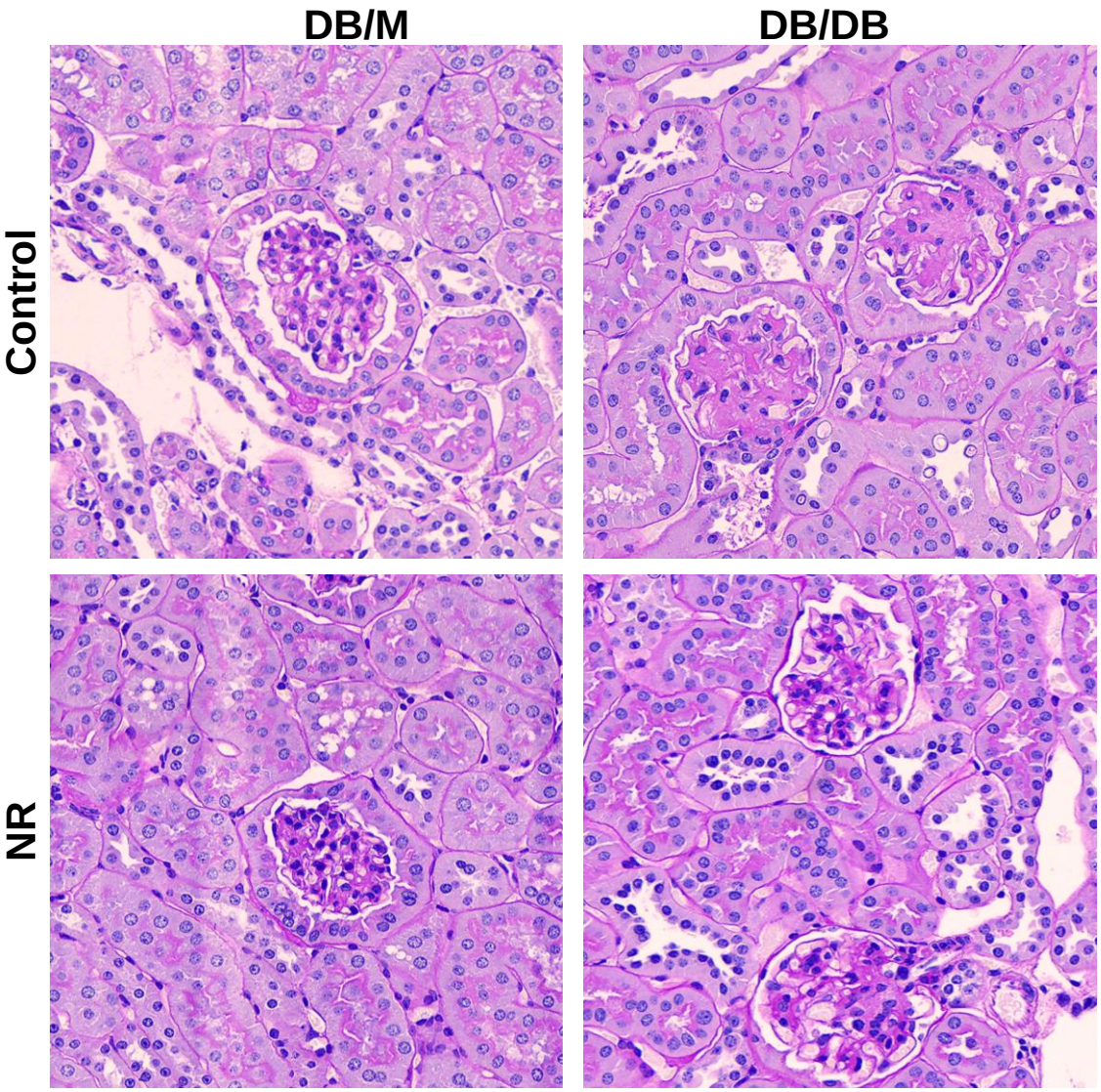

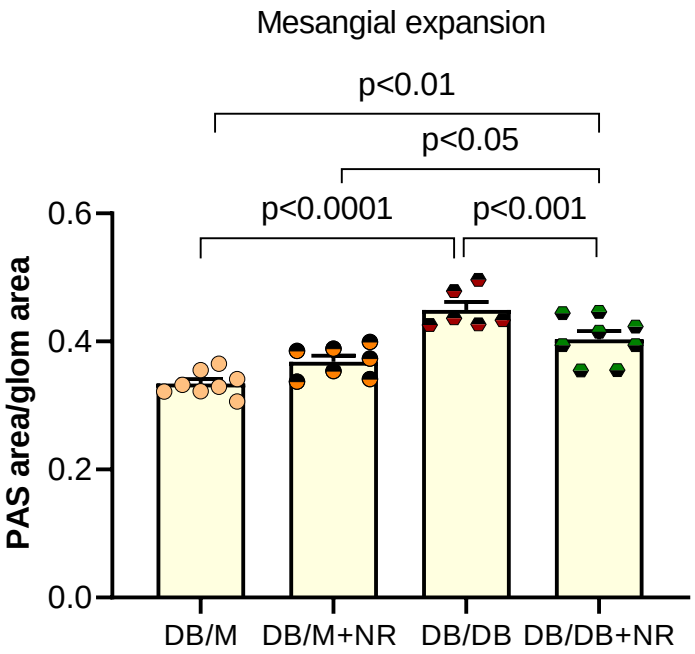

Figure 1

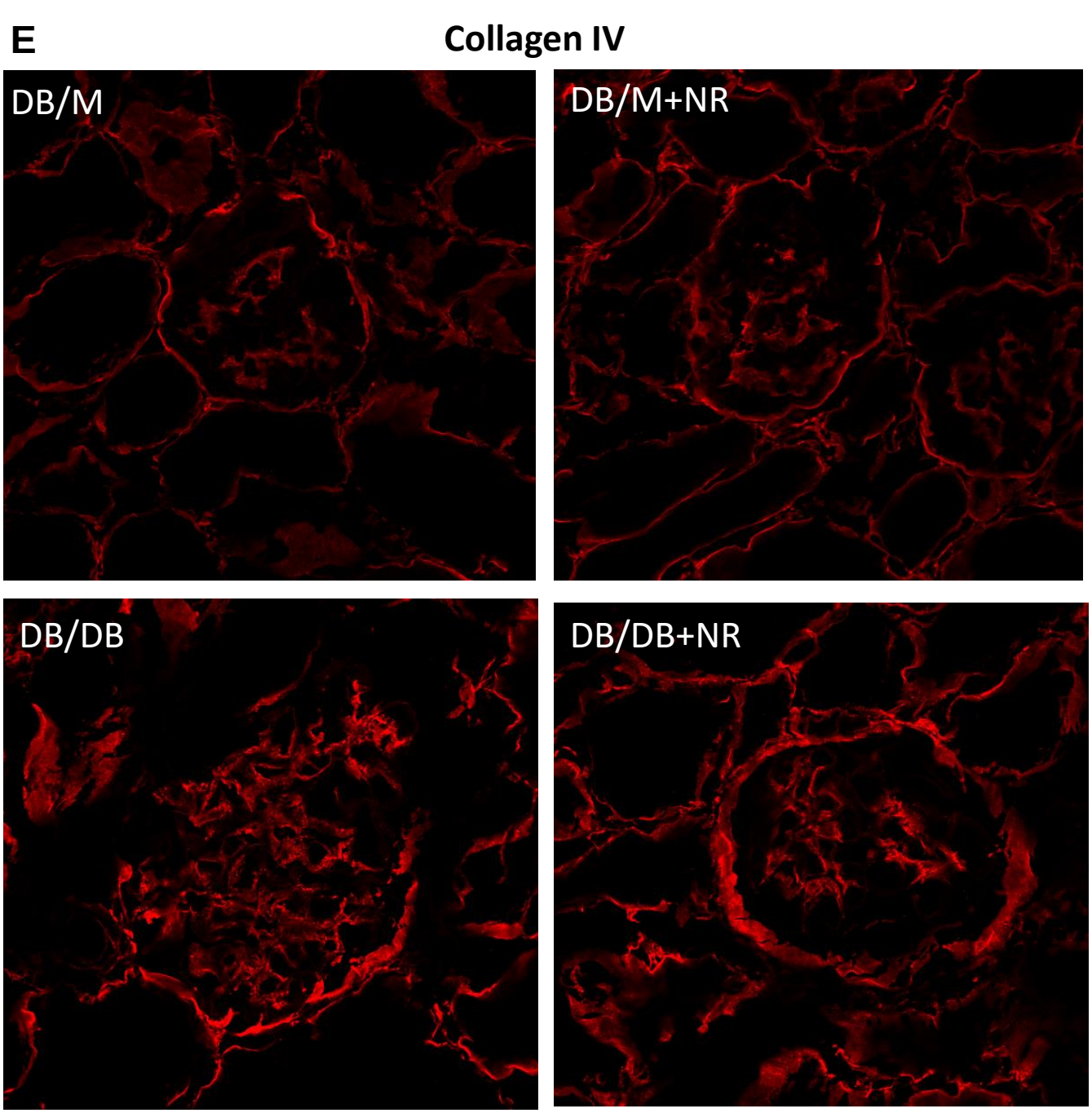

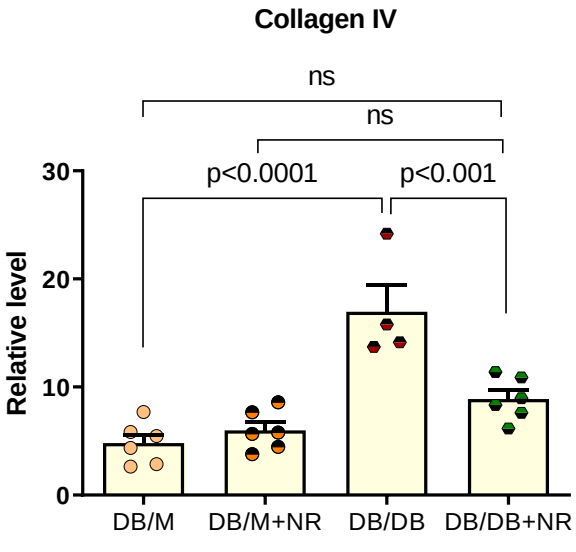

Figure 1

F

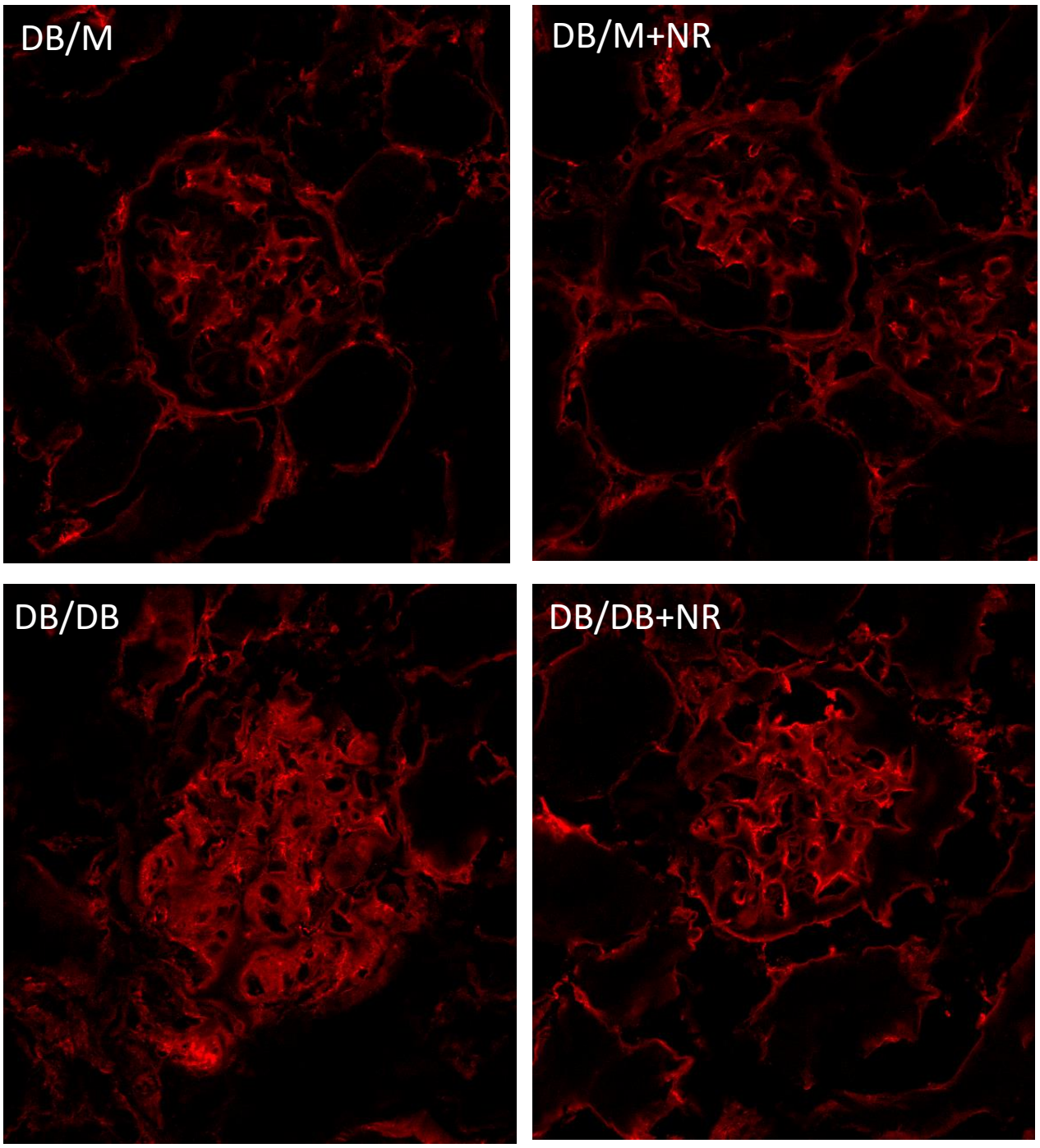

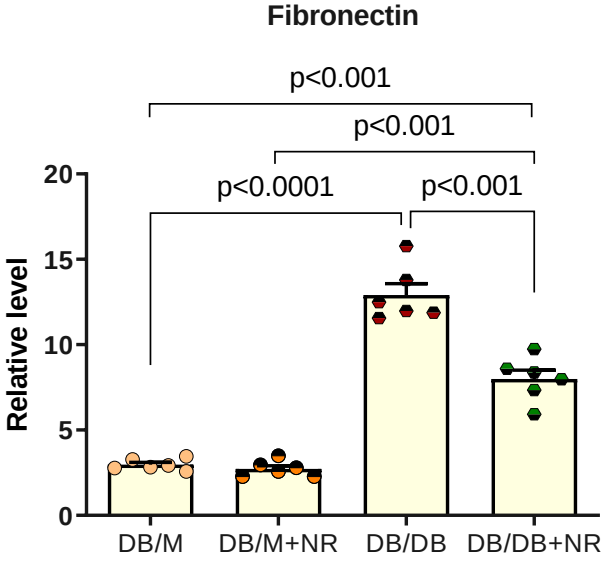

Figure 1

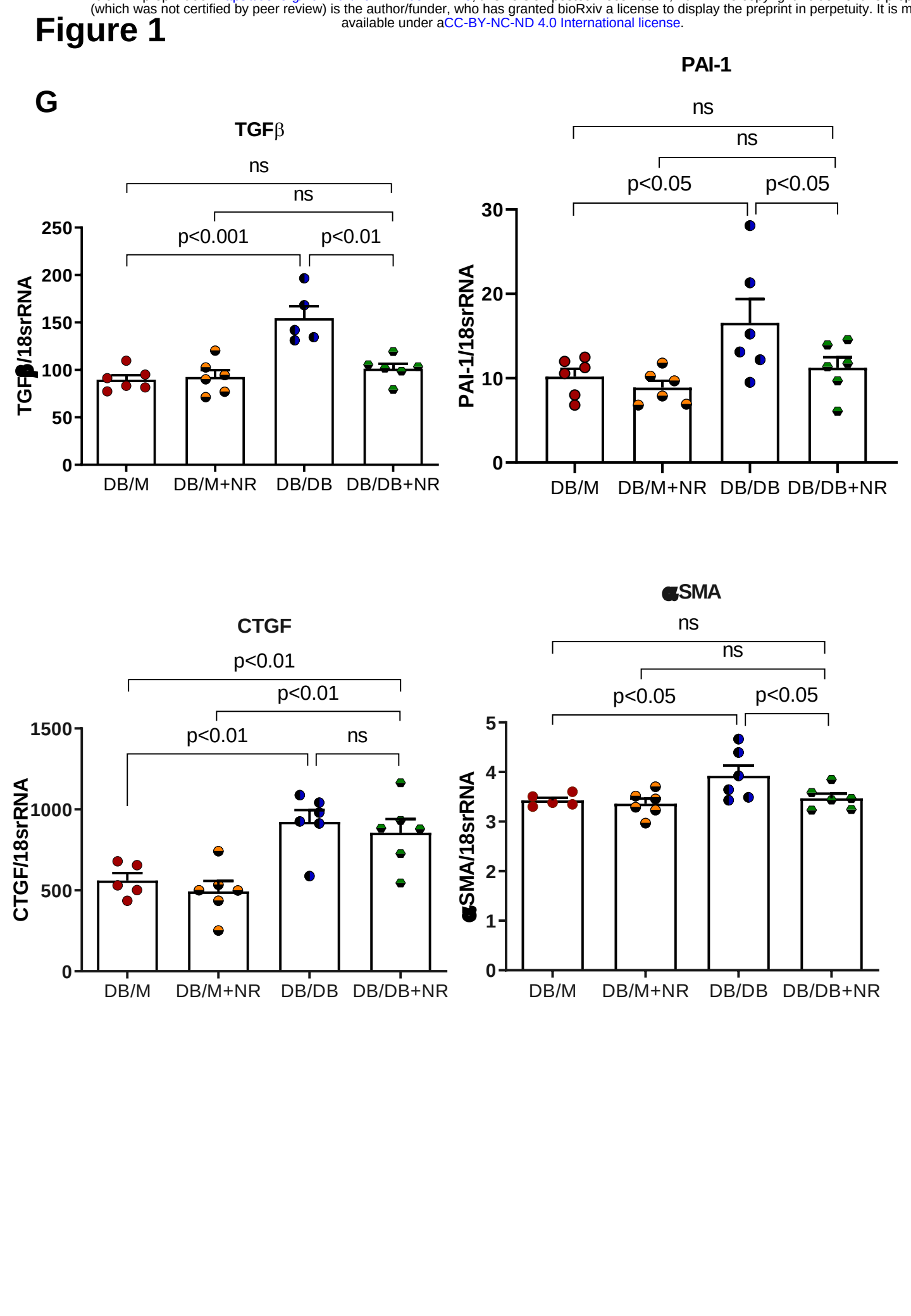

Figure 1

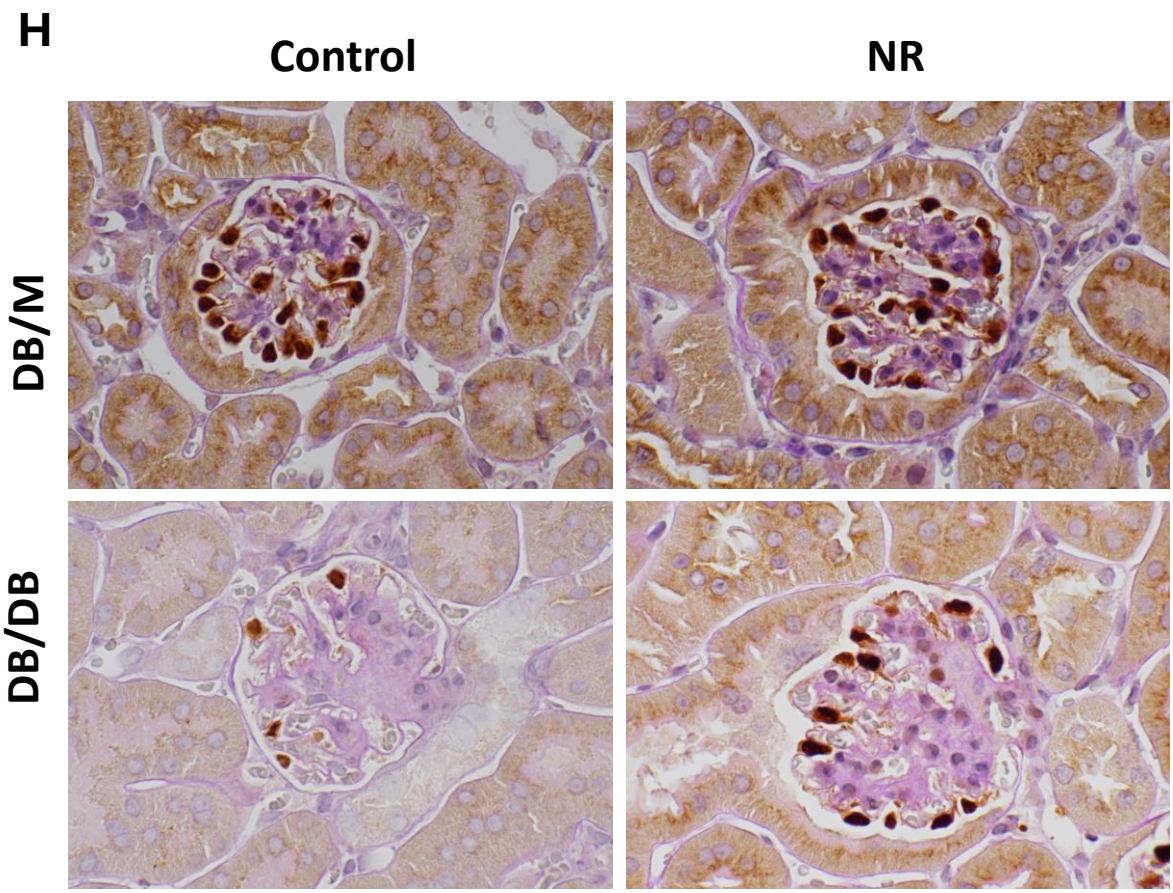

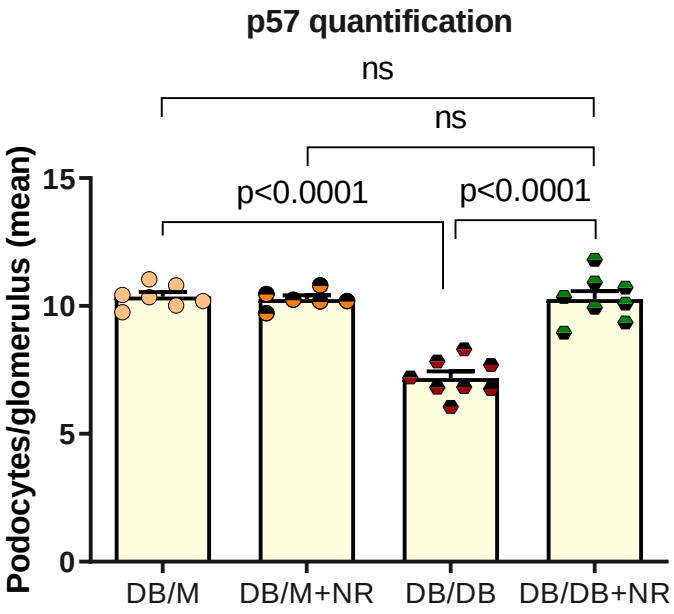

Figure 2

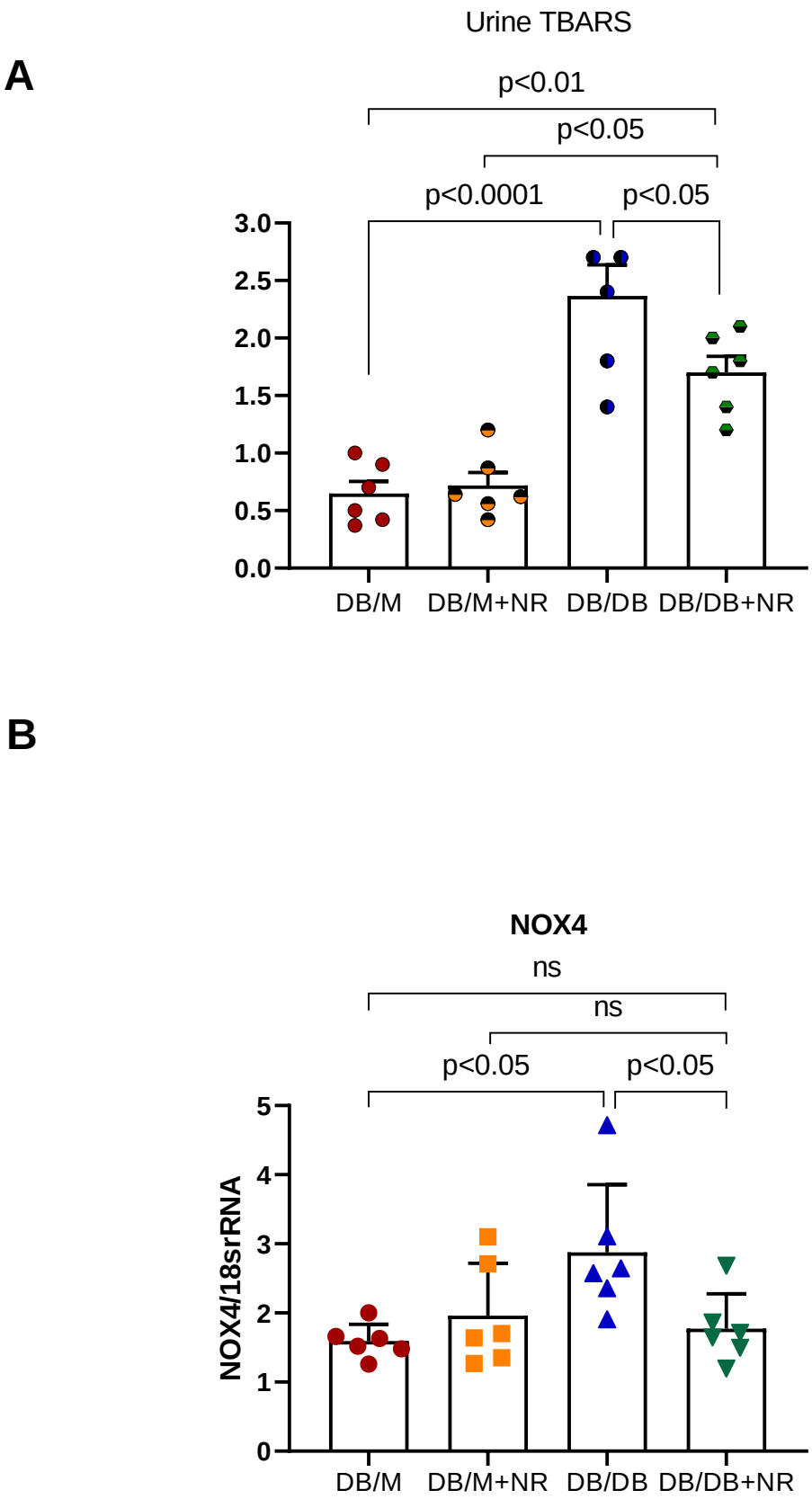

Figure 2

C

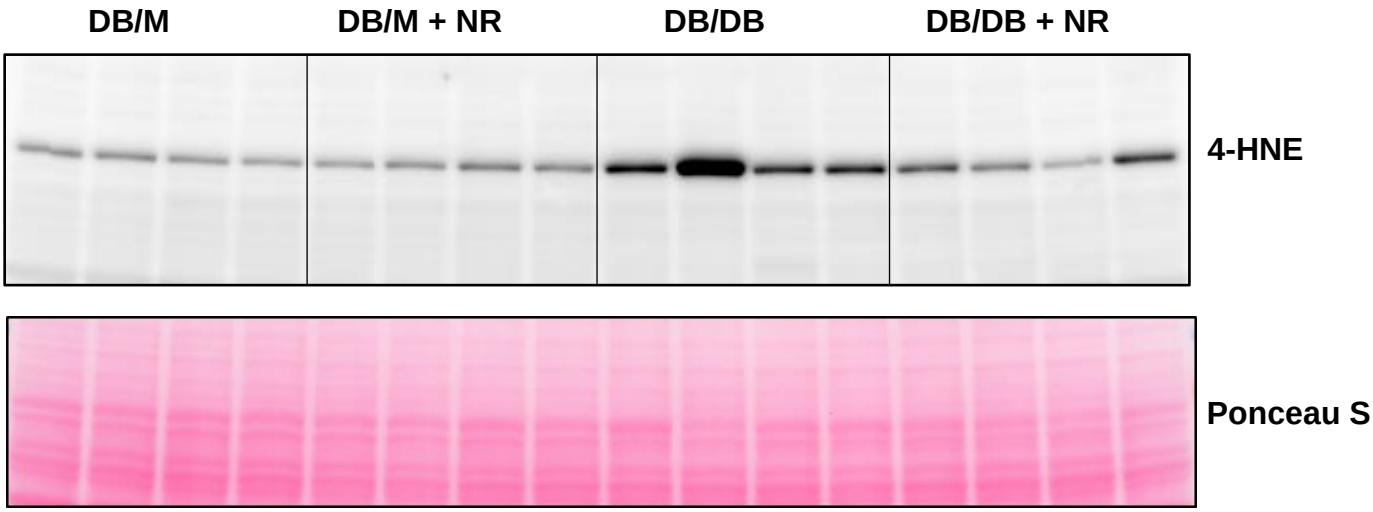

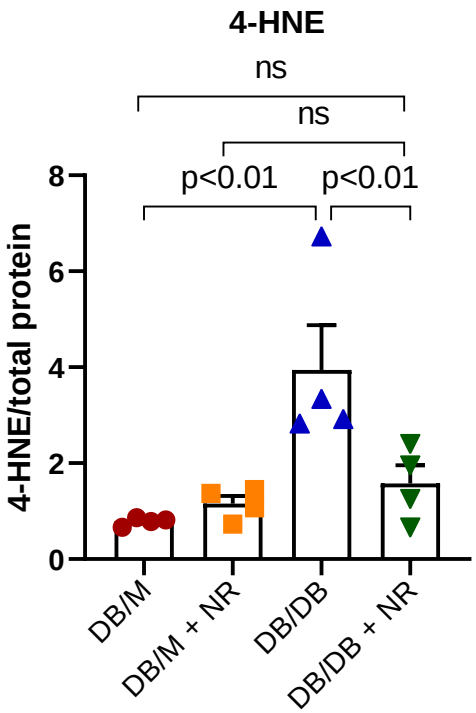

Figure 2

D

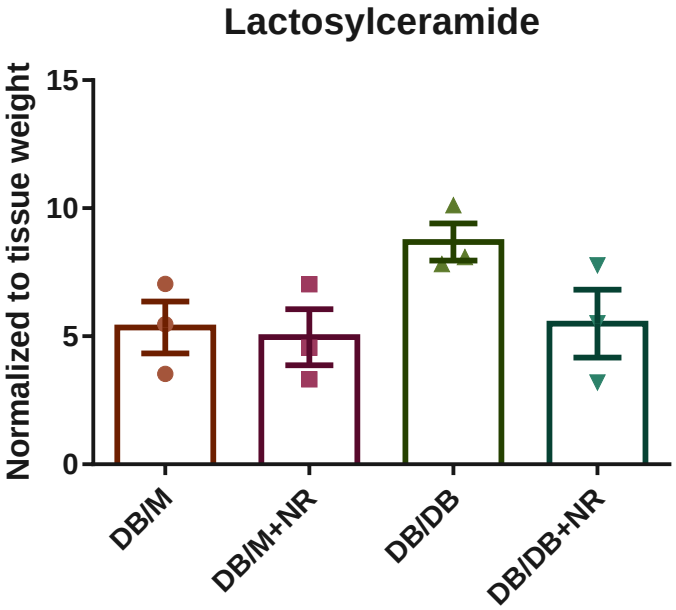

Figure 3

A

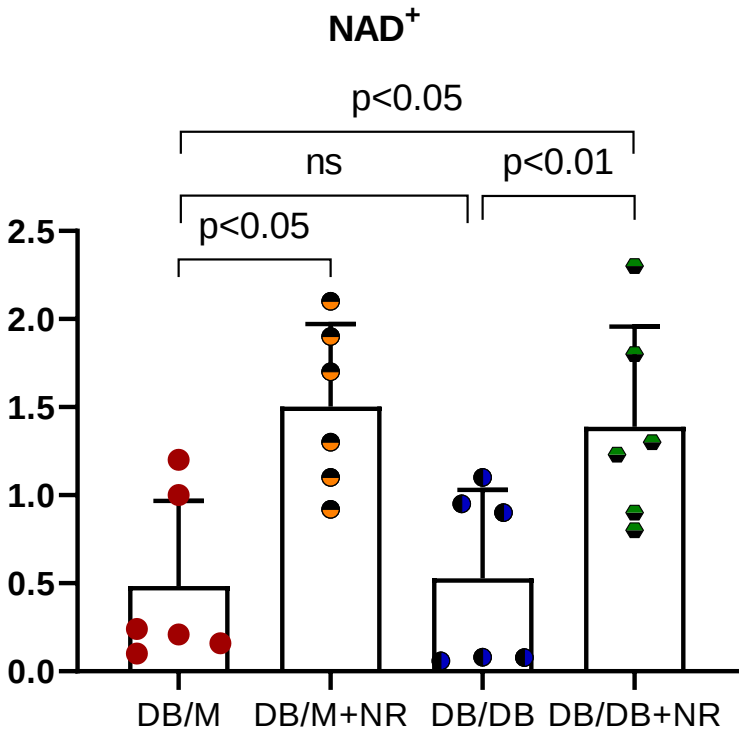

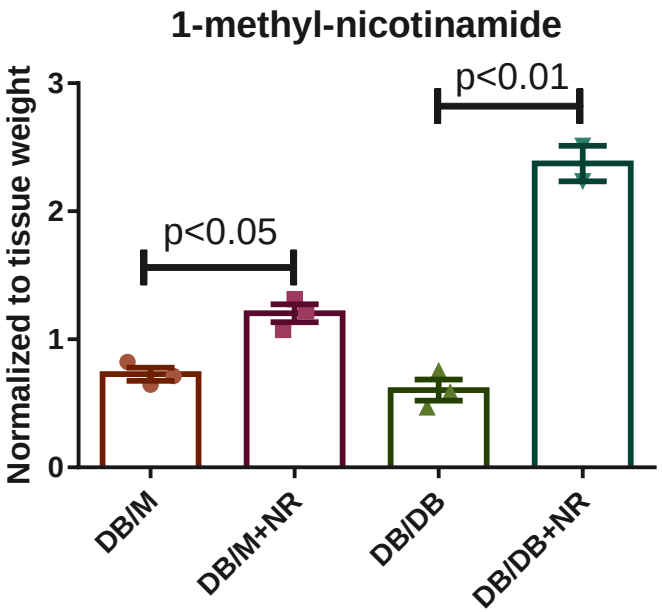

Figure 3

B

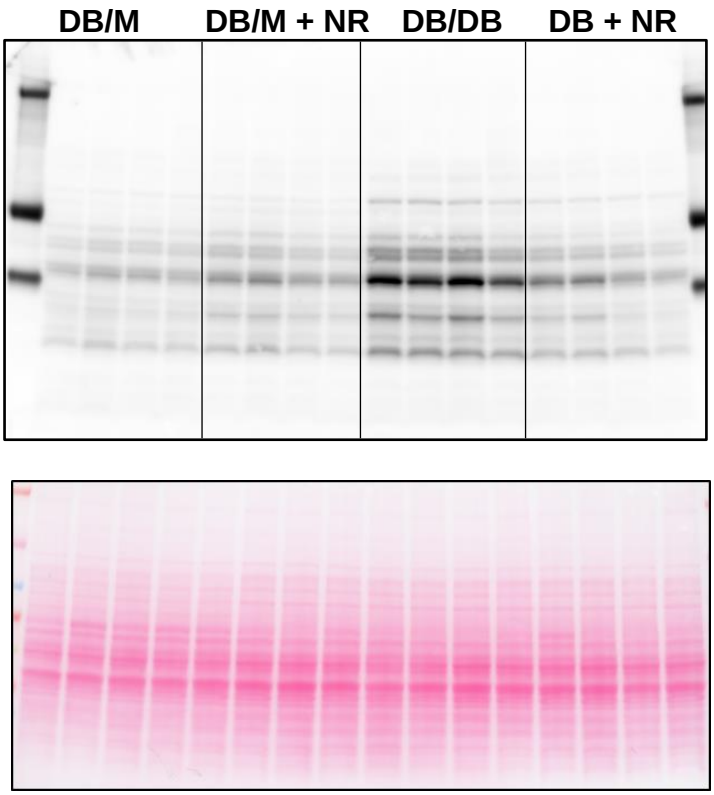

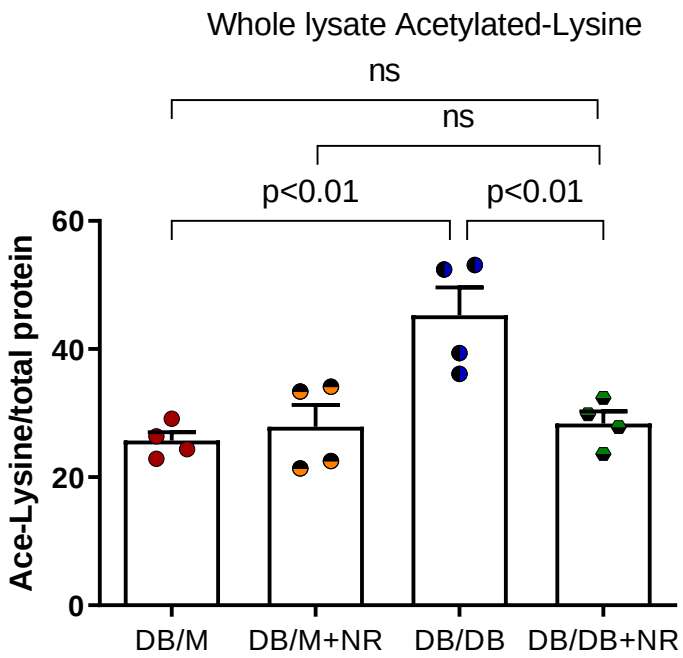

Figure 3

C

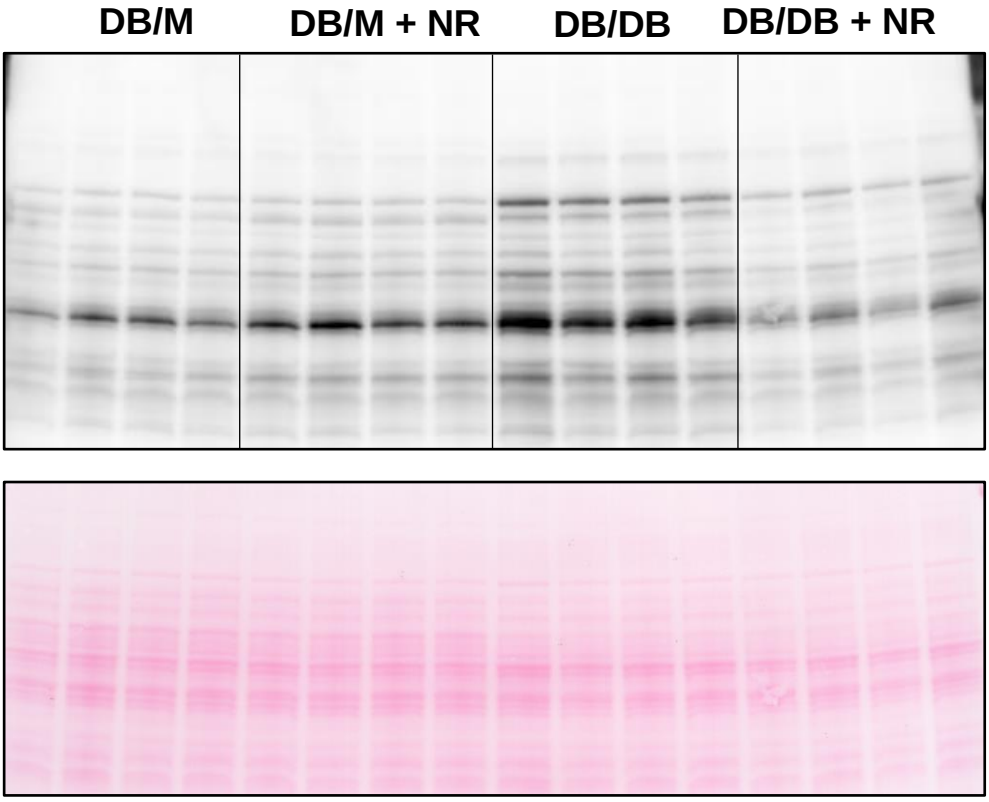

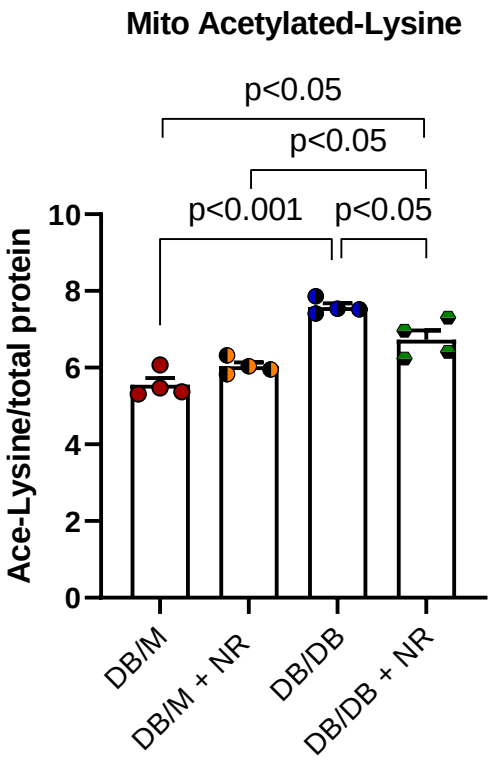

Figure 3

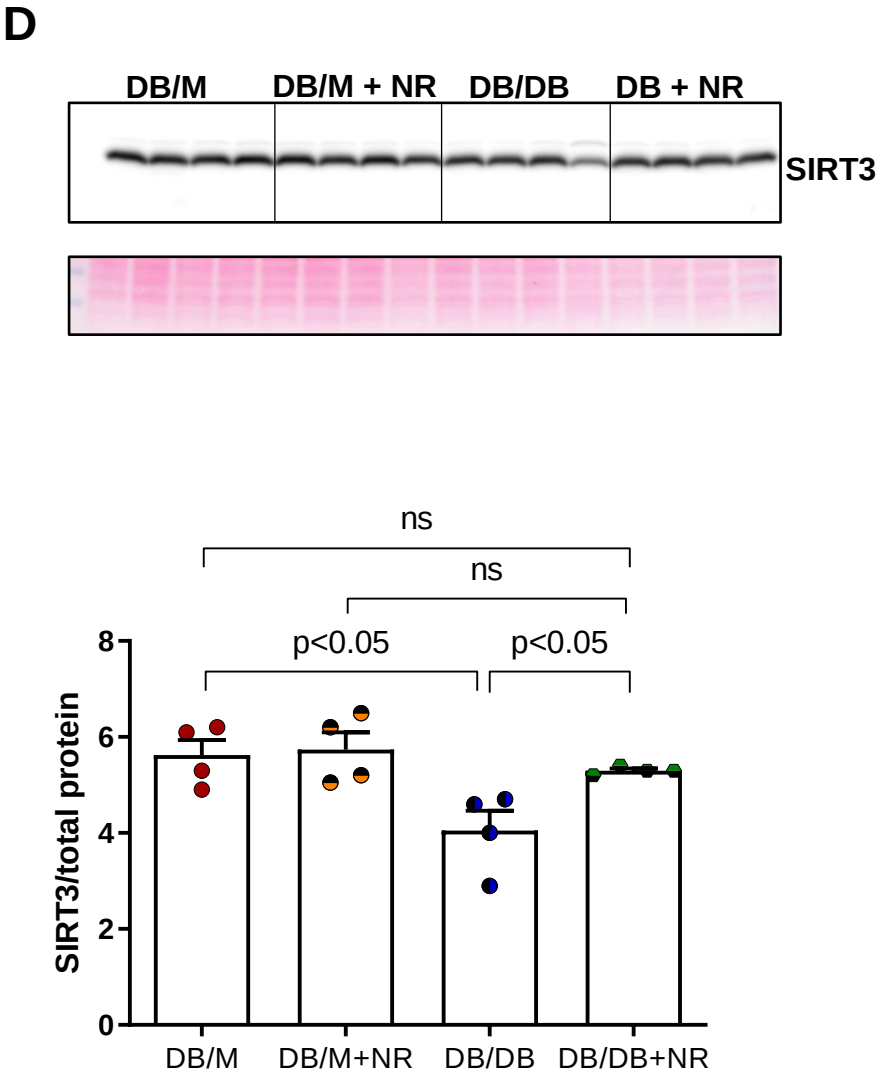

Figure 3

E

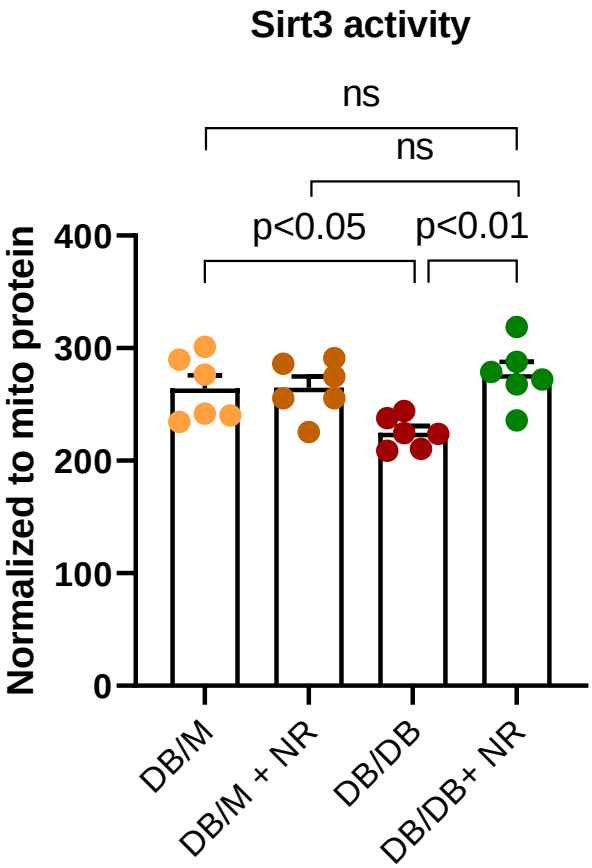

Figure 3

F

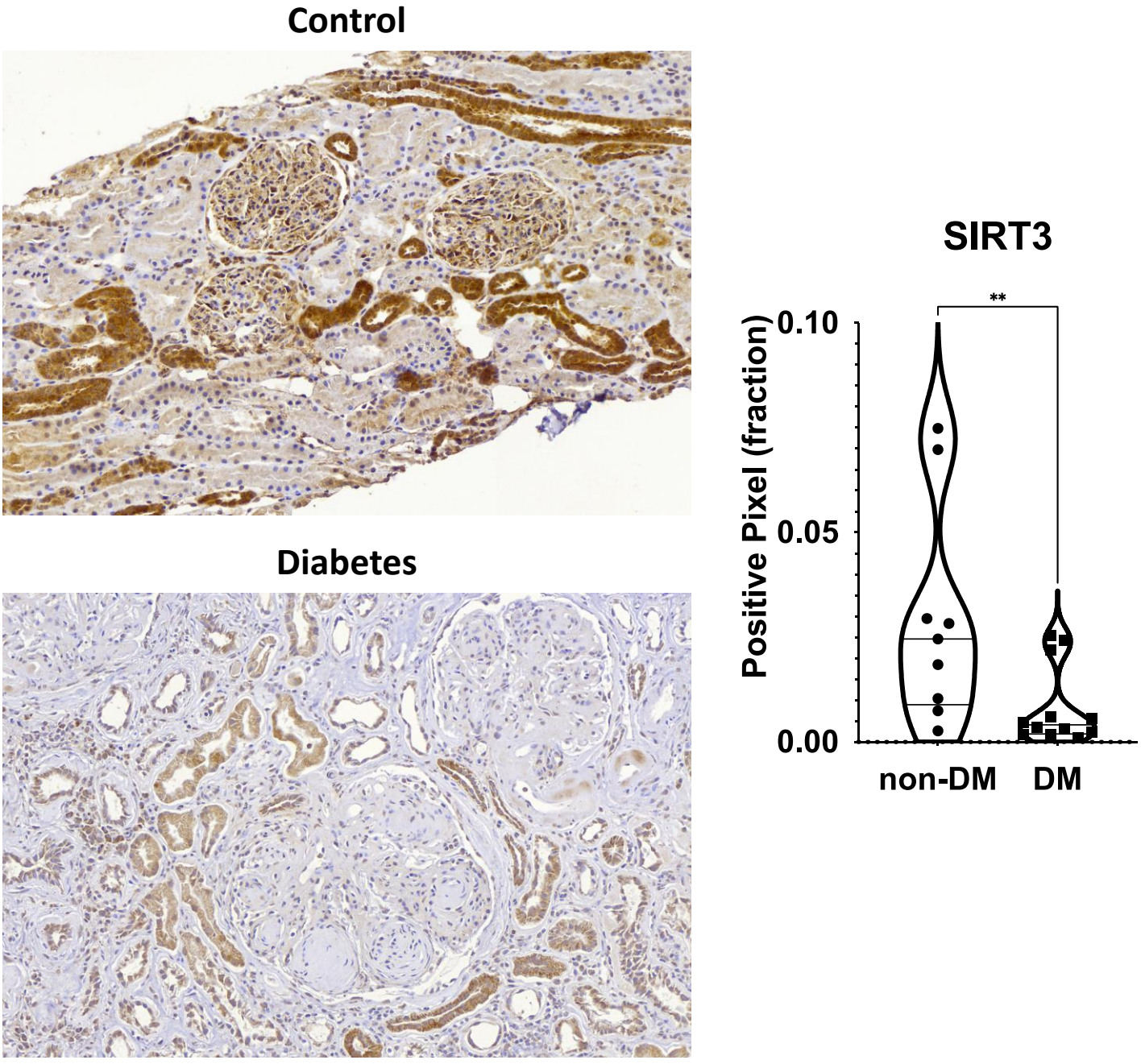

Figure 3

G

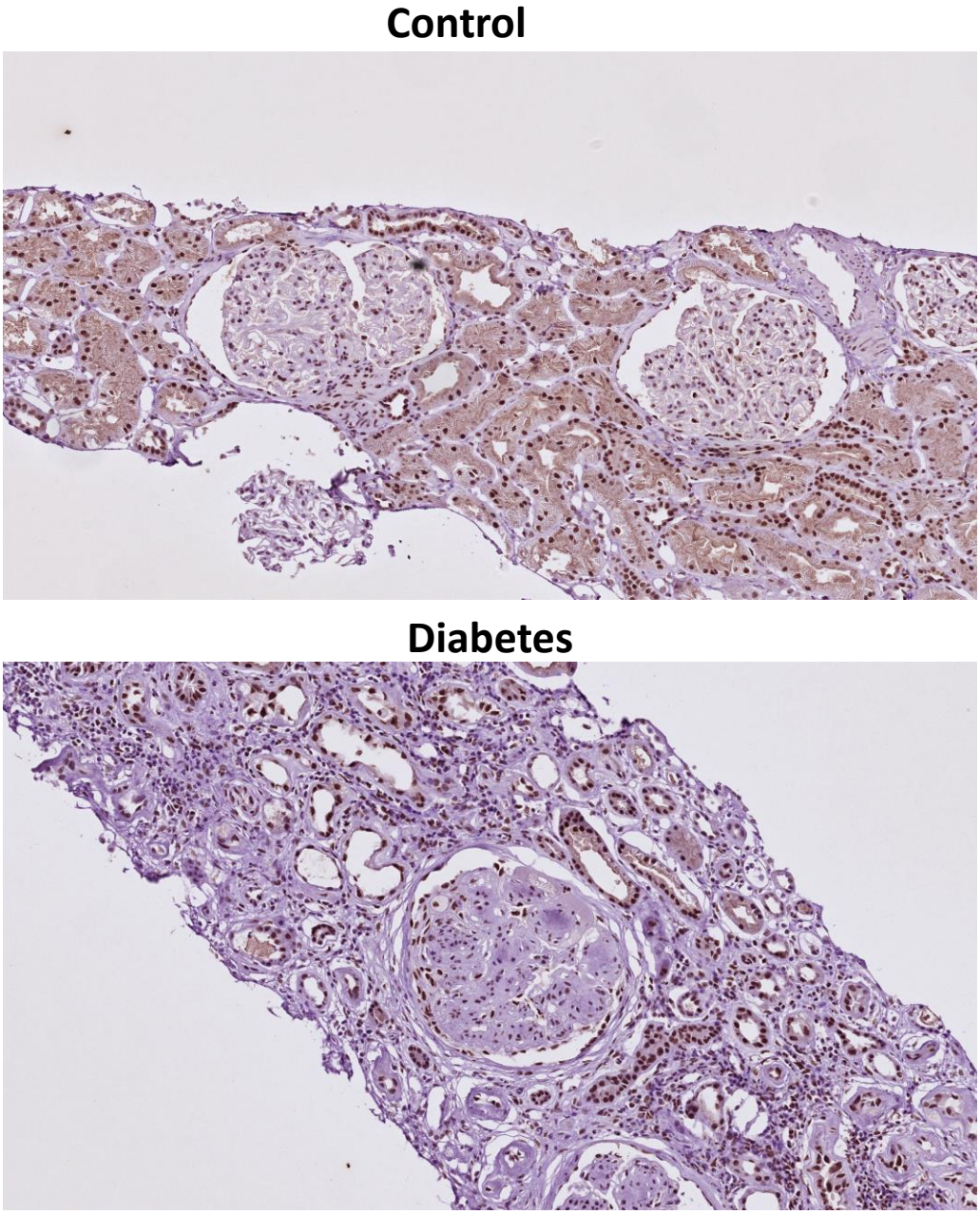

Figure 3

H

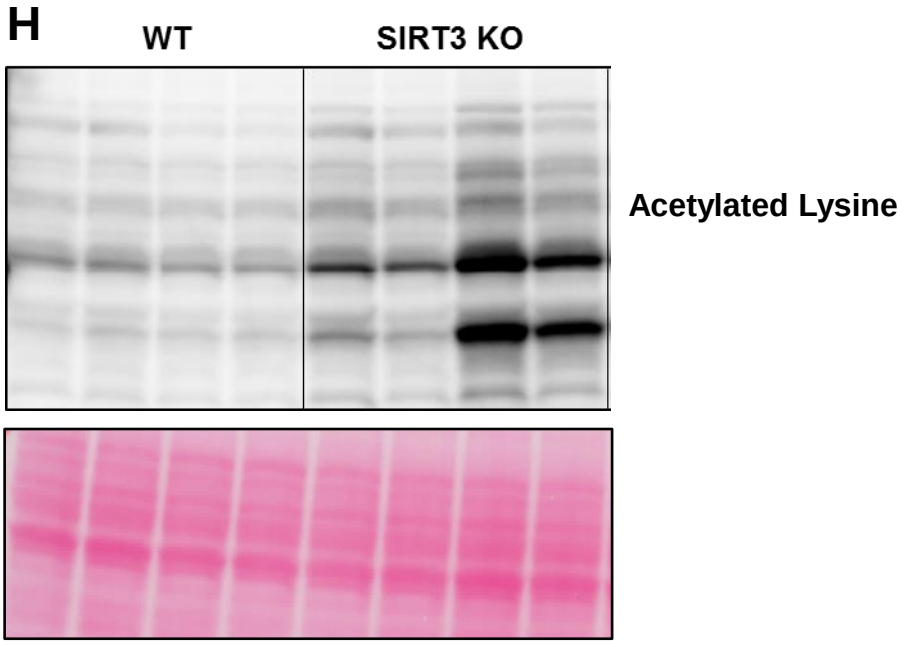

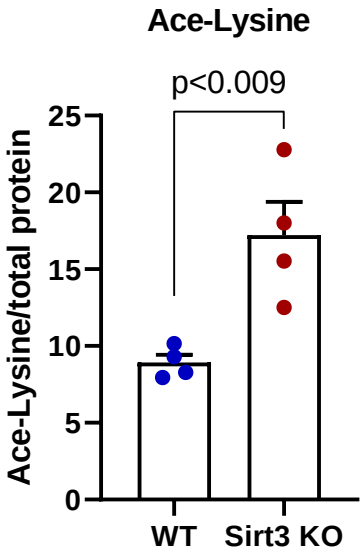

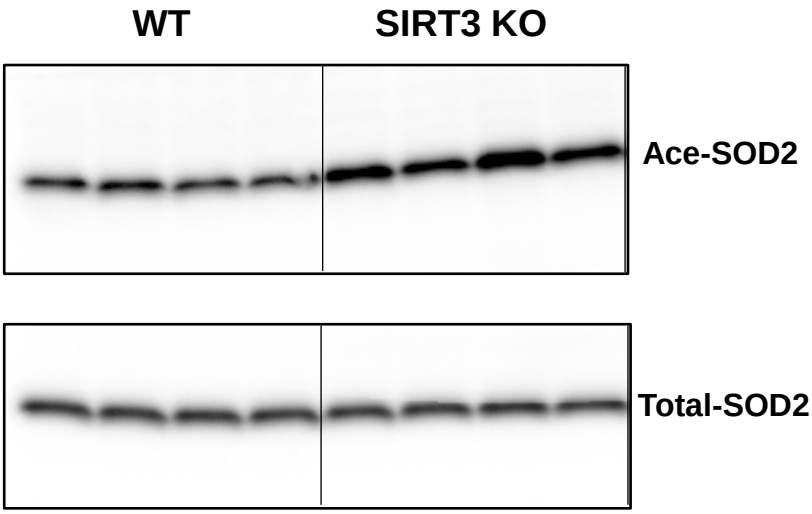

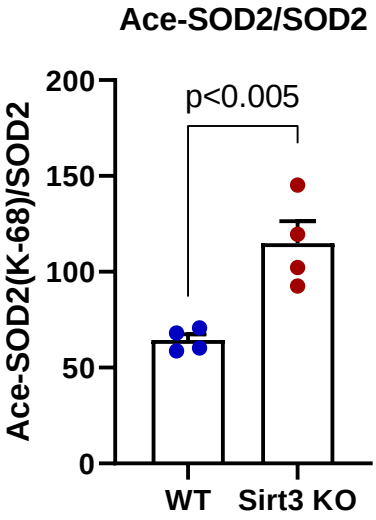

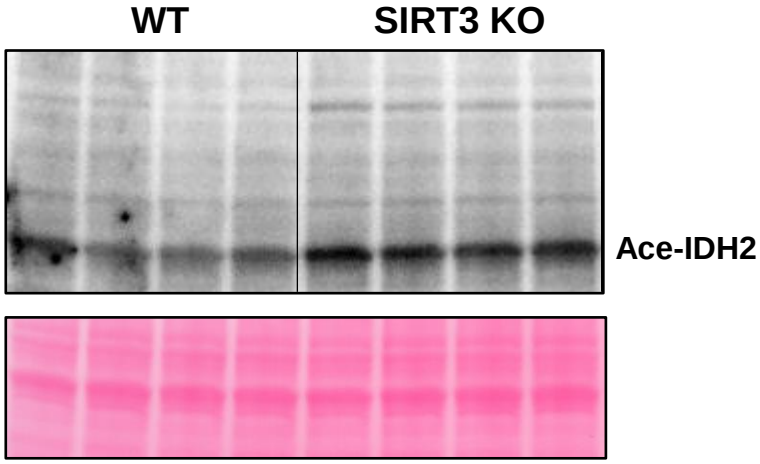

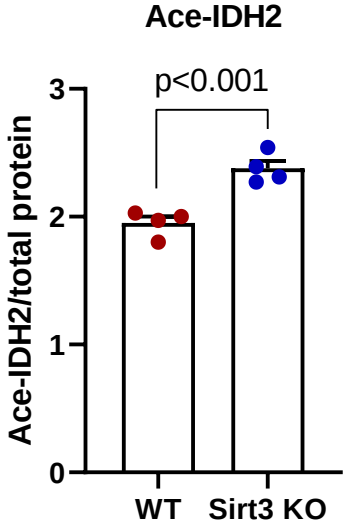

Figure 3

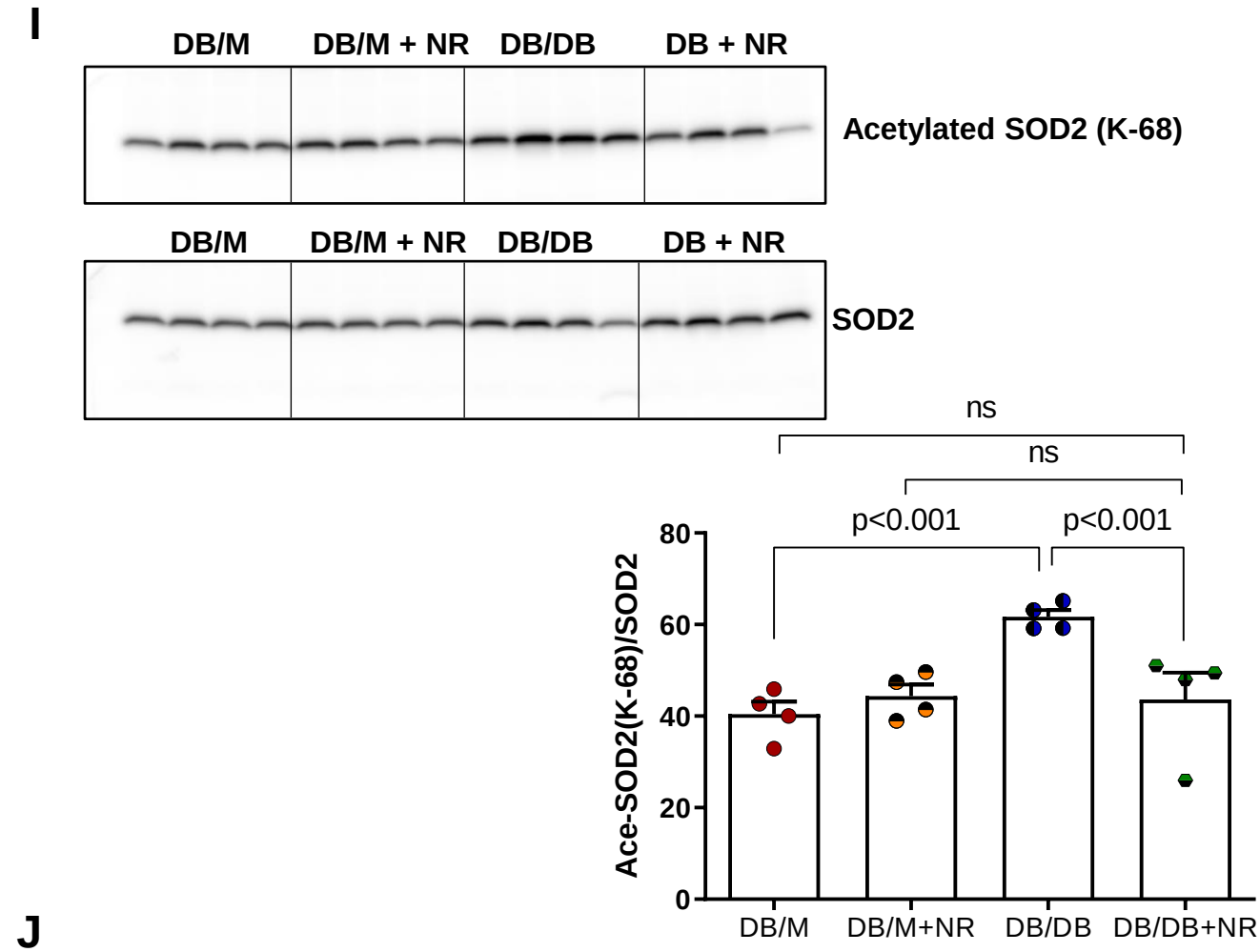

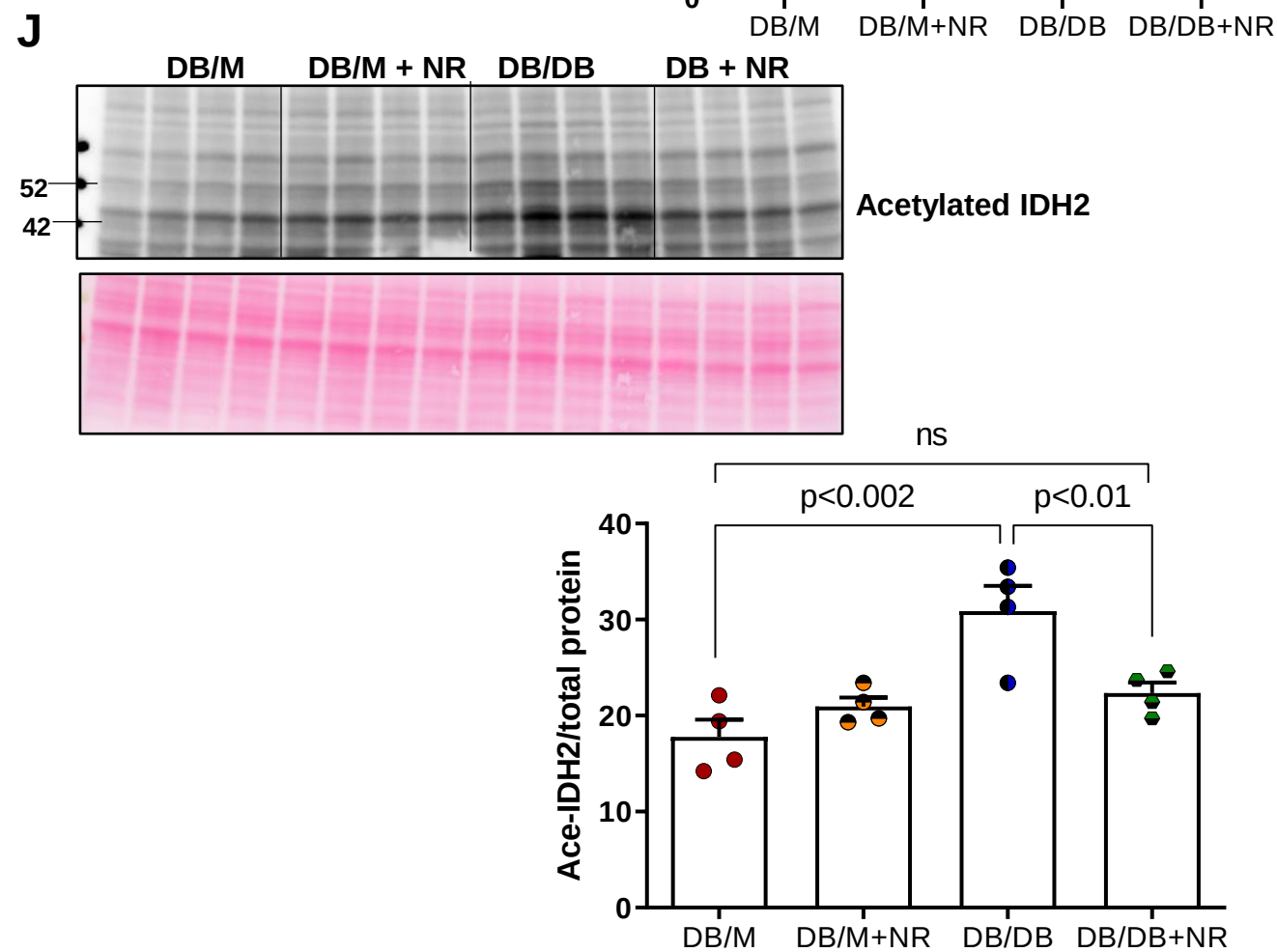

Figure 4

A

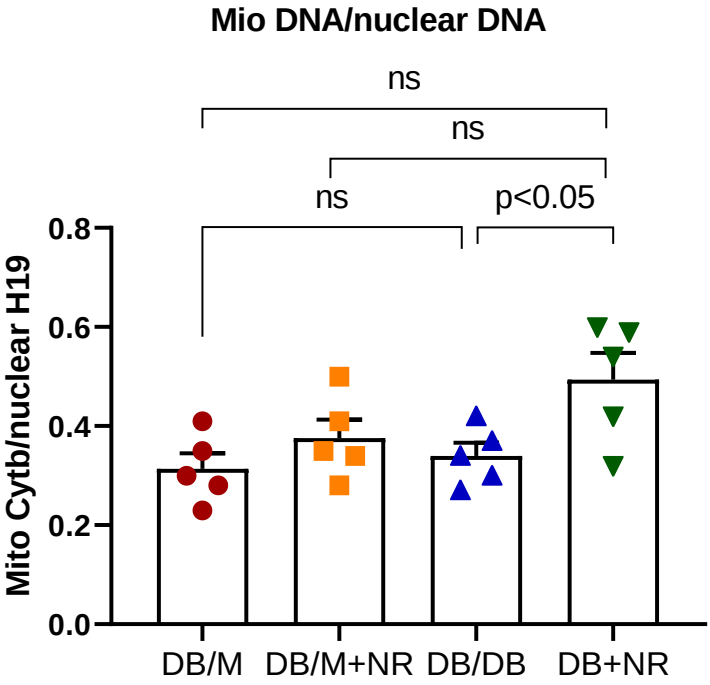

Figure 4

B

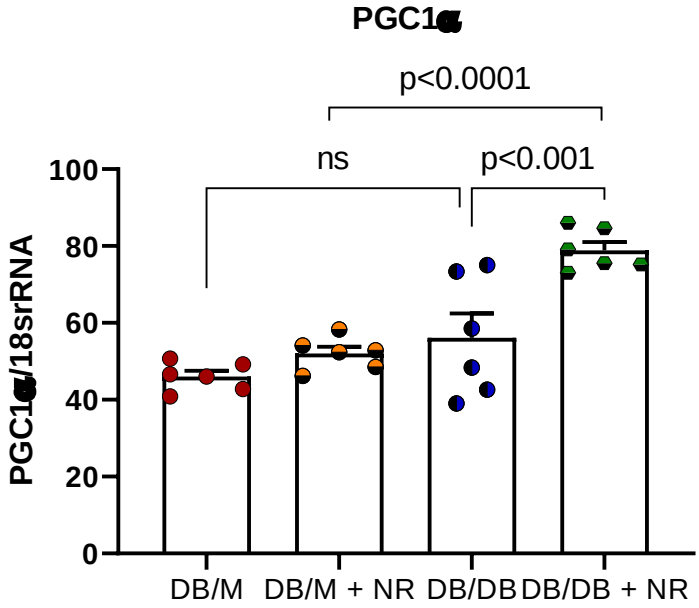

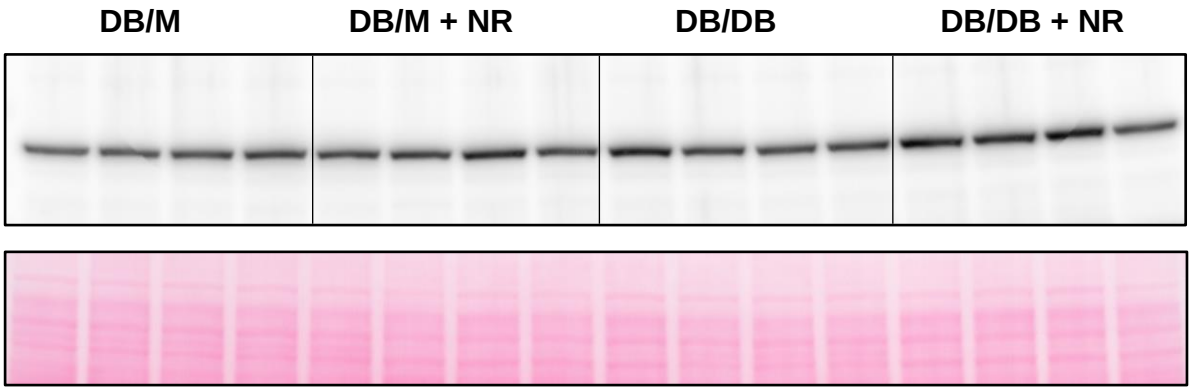

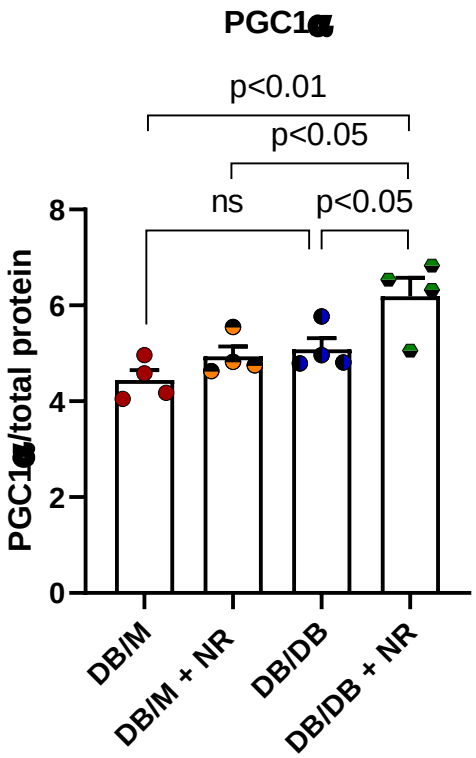

Figure 4

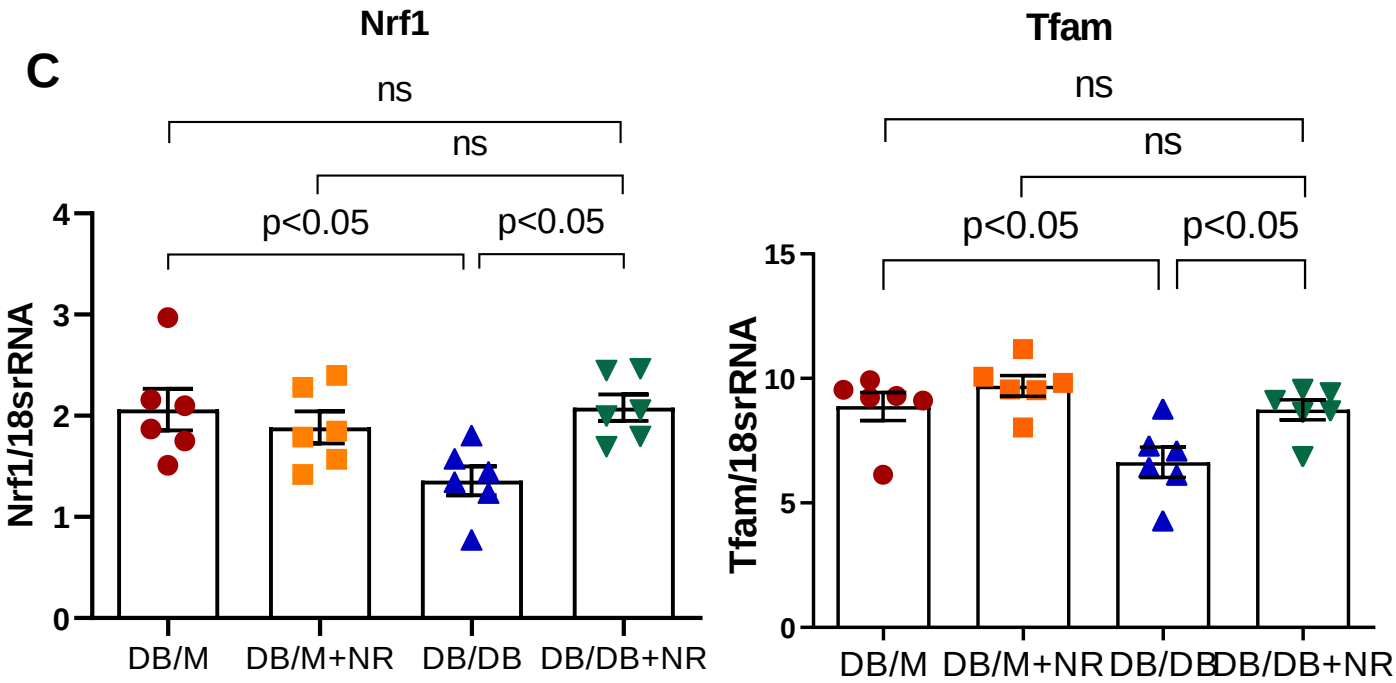

Figure 4

D

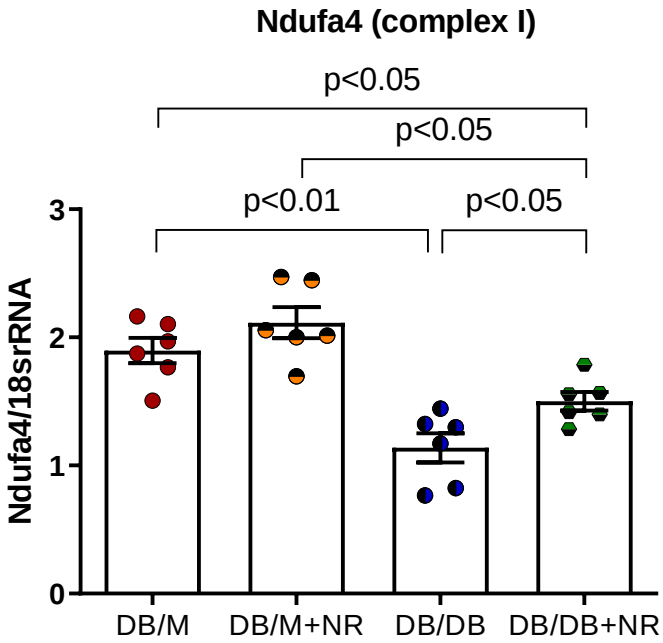

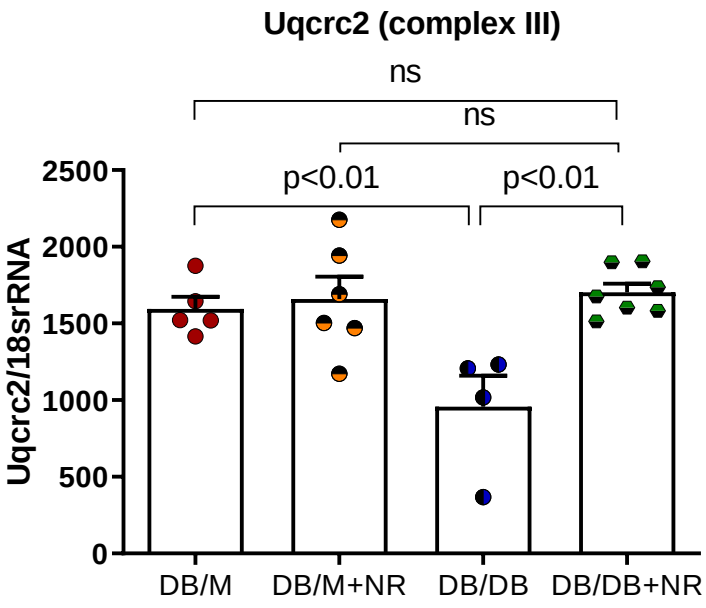

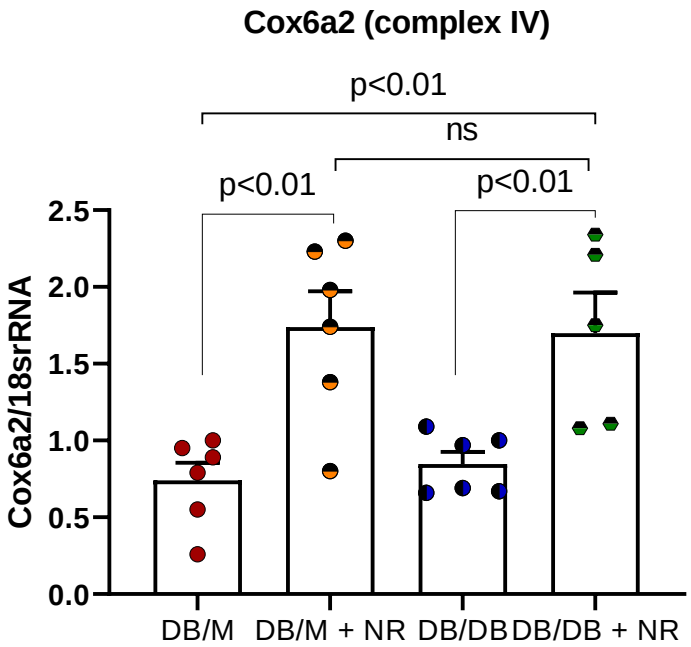

Figure 4

E

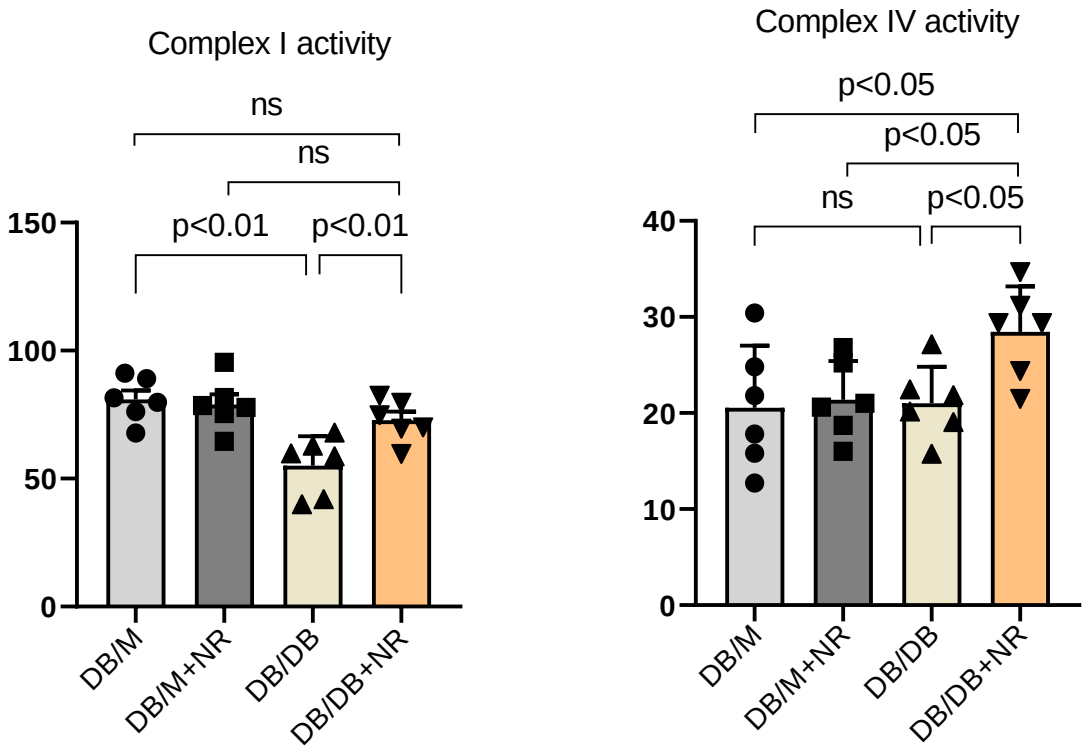

Figure 4

F

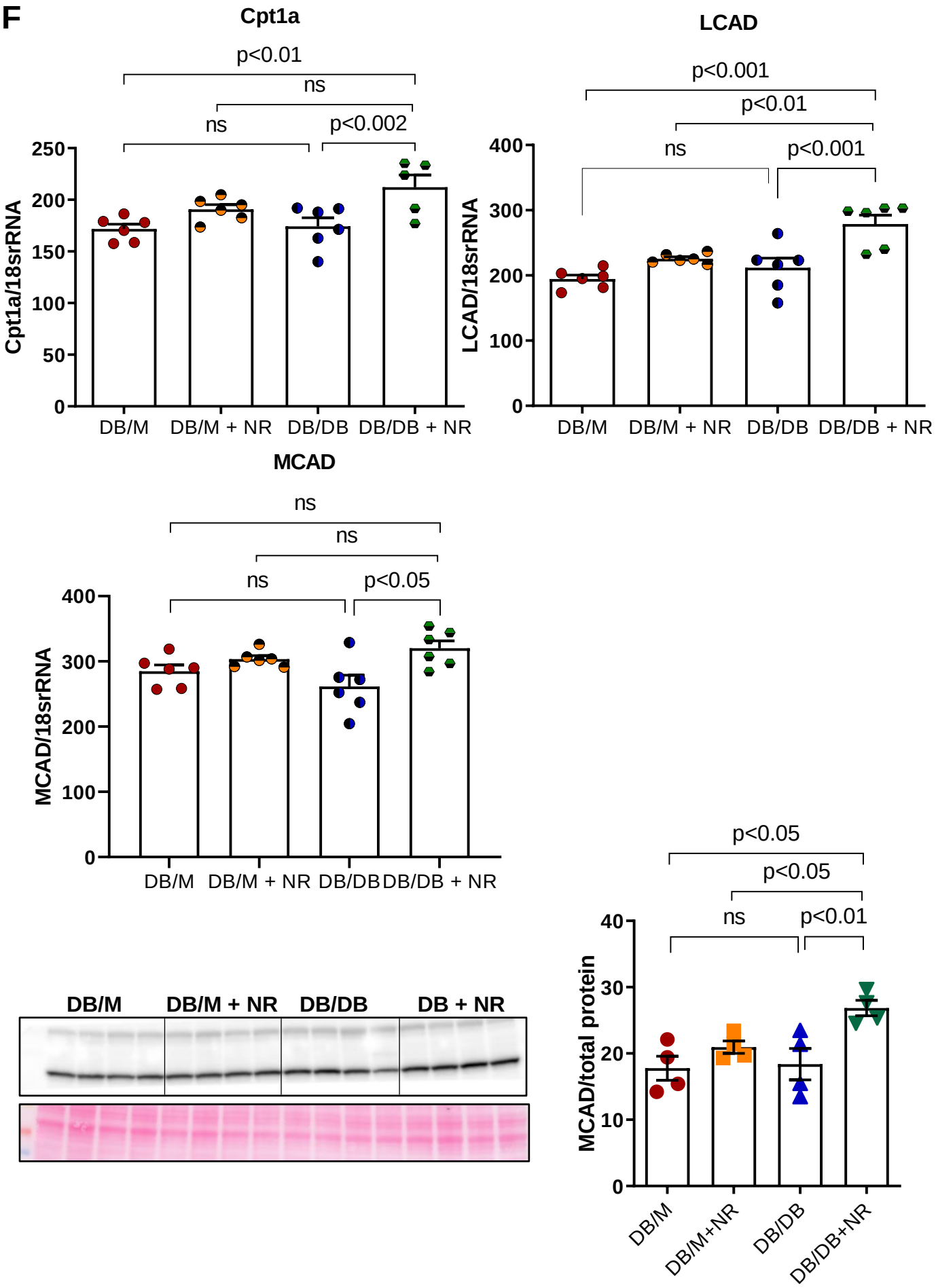

Figure 5

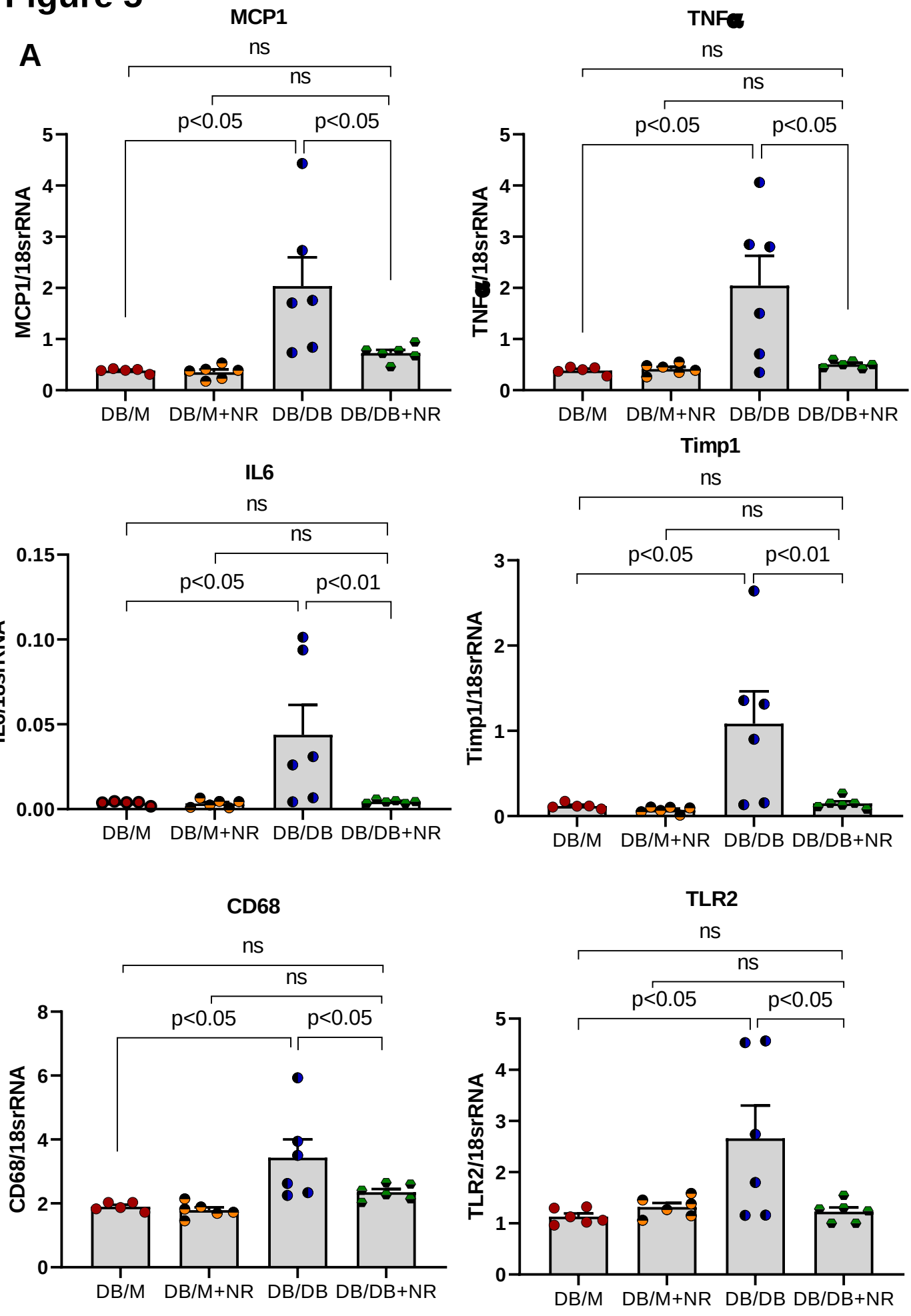

Figure 5

B **CD45**

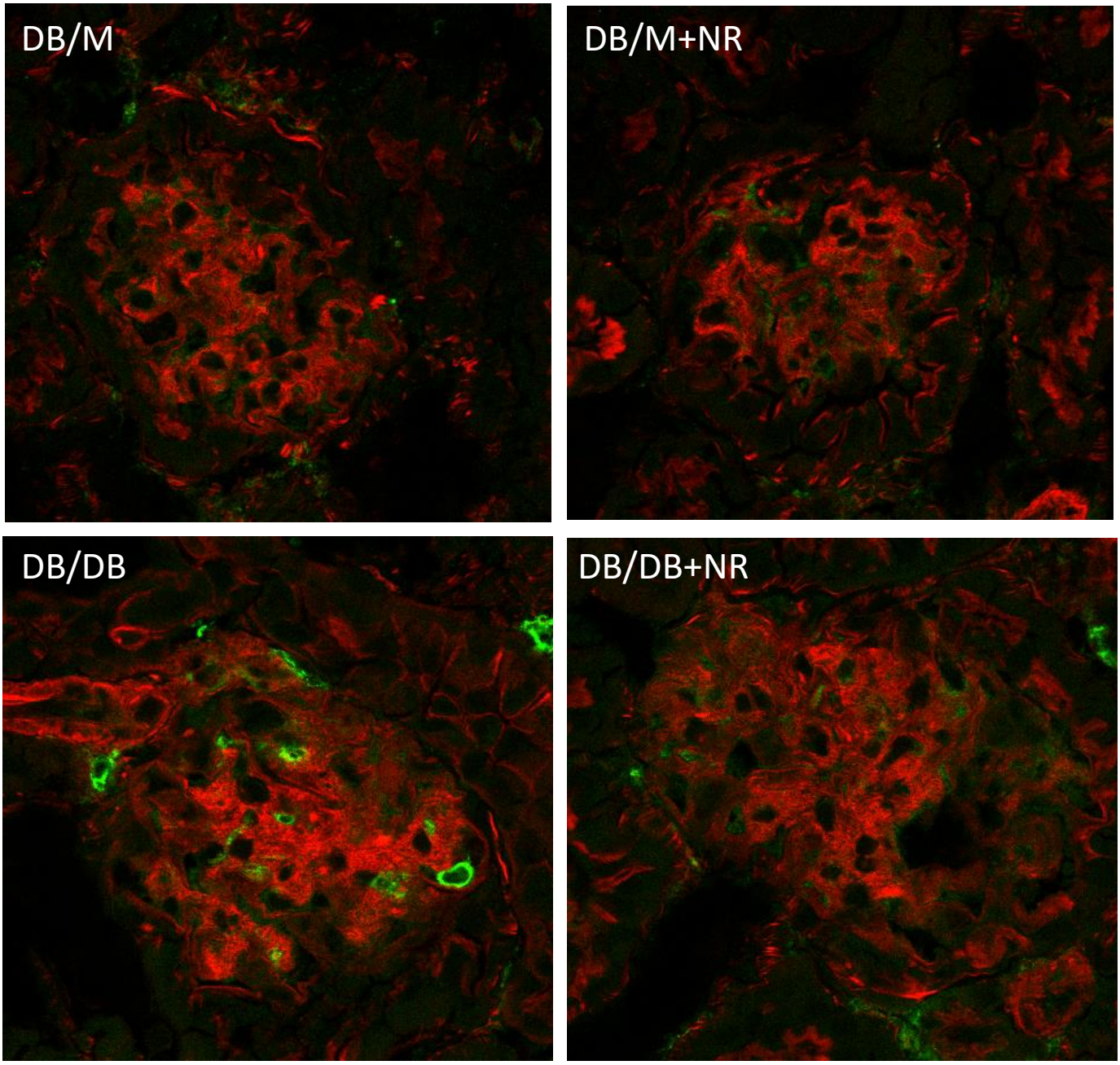

Red: Phalloidin
Green: CD45

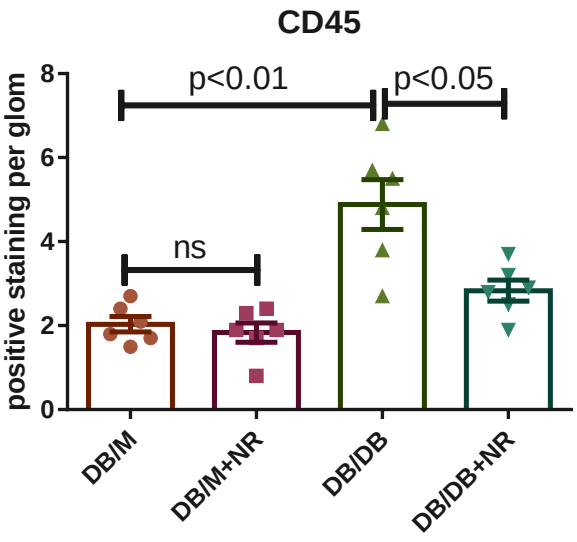

Figure 5

C

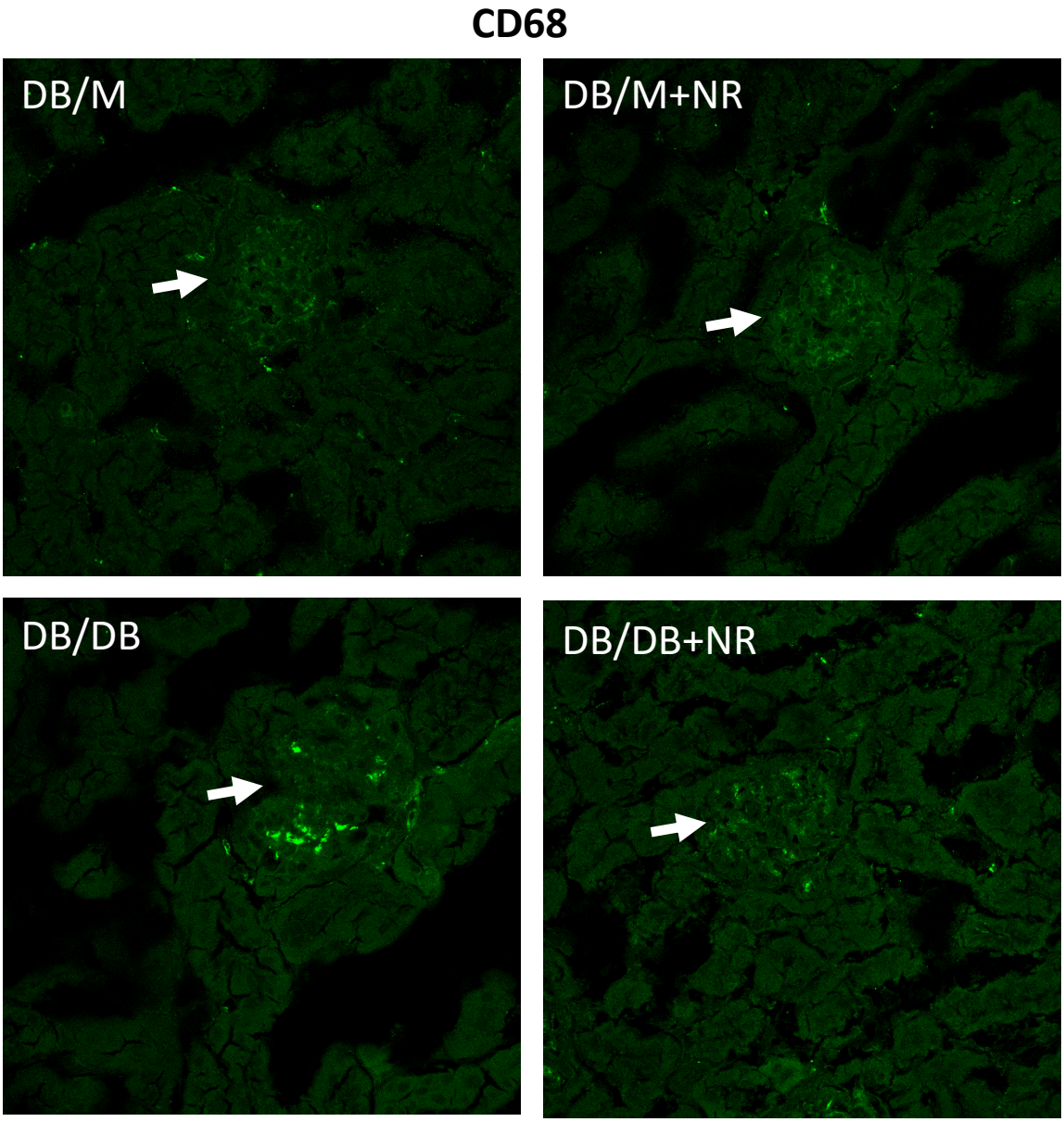

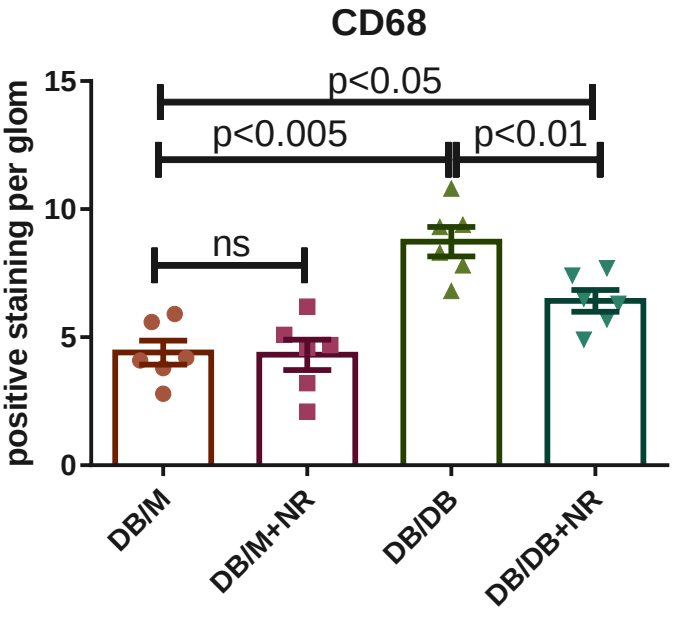

Figure 6

A

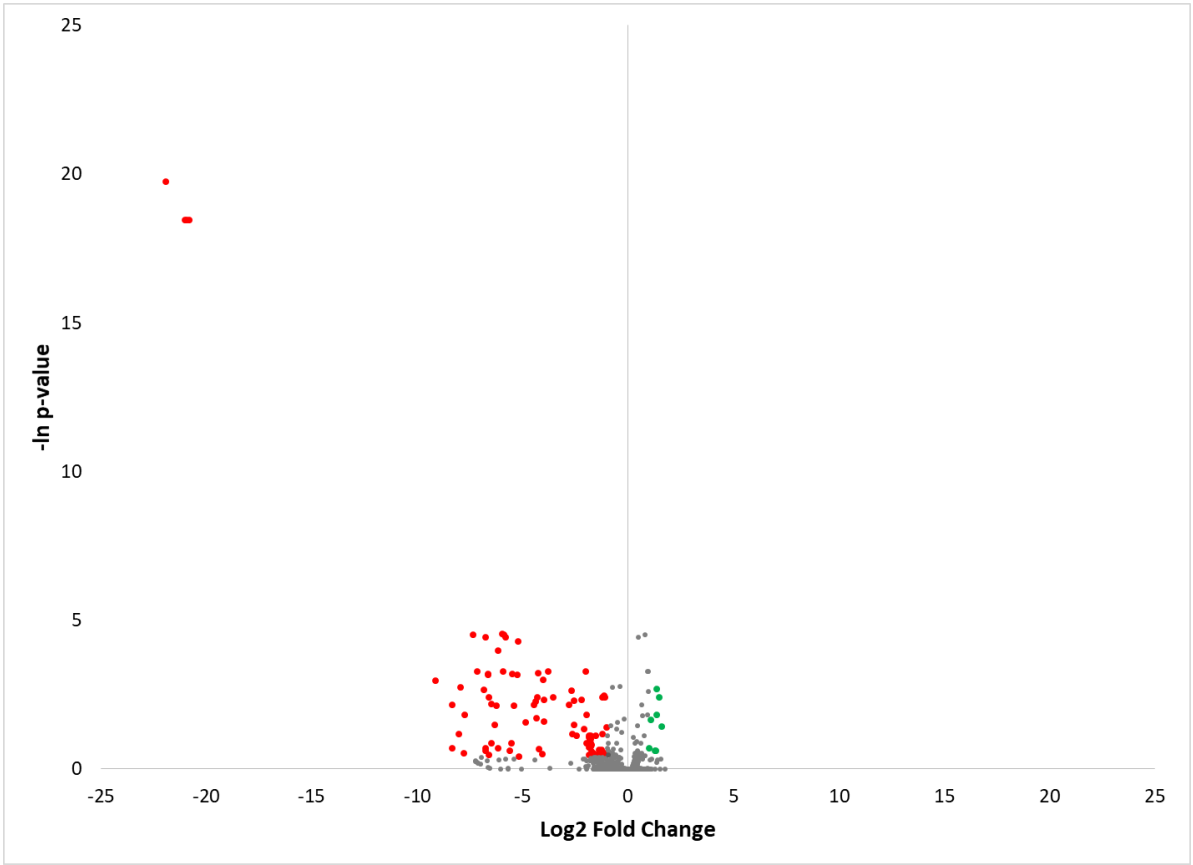

B

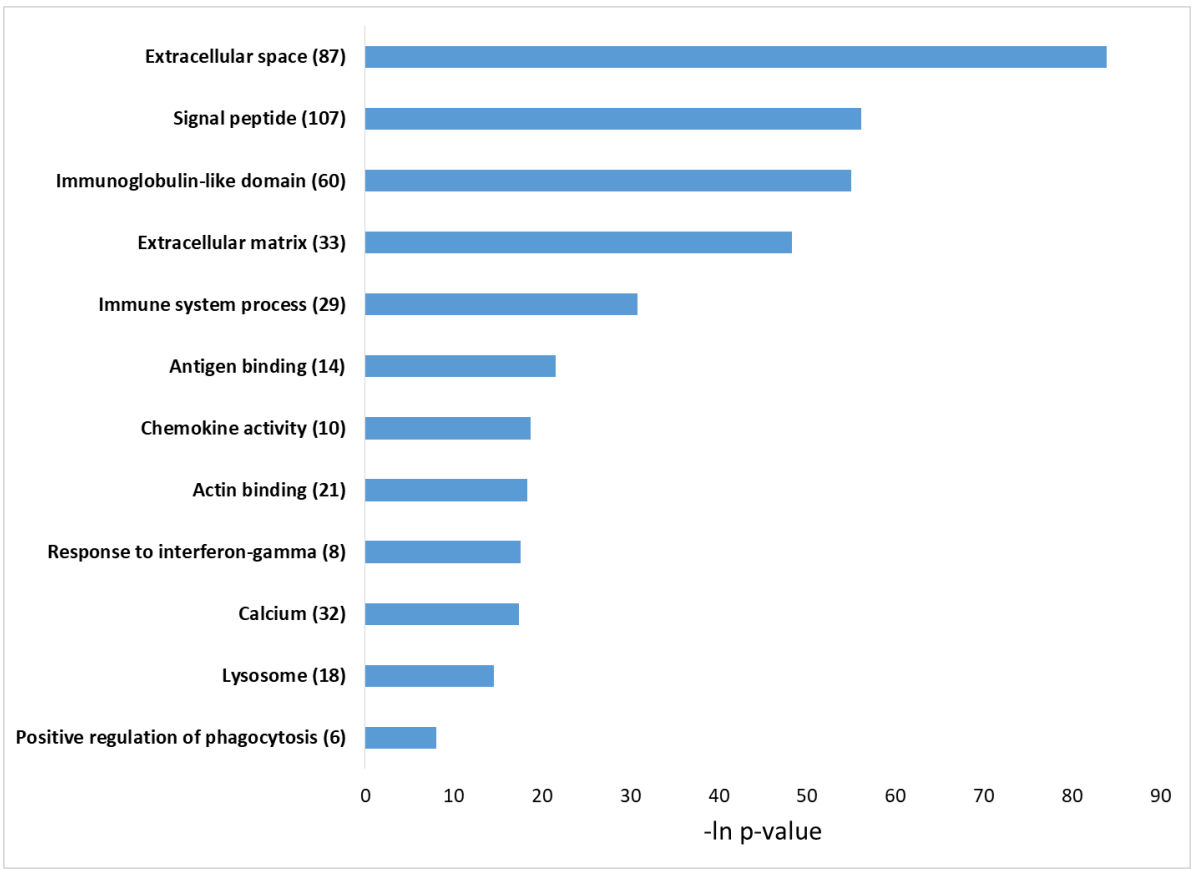

Figure 6

C

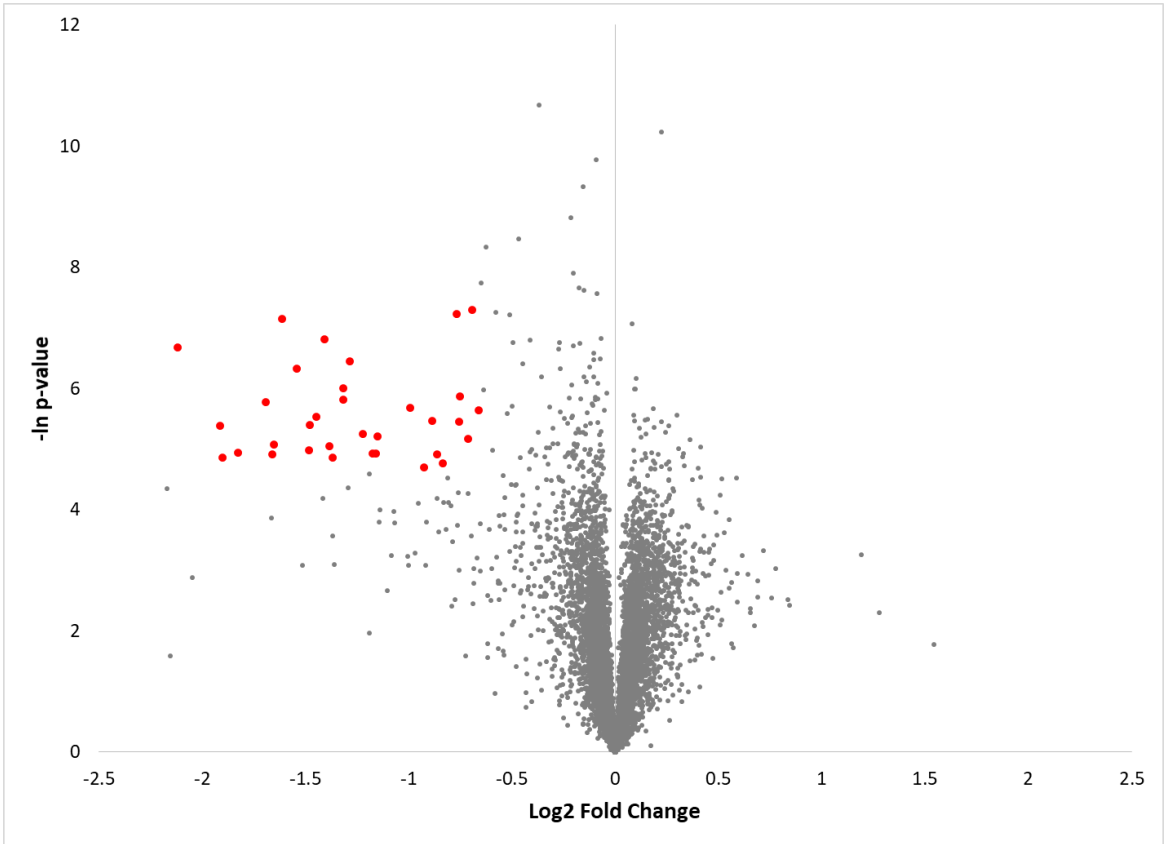

D

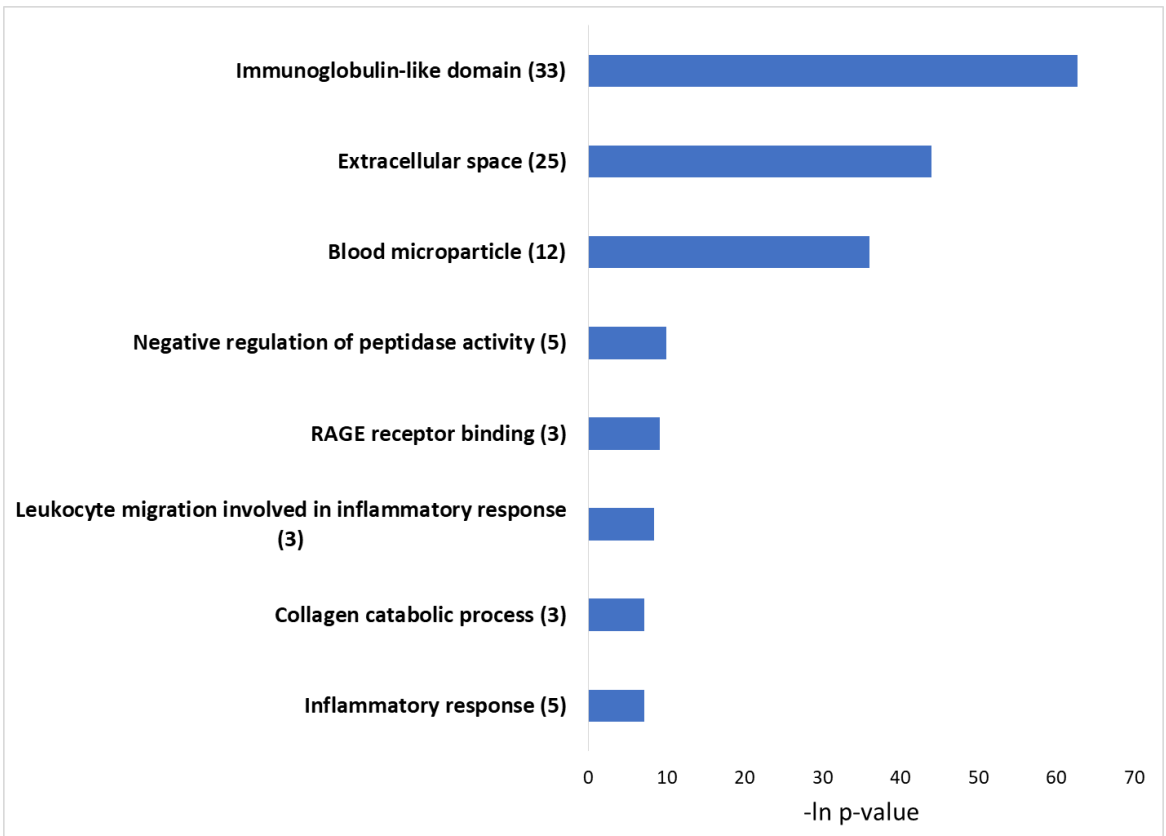

Figure 6

E

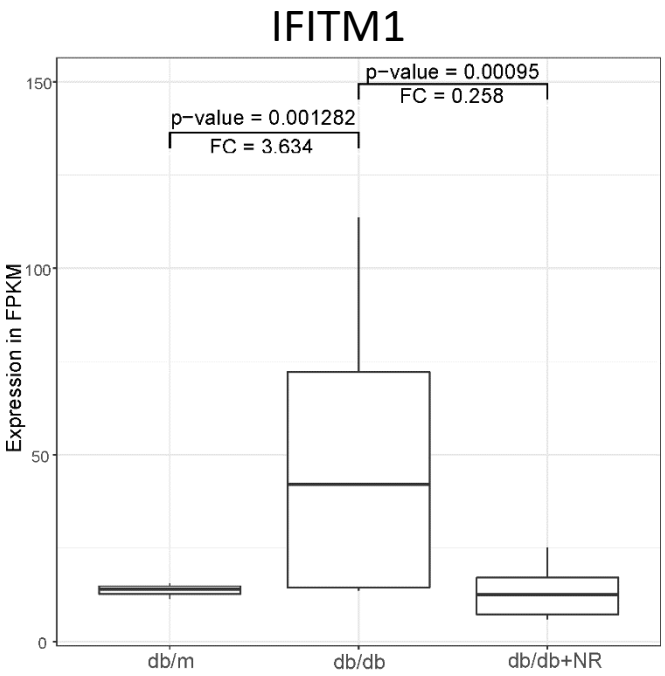

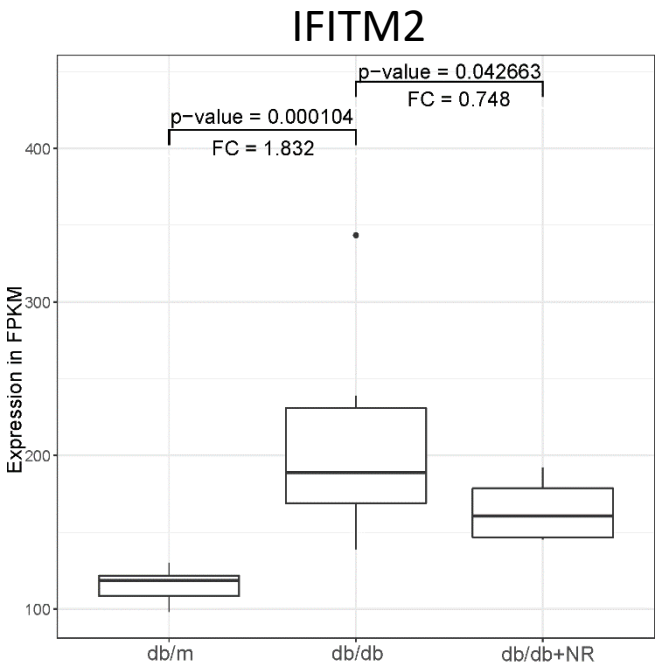

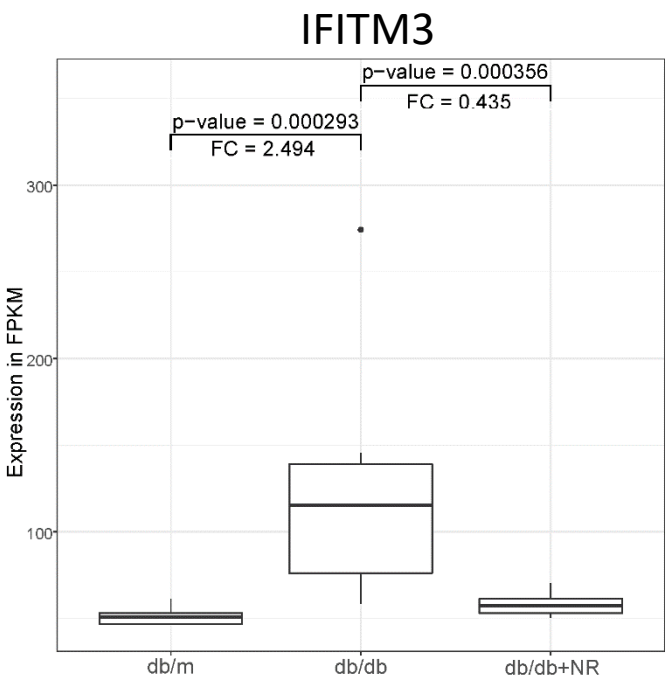

Figure 6

F

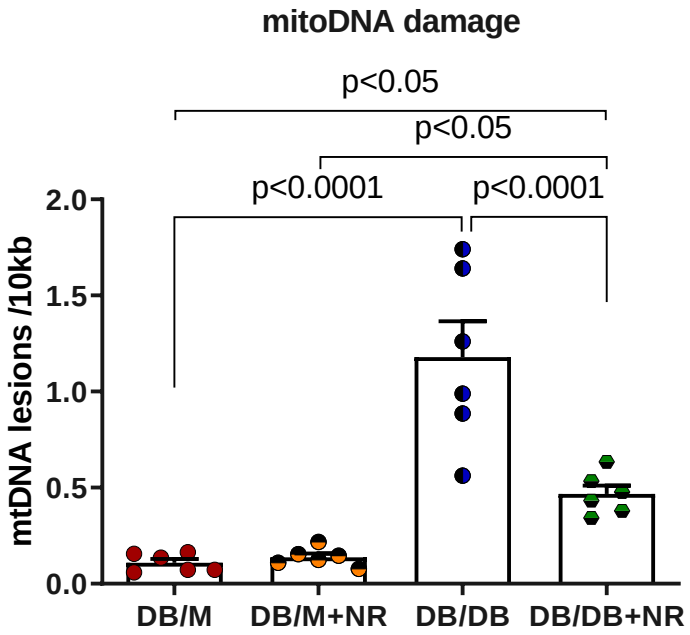

Figure 6

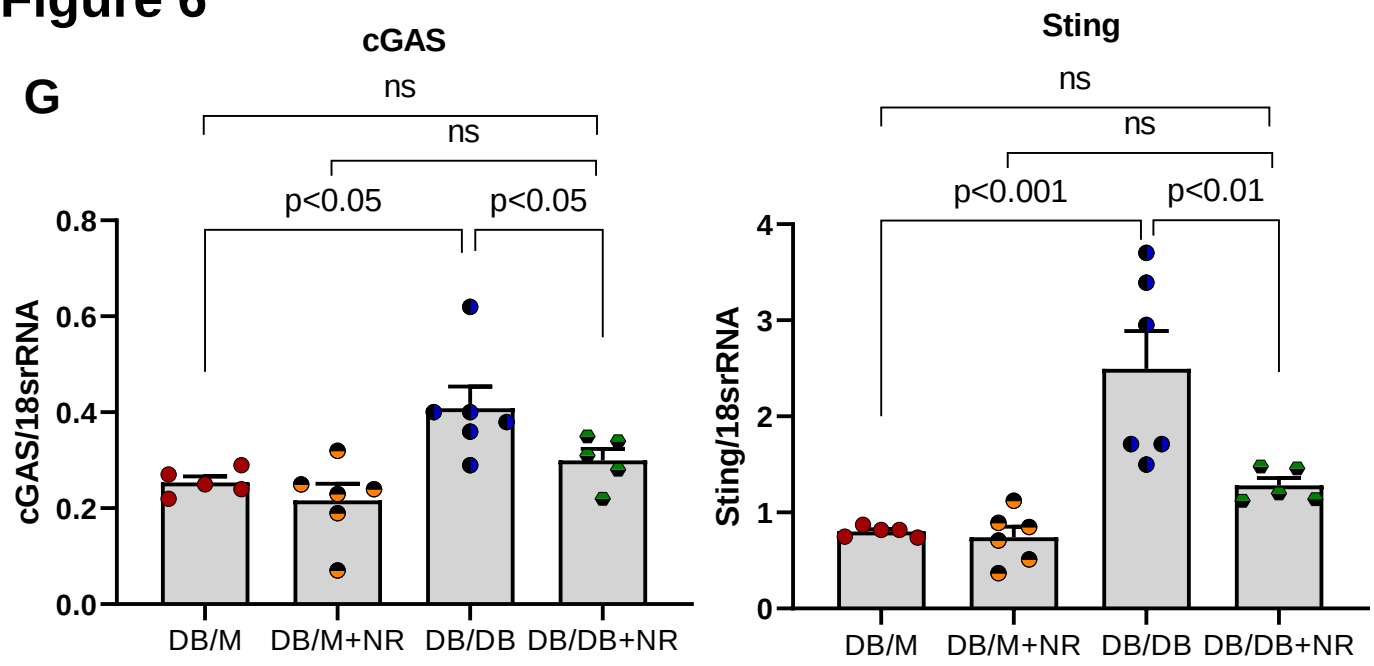

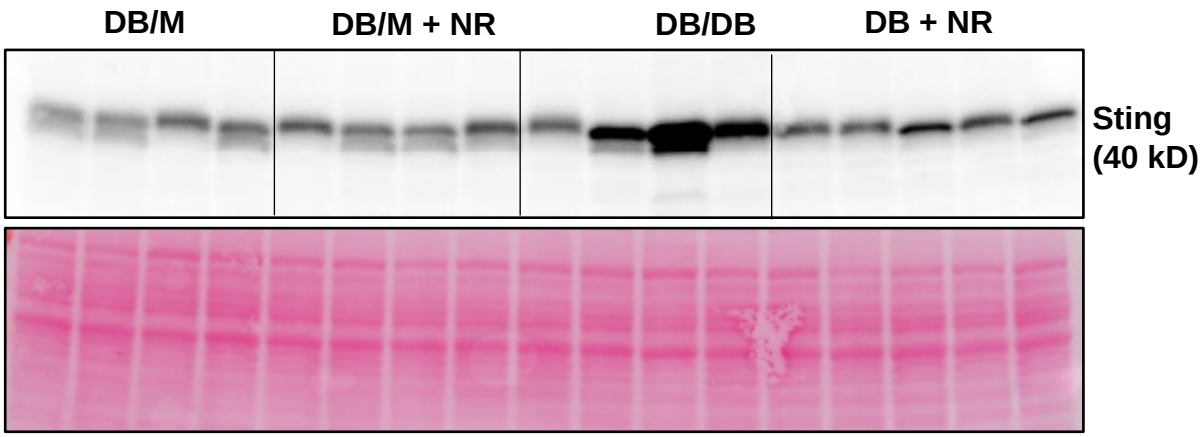

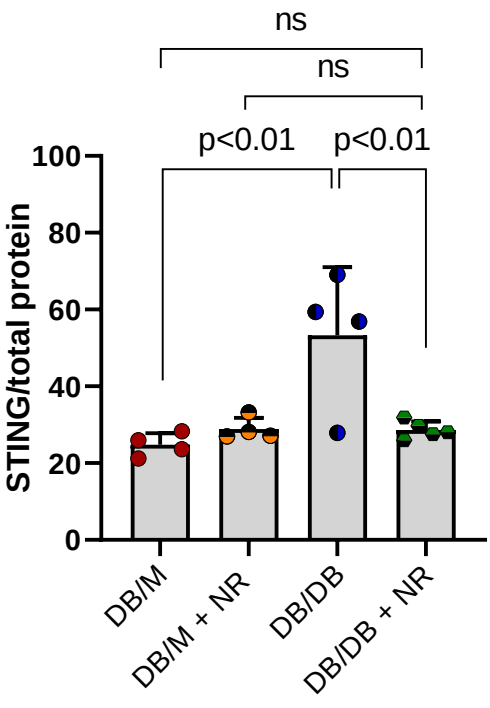

Figure 6

H

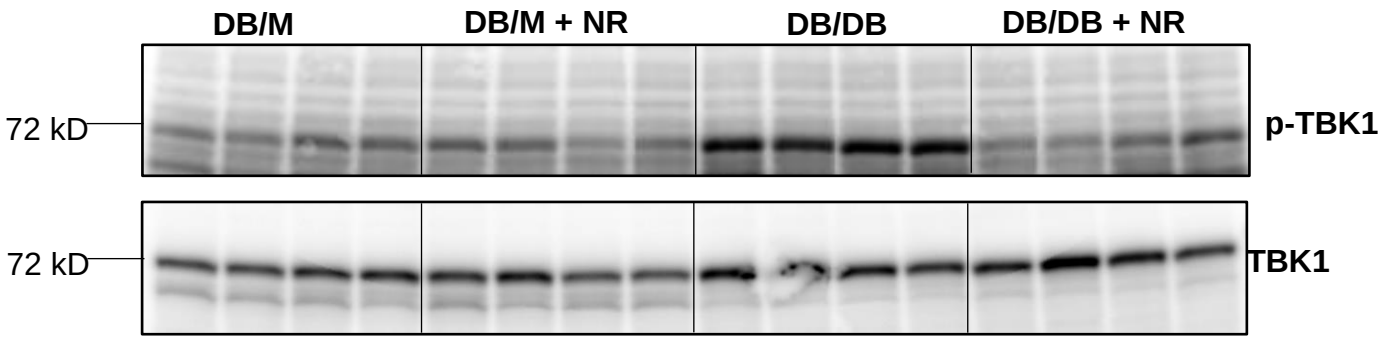

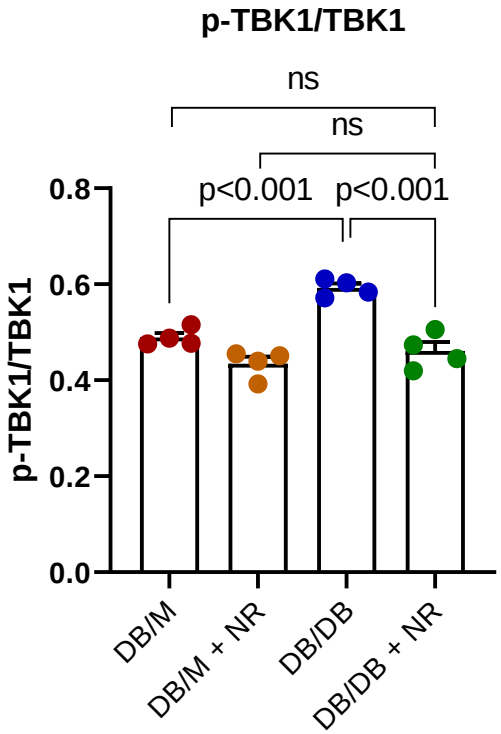

Figure 6

I

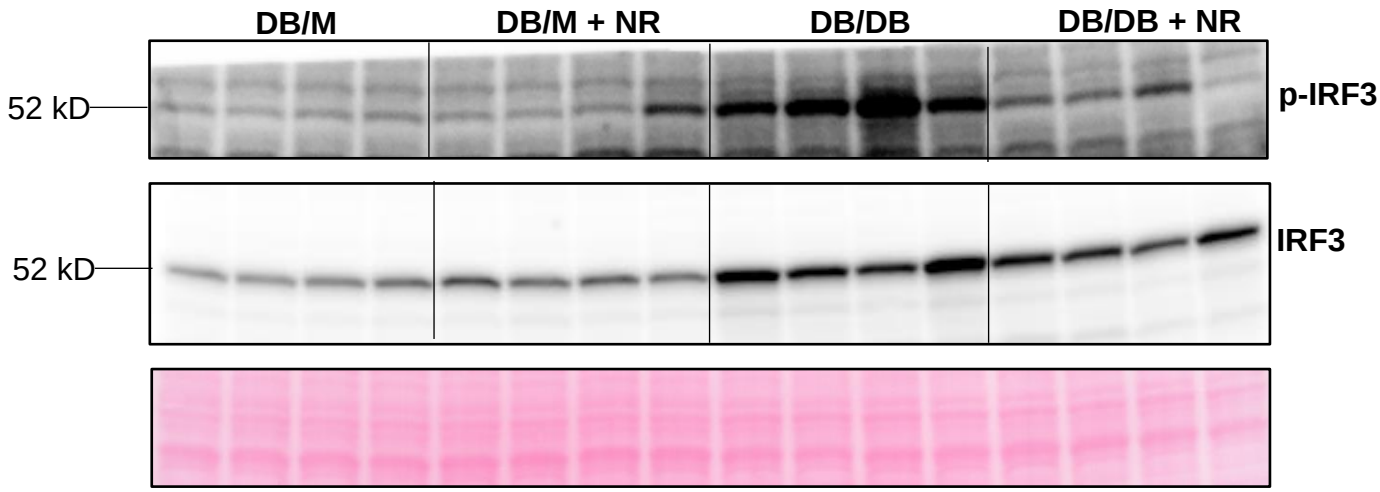

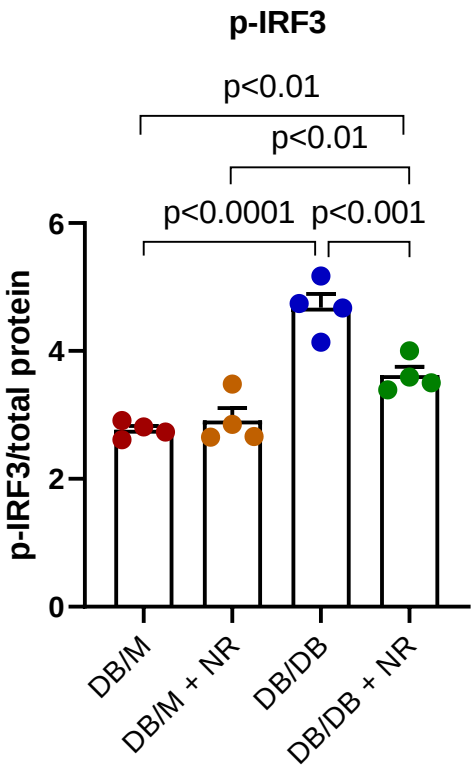

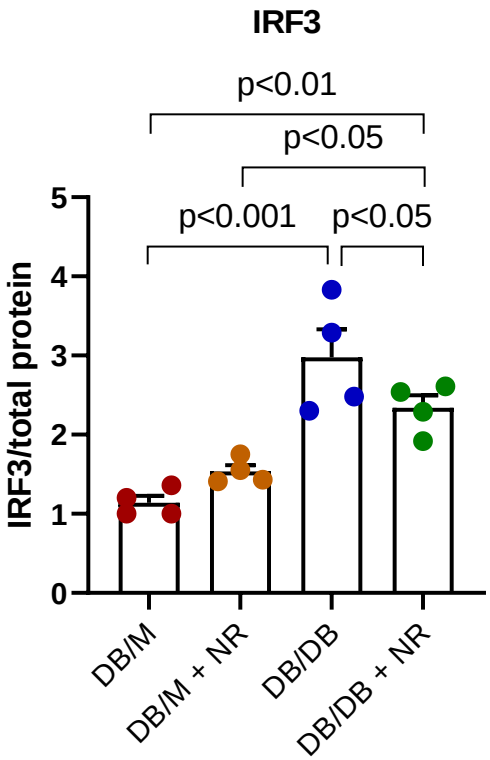

Figure 6

J

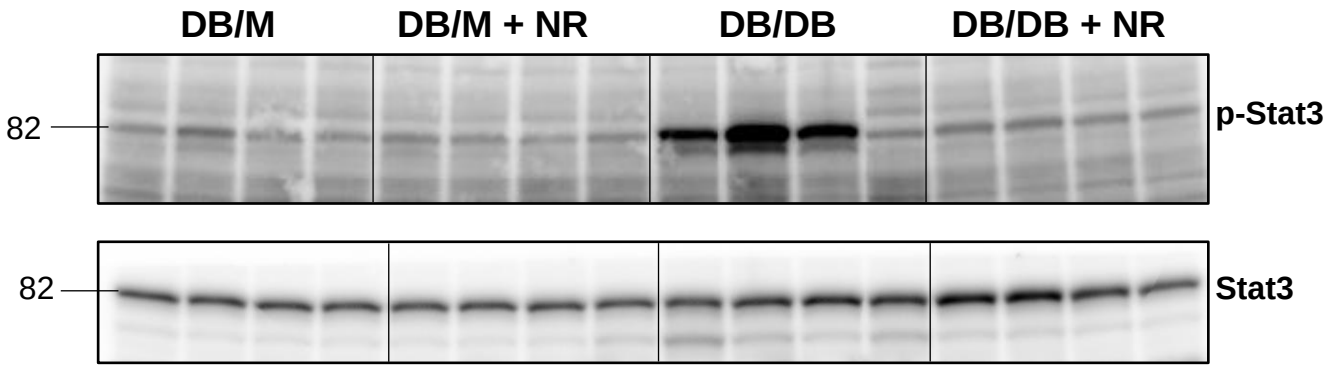

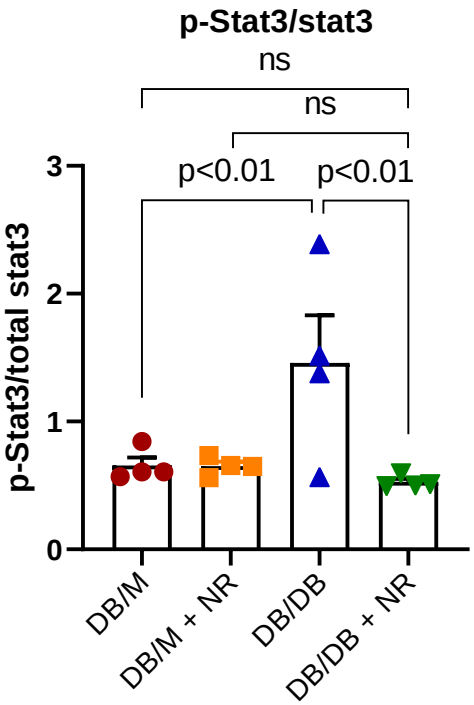

Figure 6

K

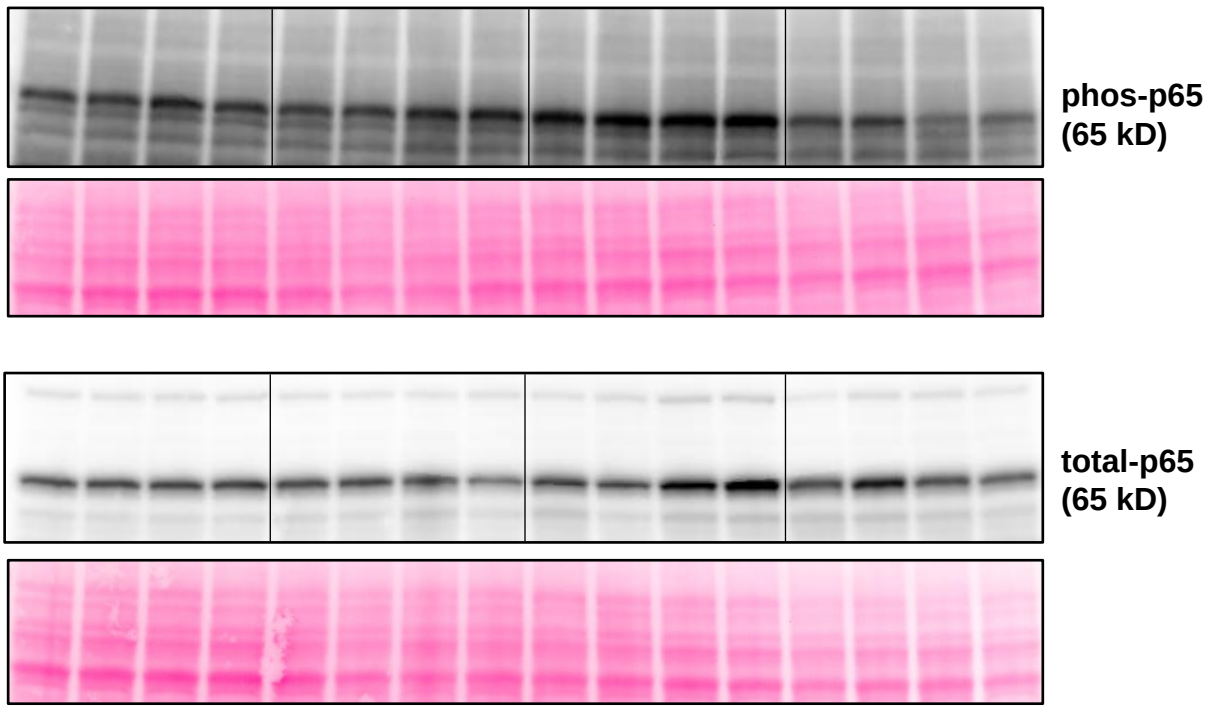

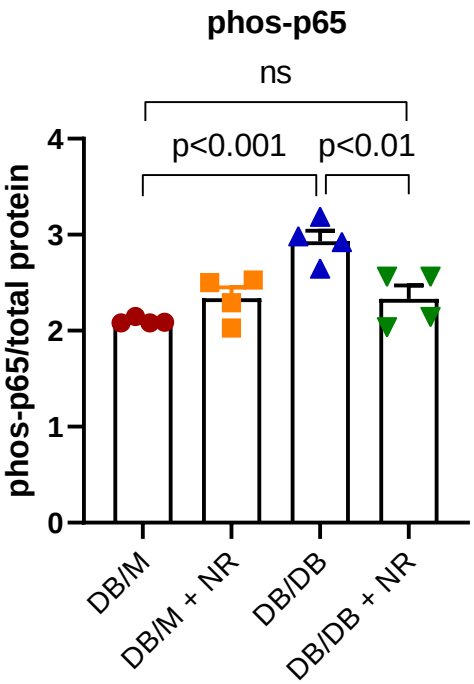

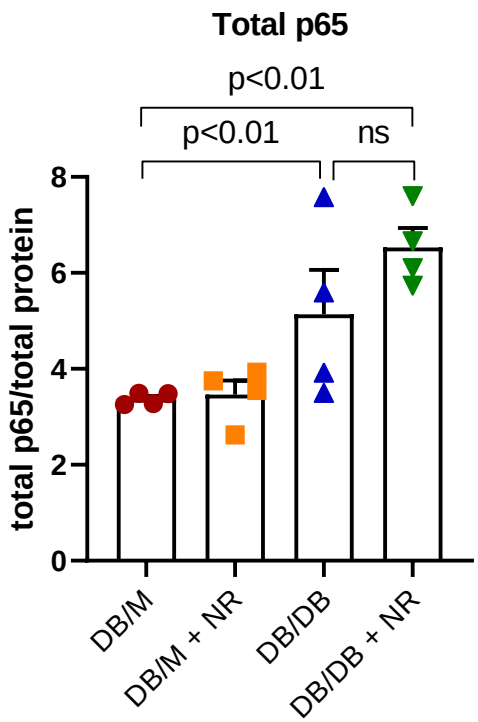

Figure 6

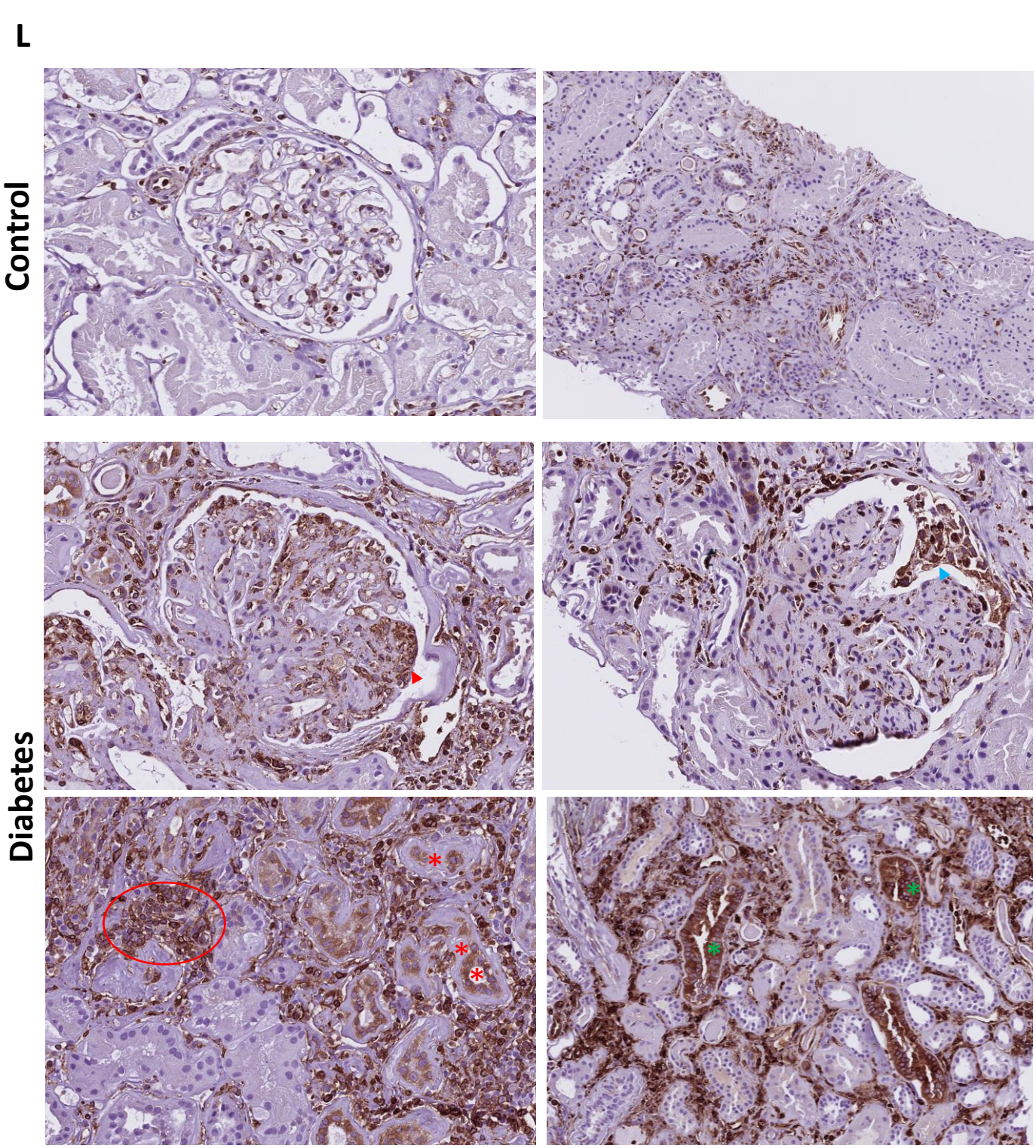

Figure 6

M

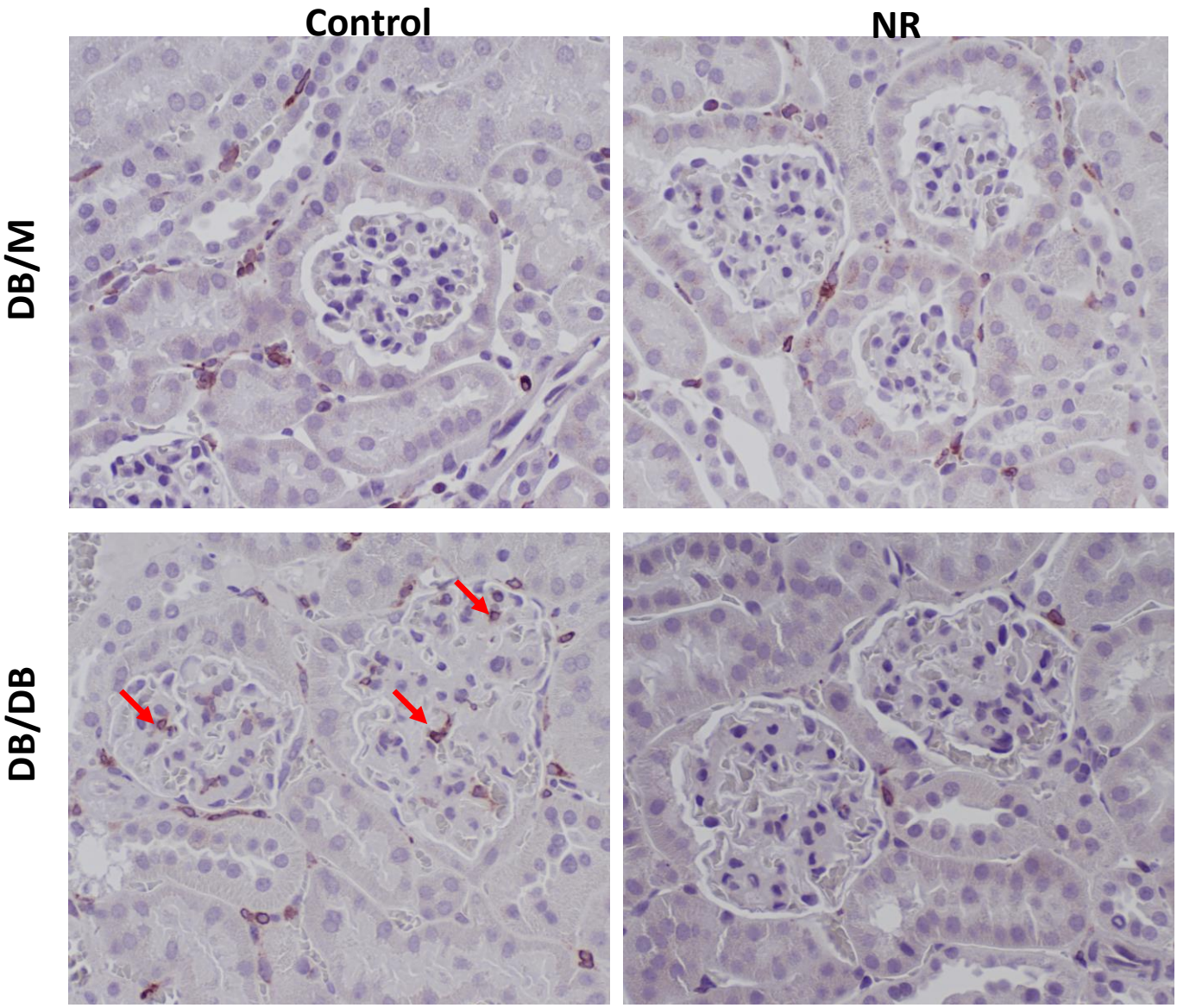

Figure 7

A

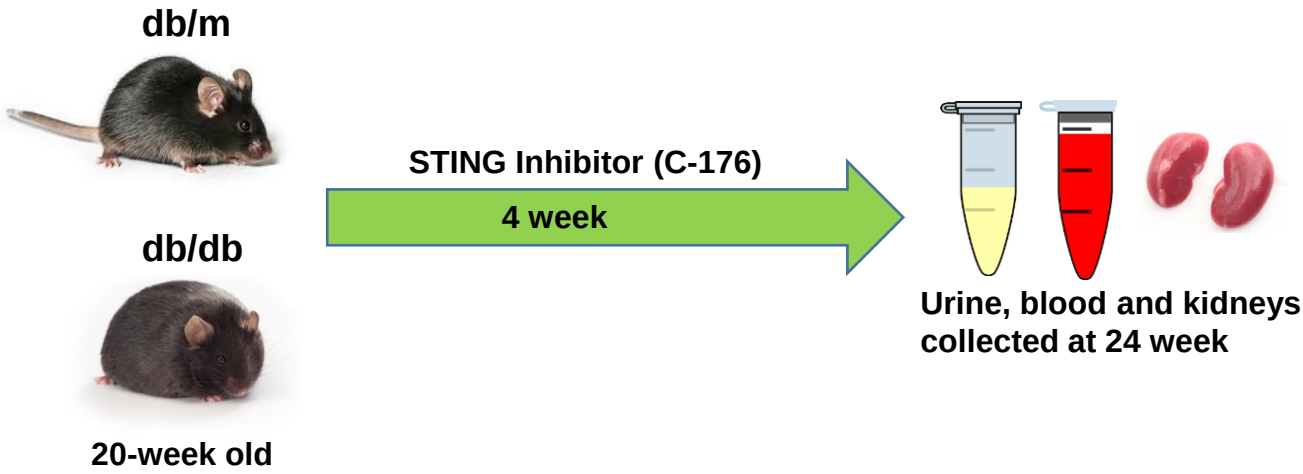

Figure 7

B

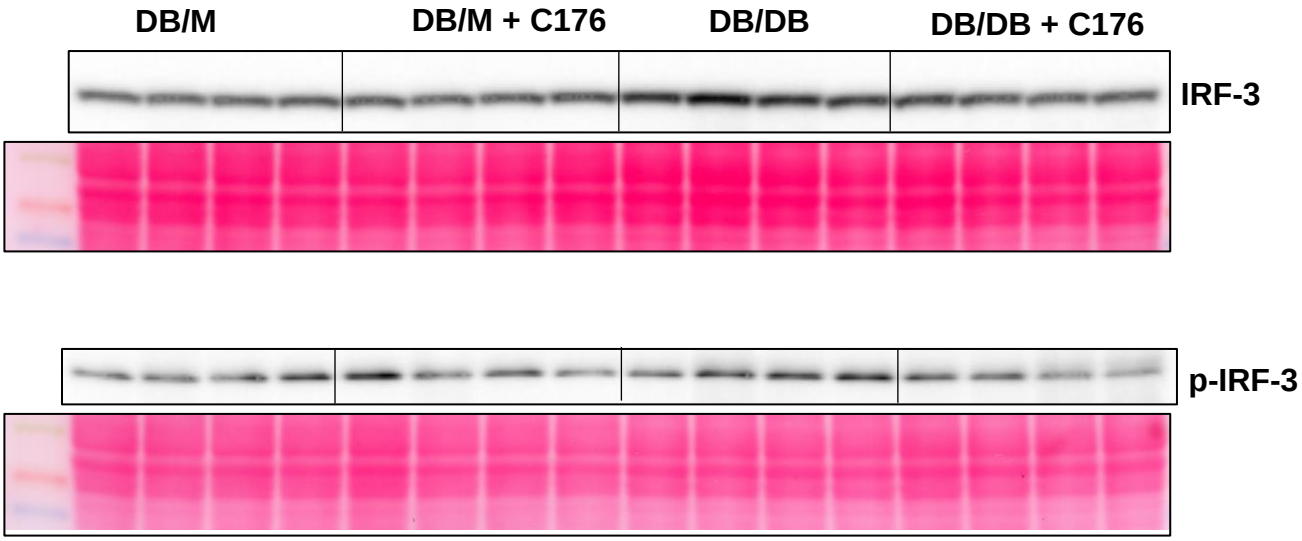

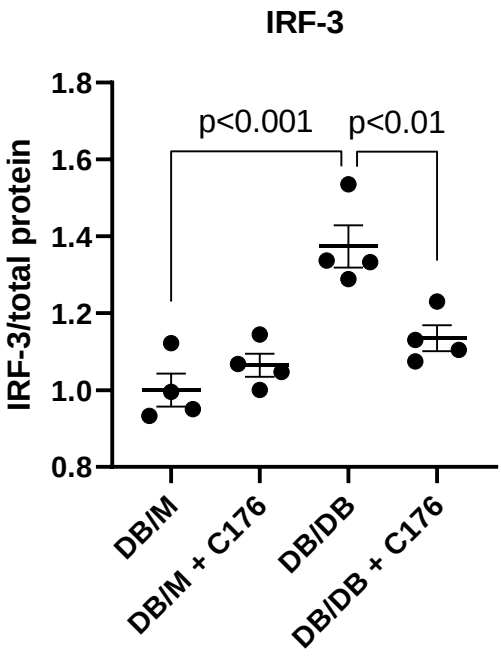

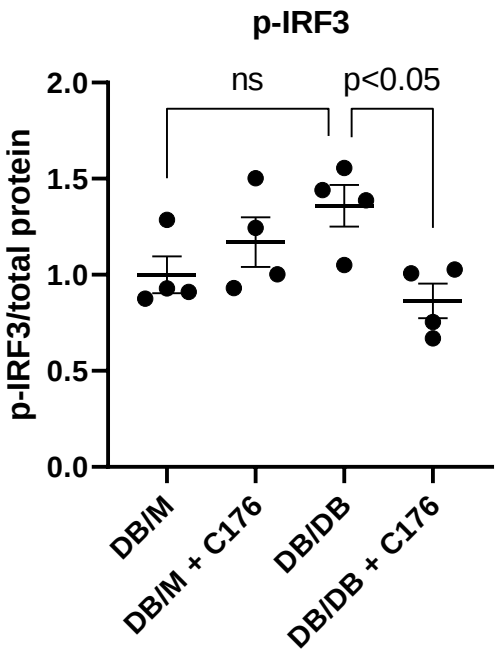

Figure 7

C

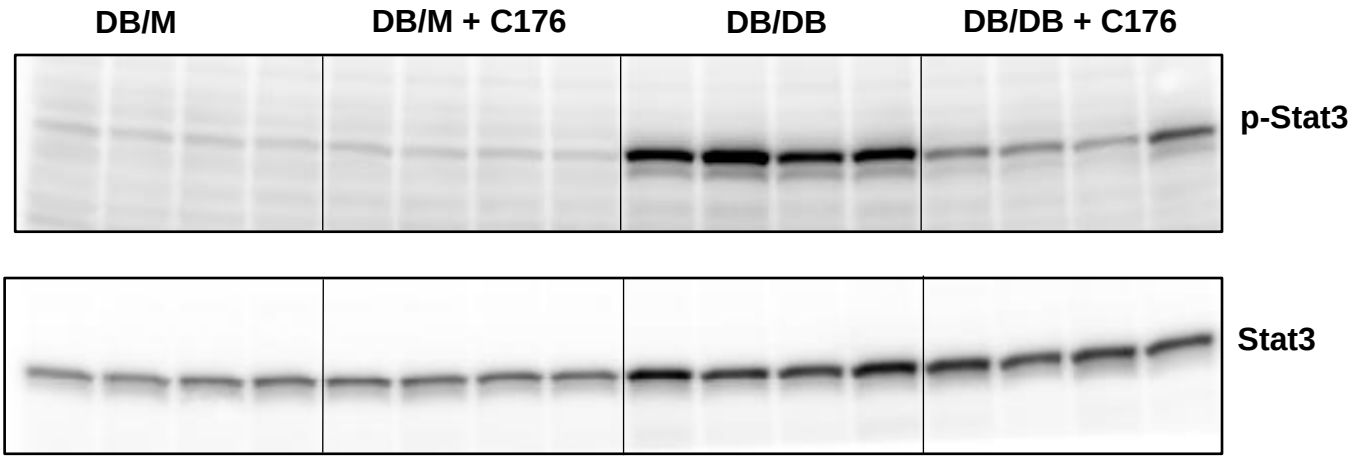

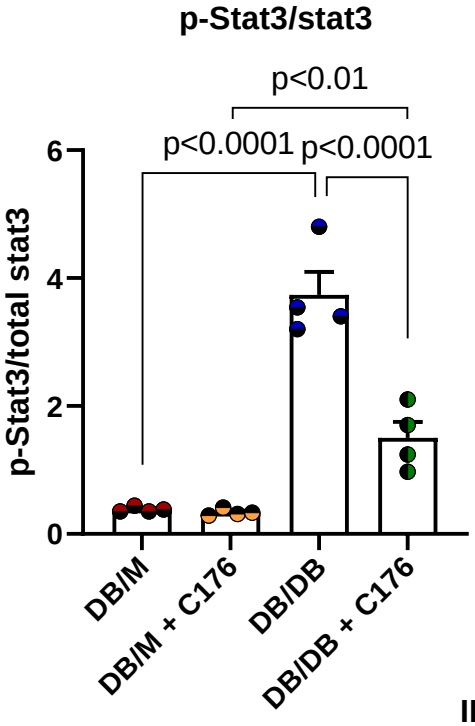

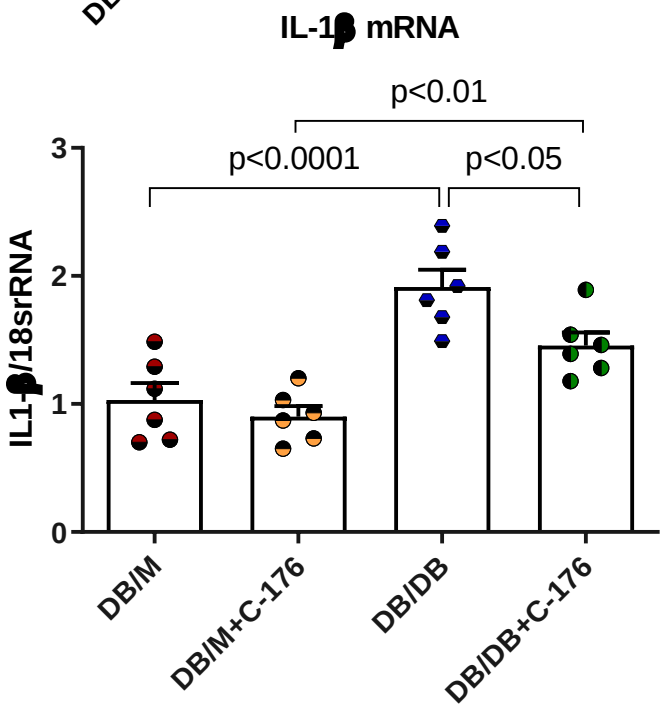

Figure 7

D

Figure 7

E

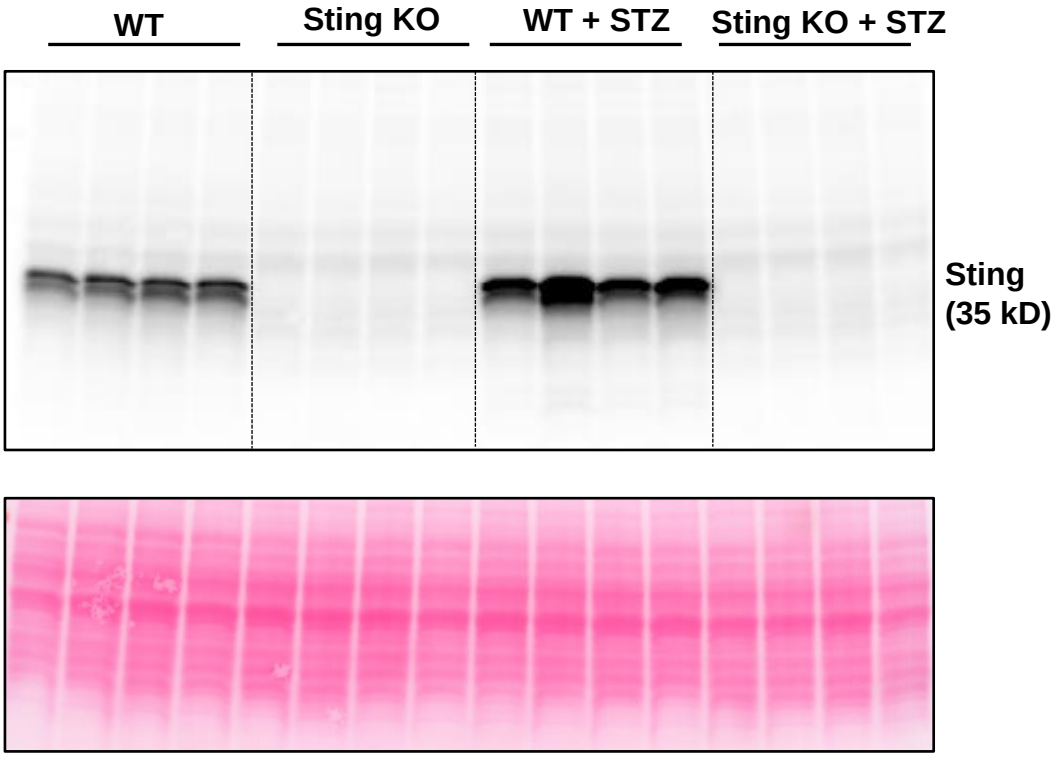

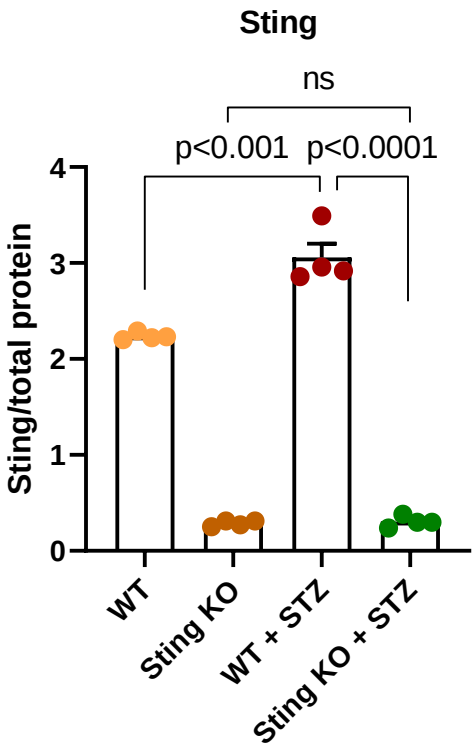

Figure 7

F

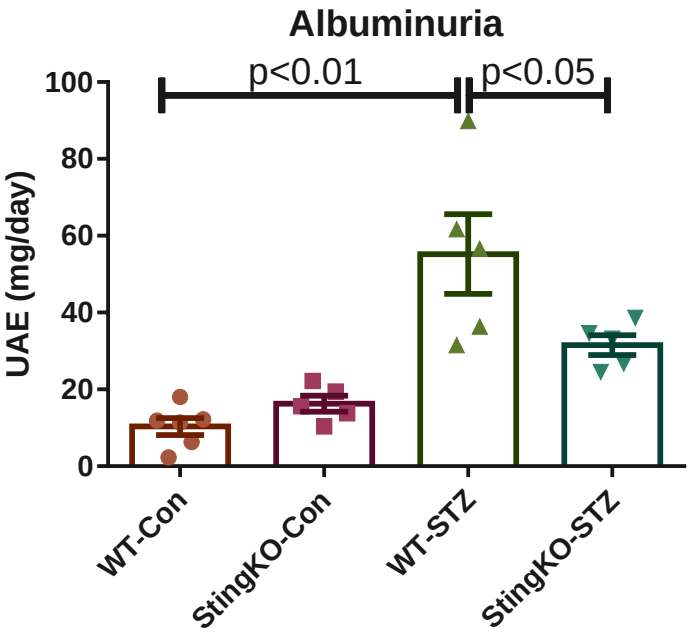

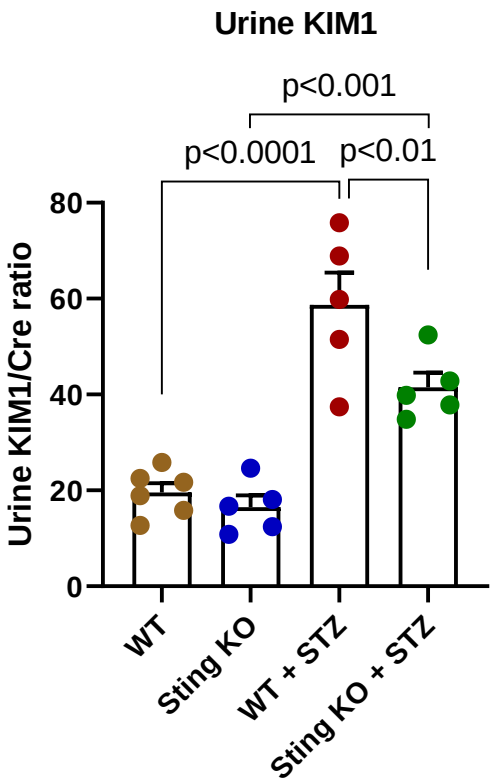

Figure 7

G